

Winter 2004

# Inter-annual and decadal variation in the pelagic marine ecosystem of the Yellow and East China seas

Seung-Hyun Son

*University of New Hampshire, Durham*

Follow this and additional works at: <https://scholars.unh.edu/dissertation>

---

## Recommended Citation

Son, Seung-Hyun, "Inter-annual and decadal variation in the pelagic marine ecosystem of the Yellow and East China seas" (2004).  
*Doctoral Dissertations*. 252.

<https://scholars.unh.edu/dissertation/252>

This Dissertation is brought to you for free and open access by the Student Scholarship at University of New Hampshire Scholars' Repository. It has been accepted for inclusion in Doctoral Dissertations by an authorized administrator of University of New Hampshire Scholars' Repository. For more information, please contact [nicole.hentz@unh.edu](mailto:nicole.hentz@unh.edu).

**INTER-ANNUAL AND DECADAL VARIATION IN THE PELAGIC MARINE  
ECOSYSTEM OF THE YELLOW AND EAST CHINA SEAS**

**BY**

**Seung-Hyun Son**

**B.S. Busan National University, Republic of Korea, 1996**

**M.S. Busan National University, Republic of Korea, 1998**

**DISSERTATION**

**Submitted to the University of New Hampshire**

**In Partial Fulfillment of**

**The Requirements for the Degree of**

**Doctor of Philosophy**

**in**

**Earth Sciences – Oceanography**

**December, 2004**

UMI Number: 3158681

### INFORMATION TO USERS

The quality of this reproduction is dependent upon the quality of the copy submitted. Broken or indistinct print, colored or poor quality illustrations and photographs, print bleed-through, substandard margins, and improper alignment can adversely affect reproduction.

In the unlikely event that the author did not send a complete manuscript and there are missing pages, these will be noted. Also, if unauthorized copyright material had to be removed, a note will indicate the deletion.

**UMI**<sup>®</sup>

---

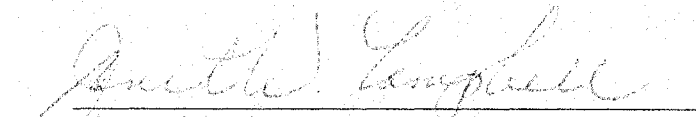
UMI Microform 3158681

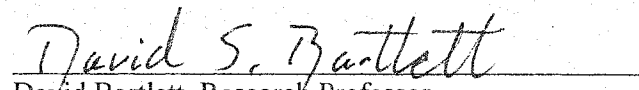
Copyright 2005 by ProQuest Information and Learning Company.

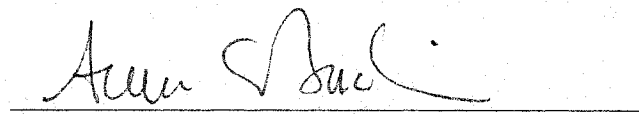
All rights reserved. This microform edition is protected against unauthorized copying under Title 17, United States Code.

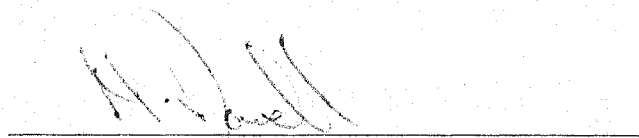
ProQuest Information and Learning Company  
300 North Zeeb Road  
P.O. Box 1346  
Ann Arbor, MI 48106-1346

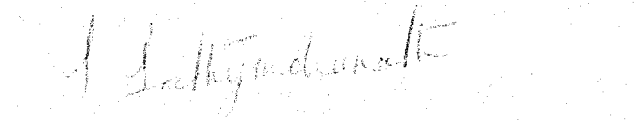
This dissertation has been examined and approved.

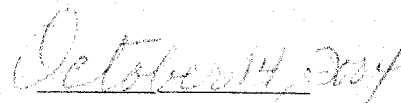
  
Dissertation Director, Janet W. Campbell  
Research Professor of Earth Sciences

  
David Bartlett, Research Professor  
Institute for the Study of Earth, Oceans, and Space

  
Ann C. Bucklin, Professor of Zoology

  
Mark Dowell, Research Scientist  
Inland and Marine Waters Unit, Joint Research Centre  
of the European Commission, Ispra, Italy

  
Shubha Sathyendranath, Honorary Research  
Scientist, Bedford Institute of Oceanography,  
Canada

  
Date

## ACKNOWLEDGEMENTS

I wish to sincerely thank my advisor Dr. Janet Campbell for her kind advice and support during all the years of my Ph.D. study. She always gave me her careful and valuable advice as well as most generous supports throughout the graduate program. Without her unfailing support, this dissertation would not have been possible. I am very grateful to Dr. Mark Dowell for his guidance and help in my research. He always gave me supportive comments and encouragement during my graduate study. I deeply appreciate Dr. Shubha Sathyendranath for giving me valuable advice in dissertation work as well as giving me great opportunities of participating and learning in the international courses. I am also honored that she agreed to be on my committee. Special thanks go to Dr. Ann Bucklin and Dr. David Bartlett for being on my committee. Their insightful comments were crucial for my dissertation.

I appreciate Dr. Sinjae Yoo, Dr. Jaehoon Noh, and Dr. Yu-Hwan Ahn in the Korea Ocean Research and Development Institute for generously providing data for the dissertation. I also wish to express my appreciation to friends, Dr. Il-Ju Moon in University of Rhode Island and Jae-Il Kwon in the Virginia Institute of Marine Science, for their professional advice and encouragement.

I like to thank Tim Moore for his technical support in data processing and general assistance. I would especially like to thank Hui Feng for his valuable discussion and encouragement during the last step in my dissertation not only as a colleague but also like an older brother. In addition, I would like to thank other colleagues in OPAL, Joe

Salisbury, Doug Vandemark, Chris Hunt, Theresa Hammer, and Cheryl Moore for their help and companionship.

Finally, I deeply appreciate my wife Chunai for the love, support, and patience during my doctoral study at UNH. I also thank my mother and sisters in Korea who understand and support me at all times.

## CONTENTS

ACKNOWLEDGEMENTS .....	iii
LIST OF TABLES .....	ix
LIST OF FIGURES .....	x
ABSTRACT .....	xvii
1. INTRODUCTION, BACKGROUND AND SCIENCE OBJECTIVES .....	1
1.1. Introduction .....	1
1.2. Background .....	2
1.3. Science objectives .....	7
2. DECADAL VARIABILITY IN THE YELLOW AND EAST CHINA SEAS AS REVEALED BY SATELLITE OCEAN COLOR DATA (1979-2003) .....	10
Abstract .....	10
2.1. Introduction .....	12
2.2. Data and Methods .....	14
2.2.1. Satellite data .....	15
2.2.2. Converting CZCS pigments to chlorophyll concentration .....	16
2.2.3. <i>in situ</i> data .....	19

2.3.	Results .....	19
2.4.	Discussion .....	22
2.5.	Conclusion .....	29
	Acknowledgements for Chapter 2 .....	30
	Tables of Chapter 2 .....	31
	Figures of Chapter 2 .....	32
3.	CLASSIFICATION OF WELL-MIXED AND STRATIFIED WATERS IN THE YELLOW SEA .....	43
	Abstract .....	43
3.1.	Introduction .....	44
3.2.	Methods .....	47
	3.2.1. Model data .....	47
	3.2.2. Satellite data .....	48
	3.2.3. Ship measurements .....	49
3.3.	Results .....	49
	3.3.1. Difference between surface and bottom temperature .....	49
	3.3.2. Simpson and Hunter's criterion .....	51
	3.3.3. Satellite observations .....	52
	3.3.4. <i>In situ</i> measurements .....	53
	3.3.5. Comparison between model result and satellite data .....	54
3.4.	Discussion .....	56



3.5. Conclusion .....	60
Acknowledgements for Chapter 3 .....	61
Figures of Chapter 3 .....	62
4. PRIMARY PRODUCTION BY OCEAN COLOR REMOTE SENSING IN THE YELLOW SEA .....	72
Abstract .....	72
4.1. Introduction .....	73
4.2. Data and Methods .....	76
4.2.1. <i>in situ</i> data .....	76
4.2.2. Satellite data .....	77
4.2.3. Parameterization of primary production model .....	79
4.2.3.1. Primary production model .....	79
4.2.3.2. Biomass profile (DCM model) .....	79
4.2.3.3. PAR profile .....	80
4.2.3.4. Photosynthetic parameters .....	82
4.2.4. Oceanographic sub-regions .....	83
4.3. Results .....	84
4.3.1. Satellite-derive primary production .....	85
4.4. Discussion and Conclusion .....	89
Acknowledgements for Chapter 4 .....	95
Tables of Chapter 4 .....	96

Figures of Chapter 4 .....	99
5. SUMMARY, SIGNIFICANCE AND FUTURE RESEARCH .....	117
BIBLIOGRAPHY .....	123

## List of Tables

<b>Table 2.1.</b> Long-term means and standard deviations of the CZCS (1979-1984) and the SeaWiFS (1998-2002) chlorophyll, $L_w443$ , and $L_w555$ for 6 sub-regions: the Bohai Sea, the western coast of the Yellow Sea, the middle of the Yellow Sea, the eastern coast of the Yellow Sea, the west-East China Sea, the middle of the East China Sea, and the east-East China Sea. Ratios and percentiles of SeaWiFS-to-CZCS long-term means were calculated. The units are $\text{mg}/\text{m}^3$ for chlorophyll and $\text{W}/\text{m}^2/\text{sr}/\text{nm}$ for water-leaving radiances .....	31
<b>Table 4.1.</b> Sources of data for the chlorophyll profiles and P-E parameters in the Yellow Sea (32-37°N and 122-127°E). Total number is 141 stations. .....	96
<b>Table 4.2.</b> P-E parameters for the 3 regions of the Yellow Sea .....	97
<b>Table 4.3.</b> Primary production in the 3 regions of the Yellow Sea .....	98
<b>Table 4.4.</b> Annual total primary production in the Yellow Sea .....	98

## List of Figures

**Figure 2.1.** Geography of the study area (BS: the Bohai Sea, WYS: the western coast of the Yellow Sea, MYS: the middle of the Yellow Sea, EYS: the eastern coast of the Yellow Sea, WECS: the western East China Sea, MECS: the middle of the East China Sea, and EECS: the eastest East China Sea) and the serial oceanographic stations of KODC (small squares, 61 stations) ..... 32

**Figure 2.2.** Results of applying the OC4 (SeaWiFS) chlorophyll algorithm (vertical axis) and the CZCS pigment algorithm (horizontal axis) to the original SeaBAM data of O'Reilly et al., (1998). The vertical dashed line marks the value pigment =  $1.5 \text{ mg m}^{-3}$  where the CZCS algorithm switched from using the 443:550 radiance ratio to the 520:550 ratio. The dashed line is the relationship  $\text{CHL} = 0.8 \text{ PIG}$  proposed by O'Reilly et al. (1998) that was subsequently used by Conkright and Gregg (2001) ..... 33

**Figure 2.3.** Yearly composite CZCS (1979-1984) and SeaWiFS (1998-2003) images of (a) nLw443, (b) nLw555 and (c) chlorophyll in the Yellow and East China Seas. The scales give water-leaving radiances in  $\text{W/m}^2/\text{sr}/\text{nm}$  and chlorophyll in  $\text{mg/m}^3$  ..... 34

**Figure 2.4.** Long-term average of CZCS (1979-1984) and SeaWiFS (1998-2003) nLw443 ..... 35

**Figure 2.5.** Long-term average of CZCS (1979-1984) and SeaWiFS (1998-2003) nLw555 ..... 36

**Figure 2.6.** Long-term average of CZCS (1979-1984) and SeaWiFS (1998-2003) chlorophylls ..... 37

**Figure 2.7.** Ratios of SeaWiFS-to-CZCS long-term means. (a) L<sub>w</sub>(443), (b) L<sub>w</sub>(555) and (c) chlorophyll. Increases are shown in yellows and reds, decreases in greens and blues, and white indicates no change ..... 38

**Figure 2.8.** The year-to-year variations of temperature, salinity, and Secchi depth from 1978 to 2002, and zooplankton biomass from 1978 to 1996 at the 61 KODC stations in the Yellow Sea. Dashed lines are the trend lines and thick horizontal lines are the means values for the CZCS (1979-1984) and SeaWiFS (1998-2002) eras. The yearly averaged chlorophyll, nLw443, and nLw555 values of the CZCS (1979-1984) and the SeaWiFS (1998-2002) are also plotted ..... 39

**Figure 2.9.** Top row: Ratios of monthly composite SeaWiFS data for November 2003 derived by two atmospheric correction algorithms. The standard algorithm products are

divided by those using a CZCS-like atmospheric correction algorithm (see text). Bottom row are the SeaWiFS-to-CZCS long-term means presented for comparison. (a)  $L_w(443)$ , (b)  $L_w(555)$  and (c) chlorophyll ..... 41

**Figure 2.10.** Histograms of the ratios shown in figure 2.9. .... 42

**Figure 3.1.** The profiles of (a) temperature (solid line) and salinity (dashed line), (b) primary production (solid line) and chlorophyll (dashed line), and (c) primary production divided by chlorophyll at a well-mixed area (126.0°E and 36.0°N; top figures) and at a stratified area (124.0°E and 36.0°E; bottom figures) in October, 1992. The data were obtained from Choi *et al.* (1995) ..... 62

**Figure 3.2.** Study area and station maps with the bathymetry contours in the Yellow and East China Seas. The filled circles denote the stations observed in the Large Marine Ecosystem (LME) cruise in 14-21 June, 2000 ..... 63

**Figure 3.3.** Distribution of well-mixed areas (filled gray) based on the temperature difference between surface and bottom ( $\Delta T < 0.8^\circ\text{C}$ ) from Moon's model for the 12 months from January to December ..... 64

**Figure 3.4.** Contours of  $\log(H/U^3)$  in (a) June and (b) August in the Yellow and East China Seas. Filled contours denote  $\log(H/U^3) = 1.5, 2.0,$  and  $2.5$  (darker  $\rightarrow$  lighter shades) and the isoline of  $\Delta T = 0.8^\circ\text{C}$  is shown as solid black line ..... 66

**Figure 3.5.** Three-year (1998-2000) averaged monthly sea surface temperature images from MODIS for March to October with the isoline of  $\Delta T = 0.8^\circ\text{C}$  (black line). The scale shows SST in degrees Celsius ( $^\circ\text{C}$ ) ..... 67

**Figure 3.6.** Three-year (1998-2000) averaged monthly 667-nm water-leaving radiance images from MODIS for March to October with the isoline of  $\Delta T = 0.8^\circ\text{C}$  (black line). The scales is nLw667 in units of  $\text{W}\cdot\text{m}^{-2}\cdot\text{nm}^{-1}\cdot\text{sr}^{-1}$  ..... 68

**Figure 3.7.** Contours of *in situ* measured (a) temperature, (b) chlorophyll-a, and (c) suspended sediment at the surface (white lines) in the southeastern Yellow Sea (June 14-21, 2000) superimposed on the monthly SST, chlorophyll-a, and nLw667 images from MODIS in June, 2000. Black line denotes the isoline of  $\Delta T = 0.8^\circ\text{C}$  and red dotted lines are the isolines of  $(H/U^3) = 1.5$  and  $2.0$  ..... 69

**Figure 3.8.** Bin averages of the composite (2000-2002) MODIS nLw667 are plotted against the model  $\Delta T$  with the error bar of one standard deviation in the southeast area of the Yellow Sea ..... 70

**Figure 3.9.** Map of well-mixed areas derived from MODIS nLw667 (gray filled) and isoline of the model  $\Delta T = 0.8^{\circ}\text{C}$  (solid black line) .....

71

**Figure 4.1.** Geography of the study area. The Yellow Sea was divided into 3 sub-regions using bathymetry and physical features (CCW: Chinese Coastal Waters, MYS: Mid-Yellow Sea, and KCW: Korean Coastal Waters) in (b). The serial oceanographic stations of KODC for Secchi depth data are shown in (a) and the observatory stations for primary production of the Yellow Sea cruise in September, 1992 (Choi et al., 1995) are shown in (b) .....

99

**Figure 4.2.** Scatter plots of measured diffuse attenuation derived from PAR in the water column versus measured Secchi depth (SD) at 17 stations in the Yellow Sea. The line of  $K_d = 1.44/\text{SD}$  is also drawn on the scatter plots .....

100

**Figure 4.3.** Secchi depth data obtained in the southeastern Yellow Sea from KODC were plotted against the SeaWiFS K490 in 286 stations during the periods of 1998 to 2002 (match up data is one day before to one day after) .....

101

**Figure 4.4.** Secchi depth data obtained in the southeastern Yellow Sea from KODC were plotted against the SeaWiFS water-leaving radiances at 555nm in 286 stations during the



periods of 1998 to 2002 (match up data is one day before to one day after)  
..... 102

**Figure 4.5.** Scatter plots of temperature and  $P_m^B$  in three different regions (CCW: Chinese Coastal Waters, MYS: Middle of Yellow Sea waters, and KCW: Korean Coastal Waters) in the Yellow Sea ..... 103

**Figure 4.6.** Mean values of  $\alpha^B$  and  $P_m^B$  in three different regions (CCW, MYS, and KCW) in May (left three) and December (right three) with 95% confidence intervals  
..... 104

**Figure 4.7.** Mean fitted biomass (chlorophyll) profiles for the 3 sub-regions of the Yellow Sea in (a) May and (b) September. Number of data used (n) and four parameters of DCM model are shown on each graph ..... 105

**Figure 4.8.** Scatter plots of primary production calculated using a uniform biomass profile (PP1) versus primary production using non-uniform biomass profile (PP2) at 37 stations of the Yellow Sea cruise in September, 1992 (Choi et al, 1995). Squares indicate primary production in deeper area (> 50m) and circles in the shallower areas (< 50m)  
..... 106

**Figure 4.9.** Monthly composite SeaWiFS images from 1998 to 2003 in May (top) and September (bottom) as well as 6-year composite images on the right of each row (a) PAR, (b) diffuse attenuation ( $K_d$ ) derived from nLw555, (c) chlorophyll derived from Ahn's algorithm ..... 107

**Figure 4.10.** Monthly-composite images of primary production based on SeaWiFS from 1998 to 2003 in May (top) and September (bottom) as well as 6-year composite images on the right of each row ..... 110

**Figure 4.11.** Year-to-year variations of the mean values of the SeaWiFS input values in the 3 sub-regions in May (top) and September (bottom). (a) PAR, (b) diffuse attenuation ( $K_d$ ) derived from nLw555, (c) chlorophyll derived from Ahn's algorithm, and (d) daily integrated primary production ..... 111

**Figure 4.12.** The values extracted from the monthly primary production images in 1998 to 2003 compared with the measured primary production at 37 stations of the Yellow Sea cruise in September, 1992 (Choi et al. 1995) ..... 115

**Figure 4.13.** Annual results based on the SeaWiFS from 1998 to 2002: (a) total primary production (unit is  $10^5 \text{ mgC m}^{-2} \text{ yr}^{-1}$ ), and composite images of (b) PAR, (c)  $K_d$ , and (d) chlorophyll from Ahn's algorithm ..... 116

# **ABSTRACT**

## **INTER-ANNUAL AND DECADEAL VARIATION IN THE PELAGIC MARINE ECOSYSTEM OF THE YELLOW AND EAST CHINA SEAS**

by

**Seung-Hyun Son**

**University of New Hampshire, December, 2004**

The water-leaving radiance measurements and chlorophyll concentrations of the Coastal Zone Color Scanner (CZCS) and the Sea-viewing Wide Field-of-view Sensor (SeaWiFS) were compared to investigate decadal trends in the Yellow and East China Seas (YECS). A unified bio-optical algorithm was derived to convert CZCS pigments to SeaWiFS chlorophyll concentrations. The conversion is applied to level-2 CZCS data. High increase of the water-leaving radiances at 443 and 555 nm and chlorophyll was shown in the area. There were increasing trends in temperature and zooplankton biomass, and decreasing trends in salinity and Secchi depth. However, in comparing CZCS with SeaWiFS data, no attempt was made to unify the atmospheric correction algorithms. Thus, it is likely that differences in the atmospheric correction between the ocean color sensors might account for the difference of water-leaving radiance at 443 nm.

We established monthly variations in the stratified and well-mixed areas using a coupled ocean wave-circulation model and the ocean color satellite data for estimating primary productivity in the Yellow Sea using satellite observations. The model results were compared with remotely sensed sea surface temperature and water-leaving radiance at 667nm derived from the Moderate Resolution Imaging Spectroradiometer (MODIS) to develop a method to differentiate stratified and well-mixed waters using remote sensing data. Maps of the well-mixed area were derived from MODIS nLw667 using the relationship between the nLw667 and the model  $\Delta T$  in the southeastern Yellow Sea for the warmer months. The well-mixed areas were located where nLw667 is higher than 2–4  $W \cdot m^{-2} \cdot nm^{-1} \cdot sr^{-1}$  depending on the month. These results provide the basis for modeling vertical biomass profiles in estimating primary production using satellite data in the Yellow Sea.

We used and modified an existing primary productivity algorithm to estimate phytoplankton primary production using satellite data in the Yellow Sea. The Yellow Sea was first partitioned into three subregions based on the bathymetry and physical features to parameterize the algorithm. A local empirical chlorophyll algorithm was applied to derive more accurate chlorophyll concentration in the Yellow Sea and an approach was presented for estimating the diffuse attenuation coefficient. We investigated whether it was necessary to model the vertical biomass profile. Finally, the algorithm was applied to derive the primary production in the Yellow Sea. The primary production derived using the local algorithm was higher in the middle of the Yellow Sea in May and September than in the shallower (<50 m) coastal areas. The low primary

production in the coastal areas is caused by high turbidity due to strong tides and shallow depths. Lower turbidity in the middle of the Yellow Sea allows the light energy for primary production to penetrate to a deeper depth. Our computation of daily total primary production for the entire the Yellow Sea is  $19.7 \times 10^4$  tonC d<sup>-1</sup> in May and  $15.8 \times 10^4$  tonC d<sup>-1</sup> in September, and the annual total primary production in the Yellow Sea was  $50.1 \times 10^6$  ton C yr<sup>-1</sup>. The resulting maps of primary production calculated from the remotely sensed data provide the first synoptic views of primary production in the Yellow Sea.

# CHAPTER 1

## INTRODUCTION, BACKGROUND AND SCIENCE OBJECTIVES

### 1.1. Introduction

The main goal of this research is to characterize and understand contemporary and long-term variations in the marine ecosystem of the Yellow Sea. The proposed research on the Yellow Sea has importance in two aspects: (i) Fishery in the Yellow Sea is one of the major food resources to adjacent countries. It has been reported that the overall biomass of fisheries has decreased considerably for the last 30 years (KORDI, 1998). Specifically, it appears rather clear that catch per unit effort in 1990s declined significantly compared to the 1970s. (ii) The Changjiang River influences the phytoplankton production and fisheries in the Yellow Sea. Variation in the discharge from the Changjiang River could be one of the main reasons for the ecological shift. In particular, the Three Gorges dam, which is being constructed in the Changjiang River, will be an issue for changes of the marine ecosystem.

First, a time series of ocean color remote sensing and in situ ecological variables is constructed. The next step for this study is to establish the stratified and well-mixed areas associated with monthly variations to examine the non-uniformity for the estimation of primary production using remote sensing data in this coastal water. Finally, a primary production model is applied to the Yellow Sea and a local primary production algorithm is developed for the Yellow Sea. This proposed study will help to understand

phytoplankton production in the coastal waters, in general, more quantitatively as well as to address long-term variations of the ecosystem and effects of climate change in the Yellow Sea.

## **1.2. Background**

The coastal zone, in which 60% of the human population lives, is very important in the human life and activities (Pernetta and Milliman, 1995). Coastal waters play an important role as food resource. While the coastal ocean occupies 8% of the ocean surface, about 90% of world commercial fish is caught in coastal waters. It is reported that coastal primary production contributes 14~25% of the global oceanic primary production (Longhurst, et al., 1995; Pernetta and Milliman, 1995). Coastal areas are affected through riverine discharge and changes due to land-use and other activities. Coastal waters are also easily affected by internal and external forcing, and the properties change on short time scales. Periodic tidal forcing causes vertical mixing in shallow areas which causes re-suspension and the interactions with bottom organisms. The biomass profile in the tidally well-mixed area can be assumed as vertically uniform while there is a deep chlorophyll maximum in the stratified area. The area vertically well-mixed due to tidal force has importance on phytoplankton growth and distribution. In addition, light limitation due to high turbidity caused by tidal mixing can inhibit primary production. It has been reported that light transparency is most important factor on primary production in the tidal mixing area of the Yellow Sea (Kang, et al., 1992; Choi,

1991; Choi, et al., 1995; Yoo and Shin, 1995). Thus, it is important to identify well-mixed and stratified regions for estimation of primary production using the ocean color satellite data.

Simpson and Hunter (1974) proposed a criterion to differentiate tidally well-mixed from stratified waters based on  $\log(H/U^3)$ , where  $H$  is the water depth and  $U$  is the depth-mean velocity of the tidal current. The threshold value of  $\log(H/U^3)$  less than 2 was used for vertically well-mixed areas and the value greater than 2 for stratified areas. In order to establish the magnitude of the productivity associated with the well-mixed regions in the Gulf of Maine, Yentsch and Garfield (1981) differentiated mixed and stratified waters in the Gulf of Maine using the criterion proposed by Simpson and Hunter (1974). They compared maps of  $\log(H/U^3)$  with infrared satellite imagery and found a good correspondence of well-mixed areas with cooler nearshore areas. Others have compared satellite infrared imagery and/or ship-measured temperature with this criterion in other regions (Pingree and Griffiths, 1978; Garrett et al. 1978; Bowman and Esaias, 1981; Baines and Fandry, 1983; Lie, 1989).

Another criterion for well-mixed areas can be based on top-to-bottom temperature differences. Mixed layer depth (MLD) is generally defined as the depth where the temperature differs by  $0.5^{\circ}\text{C}$  from the sea surface temperature (Obata et al., 1996; Monterey and Levitus, 1997). More recently, Kara et al. (2000) presented the "optimal" definition of MLD as the depth at the temperature difference of  $0.8^{\circ}\text{C}$ . In this work, we will regard waters as vertically well mixed if the temperature difference between surface and bottom ( $\Delta T$ ) is less than  $0.8^{\circ}\text{C}$ .



An important contribution of ocean color remote sensing, which can overcome the temporal and spatial limitation in ship measurements (Smith, et al., 1982; Robinson, 1985), is to understand primary productivity of the ocean. Ocean color remote sensing is now the only means to determine the basin to global scale phytoplankton abundance. Phytoplankton abundance is routinely derived from the satellite in the open ocean waters, so-called "Case 1 waters" whose optical properties are affected by the phytoplankton cells or their decay products (Morel and Prieur, 1977). However, optical properties in coastal waters are affected by non-algal materials such as suspended sediments as well as by phytoplankton pigment. These waters are called as "Case 2 waters." These properties make it difficult to estimate phytoplankton biomass and primary productivity using the ocean color remote sensing in coastal waters. The Yellow Sea is a marginal sea and primarily Case 2 water although the middle area of the Yellow Sea in summer is characterized as Case 1 water (Yoo and Park, 1998). The Yellow Sea is affected by strong tidal currents and the discharge of fresh water from the Changjiang (Yangtze) River which is the largest river in Asia (annual mean inflow of  $28,900 \text{ m}^3 \text{ s}^{-1}$ ; freshwater discharge of  $9.24 \times 10^{11} \text{ m}^3 \text{ y}^{-1}$ ; solid discharge of  $4.86 \times 10^8 \text{ tons y}^{-1}$ ). The Kuroshio Current which is characterized by comparatively high temperature and salinity also influences the southeastern area of the Yellow Sea.

Previous studies of primary productivity in the Yellow Sea have been temporally and spatially limited. Choi et al. (1988) showed that high productivity in the western coastal waters of Korea maintains the high abundance of zooplankton and fish larvae in summer. Kang et al. (1992) estimated that primary productivity along the mid-eastern

coast of Korea varied from 37 to 1104  $\text{mgC}\cdot\text{m}^{-2}\cdot\text{d}^{-1}$  and the assimilation numbers (primary production per unit chlorophyll-a at saturated light) varied from 1.13 to 24.28  $\text{mgC}\cdot(\text{mg}\cdot\text{chl-a})^{-1}\cdot\text{hr}^{-1}$ . In another study of the nearshore region (Chunsoo Bay) of the mid-eastern Yellow Sea, Yoo and Shin (1995) estimated primary productivity ranged from 28 to 197  $\text{mgC}\cdot\text{m}^{-2}\cdot\text{d}^{-1}$  in January, and increased to 1324  $\text{mgC}\cdot\text{m}^{-2}\cdot\text{d}^{-1}$  in July.

Studies describing the distribution of chlorophyll and primary productivity over all the Yellow Sea are also in the literature (Choi *et al.* 1995; Wu *et al.* 1995). Choi *et al.* (1995) measured primary productivity using C-14 methods and estimated depth-integrated primary production with the formula of Platt *et al.* (1980). According to their work, primary production varied from 147 to 2694 (mean of 740)  $\text{mgC}\cdot\text{m}^{-2}\cdot\text{d}^{-1}$  in September, 1992, in the Yellow Sea. Wu *et al.* (1995) also measured primary production using C-14 method in September 1992, but used Cadee and Hegeman's (1974) formula to estimate primary production which ranged from 65 to 927 (mean of 331)  $\text{mgC}\cdot\text{m}^{-2}\cdot\text{d}^{-1}$ . The large differences between these primary production values may be because they used different methods to estimate primary production. In addition, they found very different chlorophyll levels (0.16 to 3.20  $\mu\text{g}\cdot\text{l}^{-1}$  with mean of 0.69  $\mu\text{g}\cdot\text{l}^{-1}$  – Choi *et al.*; 0.43 to 17.43  $\text{mg}\cdot\text{m}^{-3}$  with mean of 1.362  $\text{mg}\cdot\text{m}^{-3}$  – Wu *et al.*), which were curiously opposite in magnitude to the primary productivity differences.

There have been several attempts to investigate the seasonal and temporal distribution of chlorophyll using Coastal Zone Color Scanner (CZCS) data in the Yellow and East China Seas. Ning *et al.* (1998) used the full 7.5-year CZCS level-3 data set generated by the NASA Goddard Space Flight Center (GSFC) (Feldman *et al.*, 1989). In

that study, high values of surface pigment ( $> 5 \text{ mg}\cdot\text{m}^{-3}$ ) occurred in the western coastal areas of Korea and the Changjiang River front. In the central part of the Yellow Sea, CZCS pigment values were lower than those in the other areas in most months. The CZCS level-3 data set on CD-ROM published by the NASA GSFC and the Jet Propulsion Laboratory (JPL) was used by Wang et al. (1998) to study phytoplankton variation in the East China Sea. They also reported high pigment concentration around the Changjiang River. The satellite chlorophyll concentrations used in both of these studies were over-estimated because the chlorophyll algorithms do not consider the effects of non-chlorophyll materials in Case 2 waters. Improved ocean color remote sensing algorithms must account for optically active materials other than chlorophyll to estimate chlorophyll concentration more quantitatively. A local empirical algorithm of chlorophyll-a concentration for the Yellow Sea was developed using measured remote sensing reflectance and measured chlorophyll concentrations by Ahn (2004).

Some studies have suggested that there are indications of climate change in Korean waters. Kim and Yoo (1996) reported evidence that temperature increased in the mid-1970s and fisheries resources responded to the temperature changes. There were significant increases in zooplankton biomass within the last two decades in the Yellow Sea (Kang, 1998; Son et al., 2000), in the East/Japan Sea (Kim et al., 1998; Zhang et al., 2000), and along the southern coast of Korea (Kim and Kang, 2000). Variations of fisheries biomass corresponding to climate change have also been reported during the last several decades. Reports indicate a decreased biomass of saury and increased biomass of sardine following the 1976 regime shift in the North Pacific (Zhang et al., 2000; Kang et

al., 2000) and an increase in the catch of anchovy and mackerel along the southern coast of Korea (Kim and Kang, 2000). These authors also studied the correlation between environmental variations and the chlorophyll concentration derived from water transparency (Secchi depth) in Korean waters. Ocean color remote sensing data now available provide a better means of understanding the long-term variations in primary production and phytoplankton biomass, and their relationship to environmental variables.

### **1.3. Science Objectives**

The goal of this study is to characterize and understand inter-annual and decadal variation in the pelagic marine ecosystem of the Yellow and East China Seas using satellite ocean color data. In order to address this goal, three specific objectives were undertaken as follows:

- (1) Create a multi-decadal time series of ocean color remote sensing and *in situ* ecological variables to provide the observational basis for understanding and predicting changes in marine ecosystems and biogeochemical cycles.
- (2) Develop a method to differentiate stratified and well-mixed areas for the estimation of primary production using remote sensing data in coastal waters.
- (3) Develop a local primary production algorithm to produce quantitative maps of satellite derived primary production in the Yellow Sea.

This dissertation presents three chapters that address these objectives. The dissertation is presented in the context of three self-contained papers, chapters 2-4, with each chapter addressing one of the objectives stated above. Thus, each chapter contains its own abstract, methods, results, discussion, and conclusions sections. Some overlap and redundancy among the chapters is expected because of this format of the dissertation.

Objective (1) is addressed in Chapter 2, entitled “Decadal variability in the Yellow and East China Seas as revealed by satellite ocean color data (1979-2003).” In this chapter, we constructed satellite time series of water-leaving radiance and chlorophyll concentration as well as time series of the existing long-term temperature, salinity, zooplankton, and water transparency data in the Yellow Sea. The results showed changes in satellite-derived optical properties during the past two decades in the Yellow Sea as well as increasing trends in temperature and zooplankton biomass, and decreasing trends in salinity and transparency. Some of the results in this chapter were presented at the 5<sup>th</sup> Pacific Ocean Remote Sensing Conference in Goa, India, in 2000, and later at the Joint Global Ocean Flux Study (JGOFS) Ocean Science Conference in Washington D.C. in 2003.

Chapter 3, entitled “Classification of well-mixed and stratified waters in the Yellow Sea,” focuses on objective (2). In this chapter, we established monthly variations in the stratified and well-mixed areas using the criterion of the temperature difference between bottom and surface. Temperatures were based on a model (Moon 2004). We addressed a method to differentiate stratified and well-mixed areas for estimating primary

productivity in the Yellow Sea using satellite observations. The results in this chapter were originally presented at the Ocean Optics XVI conference in Santa Fe, USA, in 2002.

Objective (3) was addressed in Chapter 4 under the title “Primary production by the ocean color remote sensing in the Yellow Sea.” In this chapter, we used and modified an existing primary productivity algorithm to estimate phytoplankton primary production in the Yellow Sea. Maps of primary production calculated from the remotely sensed data with the productivity algorithm provide the first synoptic views of primary production in the Yellow Sea.

In Chapter 5, we provide a brief summary of the thesis with the focus on the significance of the thesis, and propose further work.

## Chapter 2

### Decadal Variability in the Yellow and East China Seas as Revealed by Satellite Ocean Color Data (1979-2003)

(To be submitted to *Remote Sensing of Environment* by Seung-Hyun Son, Janet  
Campbell, Mark Dowell, and Sinjae Yoo)

#### ABSTRACT

Satellite ocean color data from the Coastal Zone Color Scanner (CZCS) and the Sea-viewing Wide Field-of-view Sensor (SeaWiFS) are examined to investigate decadal trends in the Yellow and East China Seas (YECS). Our goal is to determine whether there have been changes in chlorophyll concentration and suspended sediment as indicated by changes in satellite-derived optical properties during the past two decades. We compare water-leaving radiance measurements at 443 nm and 555 nm,<sup>1</sup> and discuss possible reasons for the changes observed (whether they are artifacts of the different sensors and algorithms or real changes in the water properties). We examine changes in the chlorophyll concentration that would be inferred from case-1 water algorithms if the water-leaving radiances are comparable and accurate. The CZCS pigment data were converted to chlorophyll concentration using an algorithm derived from *in situ* data to be comparable to the SeaWiFS chlorophyll derived by the OC4 algorithm (O'Reilly et al. 2000).

---

<sup>1</sup> The CZCS band is centered at 550 nm, but we consider this comparable to the SeaWiFS 555-nm band.

The shallow coastal areas of the YECS exhibited high water-leaving radiance in the 555-nm band ( $L_w555$ ) during both time periods, indicating that these waters are sediment-dominated case-2 waters. Between the CZCS era (1978-1984) and the SeaWiFS era (1998-2002),  $L_w443$  increased in these areas by 17%–61%, and  $L_w555$  increased by 67-108%. In the deeper waters that are considered case-1 during summer,  $L_w443$  decreased by 25%–31%, which would indicate an increase in absorbing materials such as chlorophyll and colored dissolved organic matter (CDOM). Between the CZCS and SeaWiFS eras, the average chlorophyll concentration (based on case-1 algorithms) increased by 15-60% in these offshore deep waters.

For comparison with the trends found in satellite data, we examined *in situ* data from 61 stations located off the western coast of Korea that had been sampled six times per year between 1978 and 2002. These measurements, made by the Korean National Fisheries Research and Development Institute, include temperature, salinity, Secchi depth, and zooplankton biomass. Between 1978 and 2002, there were increasing trends in temperature and zooplankton biomass, and decreasing trends in salinity and Secchi depth. The satellite data surrounding these stations showed an increase in  $L_w555$  (49 %), a decrease in the  $L_w443$  (-12 %), and an increase in chlorophyll (46 %).

No attempt was made to unify the atmospheric correction algorithms for the CZCS and SeaWiFS data. We evaluated the consequences of the differences for a limited period (November 2003) and concluded that differences in the atmospheric correction between the ocean color sensors might account for the differences we found in the water-leaving radiances.



## 2.1. INTRODUCTION

Recent climatic oscillations, such as El Nino and La Nina, have drawn attention to the effects of climate change on marine ecosystems (Wallace and Vogel, 1994). The regime shift during 1977-1978 reported in the Northern Pacific Ocean (Trenberth and Hurrell, 1994), which caused changes in phytoplankton, zooplankton, and fish production (Polovina et al., 1994, 1995; Beamishi and Bouillon, 1993; McFarlane and Beamish, 1992; Sugimoto and Tadokoro, 1997, 1998), is an example of ecological change brought about by climate change. In Korean waters, Kim and Yoo (1996) reported evidence that fisheries changed in the mid-1970s in association with increasing temperatures, and there have been other reports of climate shifts in Korean waters using zooplankton and fishery data (Kang, 1998; Kang et al., 2000; Kim and Kang, 2000; Kim et al., 1998; Park et al., 1998; Zhang et al., 2000). Significant increases in zooplankton biomass during the past two decades have been observed in the East/Japan Sea (Kim et al., 1998; Zhang et al., 2000), off the southern coast of Korea (Kim and Kang, 2000), and in the Yellow Sea (Kang, 1998). There was an apparent regime shift in Korean waters in 1976 at which time saury decreased and sardine biomass increased (Zhang et al., 2000; Kang et al., 2000); anchovy, mackerel, and sardine catches increased along the southern coast of Korea (Kim and Kang, 2000); and the catch of squid increased in Korean waters (Park et al., 1998).

The National Aeronautics and Space Administration (NASA) launched the first ocean color satellite sensor, the Coastal Zone Color Scanner (CZCS), in October, 1978. The CZCS collected ocean color data from November 1978 to June 1986. Following an 11-year gap, the Sea-viewing Wide Field-of-view Sensor (SeaWiFS) was launched in

August, 1997, and continues to provide ocean color data in 2004. To the extent that the data from these two ocean-color sensors can be compared, valuable information may be derived to understand decadal-scale variations in ocean ecosystems. However, a number of problems must be overcome before comparing data from these sensors. Among these are differences in sensor calibrations, atmospheric correction techniques, and the use of different bio-optical algorithms.

In this paper, we focus on the Yellow and the East China Seas (YECS) with the objective of comparing data from the CZCS and SeaWiFS satellite missions to determine whether there have been decadal trends in this region. The CZCS data provide a climatology of the bio-optical properties and phytoplankton pigment distributions during the period 1979-86, whereas the SeaWiFS data provide a contemporary picture of the same area. Our long-range goal is to create a multi-decadal global ocean biology time series to provide the observational basis for understanding and predicting changes in marine ecosystems and biogeochemical cycles.

We compare water-leaving radiances derived from the CZCS and SeaWiFS data in two bands, the 443-nm band centered at the chlorophyll-a absorption peak, and the 555-nm (or 550-nm) band. These measurements are the result of applying atmospheric-correction algorithms to the top-of-atmosphere radiances. Different atmospheric-correction techniques have been applied, but we did not correct for these differences. We simply offer the results here for speculation as to whether trends may be real or artifacts of sensor and algorithm differences, and later discuss possible reasons for the trends that are found.

We also compare chlorophyll concentrations derived from the two sensors, but in this case, we have attempted to adjust for differences in the bio-optical algorithms. The algorithm applied to the SeaWiFS data was the OC4 algorithm (O'Reilly et al. 2000a). It was not possible to apply this algorithm directly to CZCS data because CZCS lacked several spectral bands needed for the OC4 algorithm. Instead, pigment concentrations were derived according to the standard CZCS algorithm (Gordon et al. 1983), and then converted to chlorophyll concentration using a relationship derived from the SeaWiFS Bio-optical Algorithm Mini-Workshop (SeaBAM) data (O'Reilly et al. 1998). This conversion yields a chlorophyll concentration comparable to that derived from the OC4 algorithm.

We recognize that large areas of the YECS are case-2 waters, and thus the satellite retrievals do not give accurate chlorophyll concentrations in those areas. More realistically, the satellite-derived chlorophyll is a measure of the concentration of absorbing materials that include organic detritus and colored dissolved organic matter, as well as phytoplankton pigments. We present comparisons that suggest the possibility of decadal-scale changes in the water quality and productivity of the YECS ecosystem, but further studies will be needed to determine the nature of these changes, and whether they are real or artifacts of the differences in sensors and algorithms.

## **2.2. DATA and METHODS**

### ***2.2.1. Satellite data***

The CZCS level-0 data for the period (1978 - 1986) and all available SeaWiFS level-1a version-4 data for the Yellow and East China Seas were obtained from the NASA Goddard Space Flight Center (GSFC). Because of large gaps in the CZCS data after 1984, only the CZCS data from 1979 to 1984 were processed. The SeaWiFS data from 1998 to 2003 were processed. The data were processed from level 0 to level 2 and remapped using the SeaWiFS Data Analysis System (SeaDAS) software obtained from NASA GSFC. The standard algorithms in SeaDAS were used for the CZCS and SeaWiFS atmospheric corrections. The standard CZCS pigment algorithm and the SeaWiFS OC4 algorithm were also applied. Then a conversion algorithm was applied to the CZCS pigments to obtain a CZCS chlorophyll concentration comparable to the SeaWiFS chlorophyll concentration. Details of this conversion algorithm are described below.

Monthly composites were obtained by averaging all data within each month, and then annual composites of CZCS data from 1979 to 1984, and SeaWiFS data from 1998 to 2003 were derived by averaging the monthly composites. Finally, long-term means were derived by averaging all yearly composites during each period. The YECS was divided into seven subregions based on bathymetric contours as shown in figure 2.1, and the mean and standard deviation of the long-term composited data were calculated within each subregion for the purpose of describing apparent changes that occurred over the two decades. The Bohai Sea (BS) was defined as a subregion distinct from the Yellow Sea. This shallow sea (depths < 50 m) is affected by the Yellow River discharge. The Yellow

Sea was divided into three sub-regions: the western and eastern coastal regions shallower than 50 meters, and the middle Yellow Sea (MYS) deeper than 50 meters. The MYS stratifies in summer and is considered case-1 water at that time. The East China Sea was also divided into 3 sub-regions: the highly turbid, western coastal region shallower than 50 m, that is affected by the Changjiang (Yangtze) River discharge and tidal mixing; the middle of the East China Sea between 50 and 100 meters depth, that is also affected by the buoyant Changjiang River plume, and the eastern subregion deeper than 100 meters characterized as clear waters and influenced by the warm and saline Kuroshio current.

### ***2.2.2. Converting CZCS pigment to chlorophyll concentration***

We consider the OC4.V4 chlorophyll algorithm (O'Reilly et al., 2000) used by the SeaWiFS Project to be the standard algorithm for chlorophyll. It gives chlorophyll by the formula:

$$\log_{10}(\text{CHL}) = a_0 + a_1 \cdot X + a_2 \cdot X^2 + a_3 \cdot X^3 + a_4 \cdot X^4 \quad (1)$$

where  $X = \log_{10}(\max[R_{rs}(443), R_{rs}(490), R_{rs}(510)]/R_{rs}(555))$  and  $\mathbf{a} = [0.366, -3.067, 1.930, 0.649, -1.532]$ .

The standard pigment algorithm applied to CZCS data (Gordon et al. 1983) was:

$$\log_{10}(\text{PIG}) = a_0 + a_1 \cdot X \quad (2)$$

where  $X = \log_{10}(L_w 443/L_w 550)$  and  $\mathbf{a} = [1.130, -1.705]$  if the value of PIG  $\leq 1.5$ ;

otherwise,  $X = \log_{10}(L_w 520/L_w 550)$  and  $\mathbf{a} = [3.327, -2.44]$ . Note that this algorithm created a discontinuity at PIG = 1.5 mg m<sup>-3</sup>.

To account for differences in the CZCS pigment and SeaWiFS chlorophyll algorithms, we used the original SeaBAM data (O'Reilly et al. 1998). This data set

consists of remote sensing reflectance,  $R_{rs}(\lambda)$ , at wavelengths = 412, 443, 490, 510, 520, 555 and 565 nm, and surface chlorophyll-a concentration (CHL) measurements at 919 stations widely distributed geographically. Our objective was to apply both algorithms to this data set, and then determine a set of equations to convert PIG to CHL. Most of the stations had either the 510-nm band used by the OC4 algorithm, or the 520-nm band used by the CZCS algorithm. We eliminated stations that did not have a measured reflectance at 510 nm, thus reducing the number of stations to  $n = 539$ . To obtain  $R_{rs}(520)$ , corresponding to the CZCS band, we used the relationship:

$$R_{rs}(520) = R_{rs}(510) / [a_0 + a_1 \cdot X^1 + a_2 \cdot X^2 + a_3 \cdot X^3 + a_4 \cdot X^4] \quad (3)$$

where  $\mathbf{a} = [1.0605321, -0.1721619, 0.0295192, 0.0150622, -0.004133924]$  and  $X = \log_{10}(\text{CHL})$ . This is based on the model of Morel and Maritorena (2001) as reported by O'Reilly et al. (2000). The above-water  $R_{rs}(\lambda)$  values were multiplied by the extraterrestrial solar irradiance for each band to obtain the normalized water-leaving radiances,  $L_w(\lambda)$ . We assumed that the 555-nm band was equivalent to the 550-nm band of CZCS. Using the  $L_w(\lambda)$  values for  $\lambda = 443, 520$  and  $555$ , we calculated the CZCS pigment (PIG) according to the standard algorithm (Gordon et al., 1983) given by equation 2, and using the  $R_{rs}(\lambda)$  values for the SeaWiFS bands, we calculated chlorophyll (CHL) by the OC4.V4 algorithm (O'Reilly et al., 2000) (equation 2).

Results of plotting CHL vs. PIG are shown in figure 2.2. A discontinuity occurs when the CZCS algorithm switches from the 443:550 ratio to the 520:555 ratio (PIG =  $1.5 \text{ mg m}^{-3}$ ). At pigment values less than about  $0.12 \text{ mg m}^{-3}$ , there is a deterministic relationship because both algorithms use the 443:550 ratio. The greatest scatter occurs where pigment is between  $0.12$  and  $1.5 \text{ mg m}^{-3}$ . In this range, PIG is based on the

443:550 radiance ratio whereas CHL is based on the 490:555 ratio. At pigment levels above  $1.5 \text{ mg m}^{-3}$  (the switching point), the OC4 algorithm is probably using the 510:555 ratio, whereas PIG is using the 520:550 ratio. The scatter in this range is due to the differences between 510 and 520 nm. Also shown on figure 2.2 (dashed line) is the relationship between PIG and CHL recommended by O'Reilly et al. (1998), that was subsequently used by Conkright and Gregg (2003) for blending CZCS and *in situ* data (see discussion).

For  $\text{PIG} < 1.5 \text{ mg m}^{-3}$ , and  $\text{PIG} > 5 \text{ mg m}^{-3}$ , the OC4-derived chlorophyll exceeds the CZCS pigment (despite the conventional view that pigment includes more than just chlorophyll, a view that is reflected in the O'Reilly relationship). However, pigment values in the Yellow Sea region generally fall within the range 1.5 to  $5.0 \text{ mg m}^{-3}$  where pigment exceeds the OC4 chlorophyll. From these results, we derived formulae for converting level-2 CZCS pigments to obtain a chlorophyll concentration analogous to the OC4-derived SeaWiFS chlorophyll. The lines drawn on figure 2.2 are the formulae:

$$\log_{10} \text{CHL} = -0.1813X^4 - 0.1043X^3 + 0.6769X^2 + 1.7495X + 0.3007 \quad \text{PIG} < 0.112$$

$$\log_{10} \text{CHL} = 0.2311X^2 + 1.1916X + 0.1150 \quad 0.112 < \text{PIG} < 1.5$$

$$\log_{10} \text{CHL} = 0.2165X^2 + 1.5233X - 0.5104 \quad \text{PIG} > 1.5$$

where  $X = \log_{10}(\text{PIG})$ , and CHL is the SeaWiFS-compatible (OC4) chlorophyll concentration which we call the "CZCS chlorophyll."

### **2.2.3. *in situ* data**

For comparison with trends found in the satellite data, we examined temperature, salinity, transparency, and zooplankton data provided by the Korea Oceanographic Data Center (KODC). The serial oceanographic observations are carried out bimonthly (February, April, June, August, October, and December) in Korean waters by the National Fisheries Research and Development Institute (NFRDI). The data for 61 stations in the Yellow Sea from 1978 to 2002 were processed (Fig. 2.1).

Zooplankton data were available only from 1978 to 2000 and include the biomass of copepoda, caetognatha, euphausia, and amphipoda within the water column. Zooplankton samples were collected with NORPAC net with 0.33 mm mesh size and a 45 cm mouth diameter. The net was towed vertically from the bottom to the surface at a speed of 0.5 – 1.0 ms<sup>-1</sup>. Each sample was fixed in 5% formalin and the volume of zooplankton biomass (mg m<sup>-3</sup>) was measured excluding particles larger than 2 cm.

The surface temperature and salinity measurements, Secchi depth, and zooplankton biomass data at the 61 KODC stations were averaged within each year. In addition, the chlorophyll, Lw443, and Lw555 values were extracted within 3 × 3 pixel boxes around the 61 KODC stations from the yearly composited CZCS and SeaWiFS data.

## **2.3. RESULTS**

Individual yearly composites of CZCS data for 1979-1984 and SeaWiFS data for 1998-2002 are shown in figure 2.3. Between the two eras (or, more specifically, between



the two satellite data sets), 443-nm radiance in the middle of the Yellow Sea decreased while it increased around the Changjiang River, the southwest coast of Korea, and the Shandong Peninsula. Significant increases in 555nm radiance are seen in nearly all locations within the YECS. Likewise, chlorophyll increased nearly everywhere but the apparent increases in the shallow case-2 waters may be due to changes in other material loadings. The greater interannual variation exhibited by the CZCS data is probably due to its limited coverage.

Long-term composites of CZCS for 1979-1984 and SeaWiFS for 1998-2003 are shown in figures 2.4-2.6, and the ratios of SeaWiFS-to-CZCS long-term means are shown in figure 2.7. In terms of 443nm radiance (fig. 2.4), the spatial distribution in the CZCS image is more uniform than that of the SeaWiFS composite image. Compared with the CZCS data, the SeaWiFS  $L_w443$  values have decreased in the central Yellow Sea, but increased around the Changjiang River, along the western coast of Korea, and in the Bohai Sea. The spatial patterns of  $L_w550$  and  $L_w555$  are similar (fig. 2.5), with high values along the coastal regions and near the Changjiang River. However,  $L_w555$  of the SeaWiFS is much higher around the Changjiang River, off the western coast of Korea, and in the Bohai Sea, and has a wider range between the coastal highs and oceanic lows. The  $L_w555$  and  $L_w550$  values are almost the same, however, in the Sea of Japan/East Sea and eastern portions of the East China Sea.

The spatial pattern of chlorophyll (fig. 2.6) is similar in both data sets, with higher concentrations in coastal areas and near the Changjiang River, and relatively low values in the central area of the Yellow Sea. The higher chlorophyll concentrations near shore, especially in the western East China Sea and the Bohai Sea, are likely due to resuspended

sediments and colored dissolved organic matter. The chlorophyll concentration of SeaWiFS is overall higher than that of CZCS, especially in the area near the Changjiang River, whereas there are slight decreases in the Bohai Sea and the mid-west coastal regions of Korea. Two patches of significantly increased chlorophyll ( $\sim 3\times$  higher) appear in the Yellow Sea in figure 2.7. The more southerly patch is located around a Korean dump site where dumping has been occurring since 1992. The northerly one, located in North Korean waters, may be the location of another dump site, but this is unknown to the authors.

The means and standard deviations of these variables for the seven sub-regions are listed in Table 1. There were increases of 443 nm radiance in the year-round turbid waters of the Bohai Sea (57%), the west coast of the Yellow Sea (32%), the east coast of the Yellow Sea (17%), and the west-East China Sea (61%). Decreases of 443 nm radiance occurred in the middle of the Yellow Sea (-31%) and the east-East China Sea (-25%), both areas that can be considered as having case-1 waters at least part of the year. There were dramatic increases in water-leaving radiance at 555 nm for the very turbid shallow regions, the Bohai Sea (92%), west and east margins of the Yellow Sea (68% and 67%), and the west-East China Sea (108%). There was a smaller increase of 555 nm radiance in the middle of the Yellow Sea (28%), and a decrease in the eastern East China Sea (-5%).

The chlorophyll concentration increased over the entire study area. The greatest increase was in the middle of the Yellow Sea (60%), where the chlorophyll algorithm is more likely to be accurate than in turbid coastal (case-2) waters. The smallest increase (5%) was found in very turbid areas (the Bohai Sea and east coast of the Yellow Sea).

The clearest waters in the region were found in the eastern East China Sea where chlorophyll increased by 15 %.

Unfortunately, there are no *in situ* measurements of optical properties or chlorophyll for the CZCS era that can be used to verify the changes seen in the satellite data. However, we were able to examine long-term monitoring data on temperature, salinity, and Secchi depth for the period 1978 - 2002, and zooplankton biomass for 1978 - 1996 (fig. 2.8). Also shown in this figure are the yearly average chlorophyll, L<sub>w</sub>443, and L<sub>w</sub>555 values within 3 × 3 pixel boxes that were extracted around the 61 stations. There was an increasing trend in temperature and a decreasing trend in salinity and Secchi depth from 1978 to 2002. Zooplankton biomass showed a clear increasing trend beginning in the late 1980's. Differences between mean values during the CZCS era (1979-1984) and the SeaWiFS era (1998-2002) also reveal changes. The changes between the two satellite eras were: +0.63°C for temperature, -0.57 psu for salinity, and -0.48 m for Secchi depth, while there were increases in the mean chlorophyll (46%) and L<sub>w</sub>555 (49%), and a decrease in L<sub>w</sub>443 (-12%).

## 2.4. DISCUSSION

In the results as presented, we have described differences between the CZCS and SeaWiFS data in terms of changes in the YECS rather than differences in the sensors or algorithms. However, we are fully aware that the apparent changes may be due to differences between the sensors and algorithms. There is probably no way to differentiate

sensor and algorithm differences from true environmental changes. Here we will discuss possible reasons why the normalized water leaving radiances may be different. The changes in chlorophyll concentration are a direct result of differences in water-leaving radiances, since we have eliminated differences due to the bio-optical (chlorophyll vs. pigment) algorithms.

Water-leaving radiances are derived by applying an atmospheric correction to calibrated, top-of-atmosphere (TOA) radiances. Accurate calibration of the sensor is a critical requirement, and inaccurate calibrations are a potential source of differences between CZCS and SeaWiFS. The CZCS calibration was suspected of drifting during its 8-year mission, but there was no means to calibrate the sensor in orbit. Its calibration was adjusted retrospectively by assuming that no real environmental changes had occurred in the global radiance distributions during its lifetime (Evans and Gordon, 1994). The SeaWiFS has collected ocean color data since September 1997, and continues in 2004 to produce global products that are the best examples of climate quality ocean color data currently in existence. The SeaWiFS calibration is monitored regularly both for stability (by viewing the moon periodically) and vicariously whereby atmospherically corrected satellite radiances are compared with *in situ* water-leaving radiances, and adjustments made to the TOA calibration to force agreement.

We do not believe that differences in calibration can explain the differences between the CZCS and SeaWiFS radiances. While there are undoubtedly differences, such differences would be manifest as systematic biases (i.e., one band being systematically high or low everywhere relative to its counterpart on the other sensor).

The most likely sensor-related reason for differences in the water-leaving radiances are differences in the atmospheric corrections.

There are two major differences between the CZCS and SeaWiFS atmospheric correction algorithms. One concerns the aerosol model(s) used and the other concerns the “black pixel assumption” (namely, the assumption that water-leaving radiance is zero in the near-infrared). The CZCS used a single near-infrared band (670 nm), assumed to have zero water-leaving radiance, and a single marine aerosol scattering model which was non-spectral. Continental aerosols tend to scatter more efficiently in the blue region of the spectrum, and thus their contribution to the atmospheric scattering signal would have been underestimated at 443 nm by the CZCS. This would result in an overestimation of Lw443 by the CZCS, and consequent underestimation of chlorophyll. The black-pixel assumption, on the other hand, fails in turbid coastal waters. It certainly was not valid over the Changjiang River plume or in the Bohai Sea. The result of this assumption (by the CZCS) is that the aerosol optical thickness is overestimated, and thus Lw443 and Lw550 would be underestimated.

The SeaWiFS has two near-infrared bands that are used to estimate the aerosol optical thickness as well as to select an aerosol type. Furthermore, it uses an iterative algorithm developed by Siegel et al. (2000) which no longer makes the “black pixel” assumption. Neither sensor corrects for absorbing aerosols, however. Absorbing aerosols, such as the yellow dust often found over the YECS region, have the effect of reducing the atmospheric path radiance. If they are not included in the atmospheric correction, this reduction is attributed to absorbing materials in the water, and thus chlorophyll is overestimated (Lw443 underestimated).

It is entirely possible that the trends seen in the radiances are due to differences between the atmospheric correction algorithms. The most likely reason is the CZCS algorithm's use of the "black pixel" assumption. This could explain why the turbid coastal regions have much lower water-leaving radiances in the CZCS data compared with the SeaWiFS data. As for differences due to the aerosol models used, this is not as likely to be a reason for the decadal trends observed (figs. 2.3-2.5) because the spatial patterns are more oceanic than atmospheric. Continental aerosols, for example, would not be confined to the shallow coastal areas but would extend across the entire region. The prominent Changjiang River river plume is clearly a feature in the water rather than the atmosphere. Its apparent increased turbidity between CZCS and SeaWiFS cannot be explained by differences in aerosol models, whereas it can be explained by the black pixel assumption of CZCS. It might be possible to eliminate this problem by reprocessing the CZCS data using the iterative scheme of Siegel et al. (2000).

To investigate this further, we reprocessed 23 SeaWiFS images for November 2003 from level 1a to level 2 using the "single-scattering white aerosols (CZCS type)" atmospheric correction offered by SeaDAS. All results presented so far were processed using the "multiple-scattering with 765/865 Gordon and Wang model and NIR (SeaWiFS type)" atmospheric correction algorithm. The reprocessed scenes were then remapped and averaged to simulate CZCS-like composite images, and the original November composites were ratioed to the new CZCS-like composites. These are shown in figure 2.9 where they are compared with the ratios of SeaWiFS to CZCS long-term means (from fig. 2.7). There are similarities, particularly in the nLw443 ratios, suggesting that the differences we found between CZCS and SeaWiFS might well be the result of differences

in the atmospheric correction. Histograms of the ratios shown in figure 2.9 and shown in figure 2.10.

Another important caveat that should be mentioned concerns the chlorophyll distributions. Much of the Yellow and East China Seas are case-2 waters throughout the year, and therefore the case-1 algorithms for pigment and chlorophyll are not accurate. Here we were not so much concerned with their accuracy as with the question of whether long-term environmental changes have occurred. If the water-leaving radiances were correct, these results would suggest that absorbing materials (including chlorophyll and CDOM) have increased everywhere in the YECS between the CZCS and SeaWiFS eras. The two regions that can be considered as case-1 waters, at least part of the year, are the middle of the Yellow Sea in summer and the eastern East China Sea. The middle of the Yellow Sea showed the most extreme increase in chlorophyll (60%) whereas the eastern East China Sea had a smaller change (15%).

The CZCS climatology was compared to a large *in situ* database by Gregg and Conkright (2001), and a comprehensive comparison of CZCS and SeaWiFS chlorophyll climatologies has been presented by Conkright and Gregg (2003). They used the *in situ* measured chlorophyll as “internal boundary conditions” to blend with the CZCS data, thus producing a blended climatology that was considered to be a better representation of global chlorophyll distributions. The SeaWiFS climatology (October 1997- June 2001) was within ~10% of the blended climatology derived from CZCS and *in situ* data. In this work, the CZCS pigment was converted to chlorophyll using a formula prescribed by O’Reilly et al. 1998 (shown as the dashed line in figure 2.2). They found that the CZCS

chlorophyll, thus derived, was significantly lower than the *in situ* chlorophyll measurements. Here we ask whether this would apply to our comparisons.

The first thing to notice is that their formula for converting PIG to CHL was substantially different from ours (see fig. 2.2). The ratio of our CZCS chlorophyll to theirs (based on their formula) ranges from 0.76 to 2.5 with only a narrow PIG range where the ratio is below 1. In the open ocean, below the switching point of the CZCS algorithm, the ratio is always above 1 (ranging from 1.27 to 2.5). Thus, presumably if Gregg and Conkright (2001) had used our formula, their CZCS chlorophyll values would be much higher, and the discrepancies with the *in situ* data would be less.

The difference between CZCS and SeaWiFS chlorophylls in the very turbid waters from our results is much smaller compared with that in Conkright and Gregg's result (2003) while the range of the chlorophyll difference in the other areas is similar to the result of Conkright and Gregg (2003). The difference between CZCS and SeaWiFS chlorophyll was relatively small in the east-East China Sea characterized as open ocean which is affected by the Kuroshio current (+0.06 mg/m<sup>3</sup>).

The ratios of radiances at 443 and 555 nm between long-term composite SeaWiFS and CZCS show a very high increase in the SeaWiFS era in the same turbid areas. The Bohai Sea is affected by the Yellow (Hwanghe) River. It has been reported that construction of dams and low rainfall have led to about 50% decrease in both water and sediment discharge on the Yellow River in recent years, and the river was dry for four months in 1995 (Milliman, 1997). The Three Gorges dam, which is the largest one in the world, was being constructed on the Changjiang River since 1992 and recently completed (May, 2003). The dam will be operating in 2009. A recent study has shown that there was



more than 20% decrease of sediment discharge in the Changjiang River from 1980s to 1990s while there was increase of water discharge by 10% as a result of human activities such as deforestation and impoundments (Yang et al. 2002). Increases in water-leaving radiances at 443 and 555 nm are spatially coherent with higher turbidity occurring in shallow regions and in the river plumes. The changes in water-leaving radiances could be related to the changes of fresh water and sediment discharges. Changes of discharge in major rivers in Korea are not known, although the amount is smaller compared with that of the Changjiang River (Chen et al. 1994).

In the ratio of SeaWiFS to CZCS chlorophyll, there were two chlorophyll patches in the middle of the Yellow Sea where the chlorophyll had increased much more than in the surrounding area. The more southerly patch is located around a Korean dump site that has been used since 1995. Organic matter dumped in the area could affect the increased chlorophyll concentration. The more northerly patch is located in North Korean waters, and thus it is difficult to know what caused the increase because there is no information for that area. The ratio of chlorophyll is relatively low in the very high turbid waters, the Bohai Sea, the mid-west coast of Korea, and along the east coast of China (especially, along the Shandong Peninsula and the Changjiang River).

From the comparison of year-to-year variation in July and November, we have seen that the chlorophyll values are clearly higher in SeaWiFS images in most of the region, and notably in the central waters of the Yellow Sea which are Case 1 in the summer. There were comparisons between two periods for the satellite ocean-color data and *in situ* data over the 61 KODC stations in the Yellow Sea. In the *in situ* data, there were increasing trends in temperatures and zooplankton biomass and decreasing trends in

Secchi depth and salinity. While there were increases in the mean chlorophyll and  $L_w555$ , the  $L_w443$  decreased. The increase of temperature and zooplankton could be associated with increases of chlorophyll, and the decrease of salinity and Secchi depth with increased turbidity due to increase of chlorophyll and/or river runoff. The central regions of the Yellow Sea may be affected by higher levels of atmospheric pollution (e.g., nitrogen species acting as a fertilizer and changes in the deposition of Yellow Dust, which may enhance biomass increasing).

## 2.5. CONCLUSION

In comparing CZCS with SeaWiFS data, no attempt was made to unify the atmospheric correction algorithms. Thus, it is likely that differences in the atmospheric correction between the ocean color sensors might account for the difference of water-leaving radiance at 443 nm, especially in this area which is strongly affected by the high Yellow Dust. To resolve this we would need a unified algorithm that can correct for absorbing aerosols. Furthermore, for these Case 2 waters where mixtures of organic and inorganic materials affect the color of the water, more sophisticated bio-optical algorithms must be developed to account for the unique optical characteristics and variation of environmental parameters.

## **Acknowledgements**

This work was supported by a NASA MODIS Instrument Team investigation contract (NAS5-96063). The authors are indebted to Dr. YoungShil Kang for digitizing the zooplankton data.

**Table 2.1.** Long-term means and standard deviations of the CZCS (1979-1984) and the SeaWiFS (1998-2002) chlorophyll,  $L_w443$ , and  $L_w555$  for 6 sub-regions: the Bohai Sea, the western coast of the Yellow Sea, the middle of the Yellow Sea, the eastern coast of the Yellow Sea, the west-East China Sea, the middle of the East China Sea, and the east-East China Sea. Ratios and percentiles of SeaWiFS-to-CZCS long-term means were calculated. The units are  $mg/m^3$  for chlorophyll and  $W/m^2/sr/nm$  for water-leaving radiances.

variable	region	CZCS		SeaWiFS		ratio	%
		mean	stddev	mean	stddev		
Chl	BS	5.46	4.10	5.72	2.52	1.05	5
	WYS	2.74	2.11	3.67	2.13	1.34	34
	MYS	0.89	0.31	1.43	0.35	1.60	60
	EYS	3.97	3.54	4.17	2.03	1.05	5
	WECS	3.81	3.06	5.53	3.21	1.45	45
	MECS	1.04	0.68	1.41	0.75	1.36	36
	EECS	0.39	0.20	0.45	0.21	1.15	15
nLw443	BS	0.71	0.23	1.11	0.42	1.57	57
	WYS	1.00	0.23	1.33	0.67	1.32	32
	MYS	0.89	0.15	0.62	0.22	0.69	-31
	EYS	0.79	0.32	0.93	0.53	1.17	17
	WECS	1.02	0.31	1.65	0.34	1.61	61
	MECS	1.11	0.13	1.07	0.22	0.96	-4
	EECS	1.16	0.14	0.87	0.16	0.75	-25
nLw555	BS	1.50	0.39	2.88	1.17	1.92	92
	WYS	1.53	0.64	2.58	0.28	1.68	68
	MYS	0.60	0.15	0.77	0.28	1.28	28
	EYS	1.21	0.41	2.02	1.00	1.67	67
	WECS	1.56	0.34	3.24	1.11	2.08	108
	MECS	0.80	0.26	1.09	0.44	1.36	36

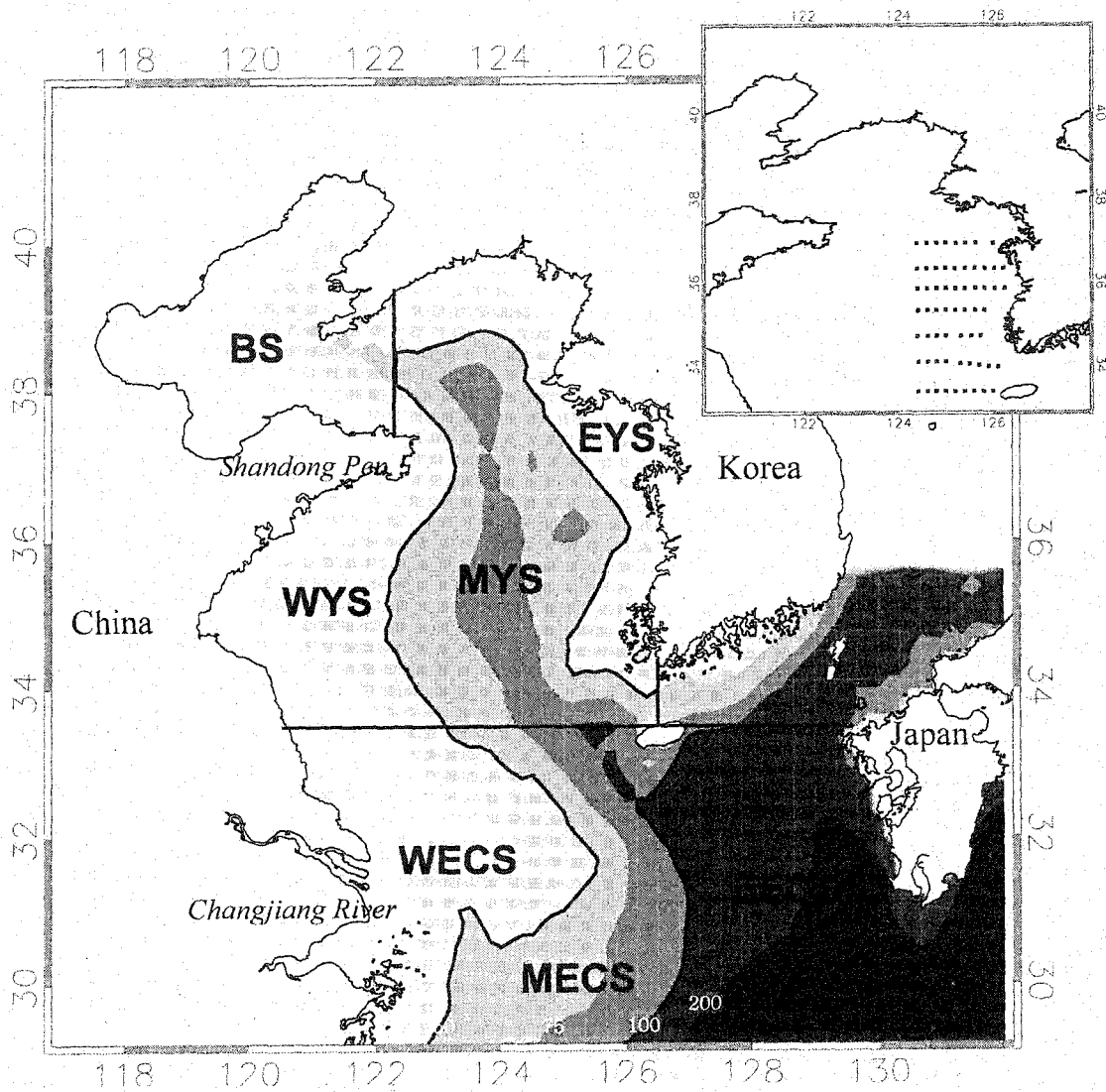


**Figure 2.1.** Geography of the study area (BS: the Bohai Sea, WYS: the western coast of the Yellow Sea, MYS: the middle of the Yellow Sea, EYS: the eastern coast of the Yellow Sea, WECS: the western East China Sea, MECS: the middle of the East China Sea, and EECS: the eastest East China Sea) and the serial oceanographic stations of KODC (small squares, 61 stations).

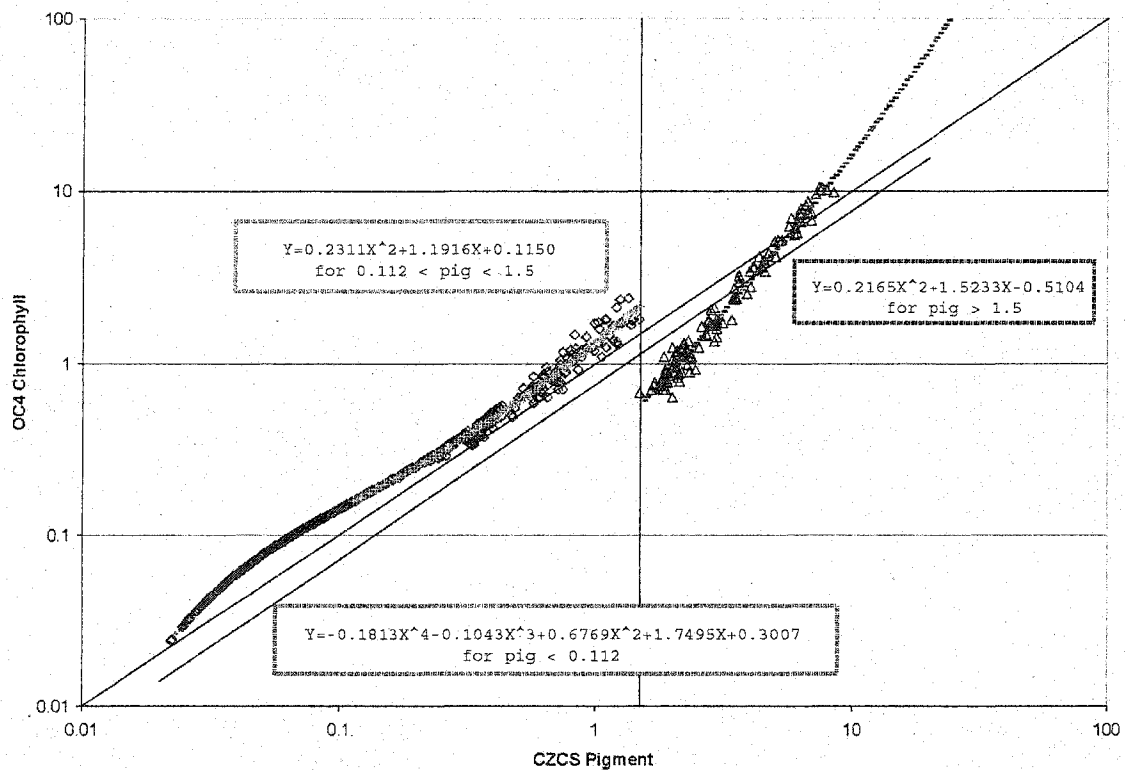
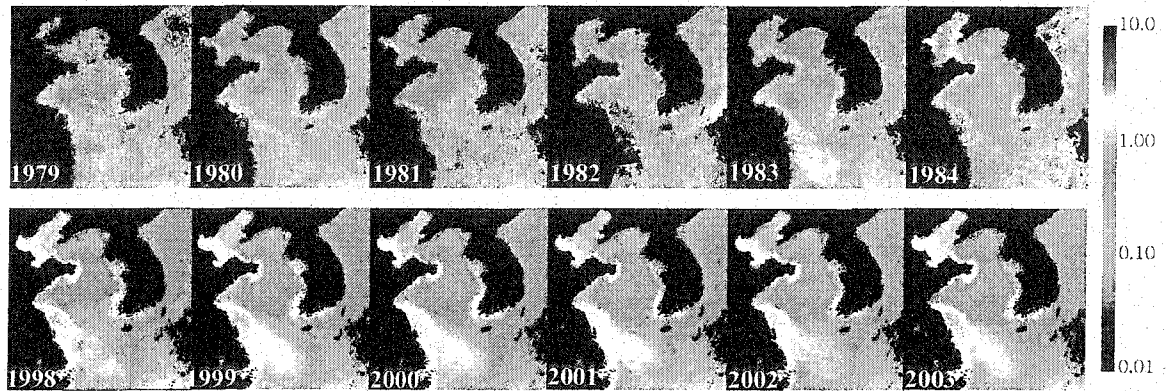
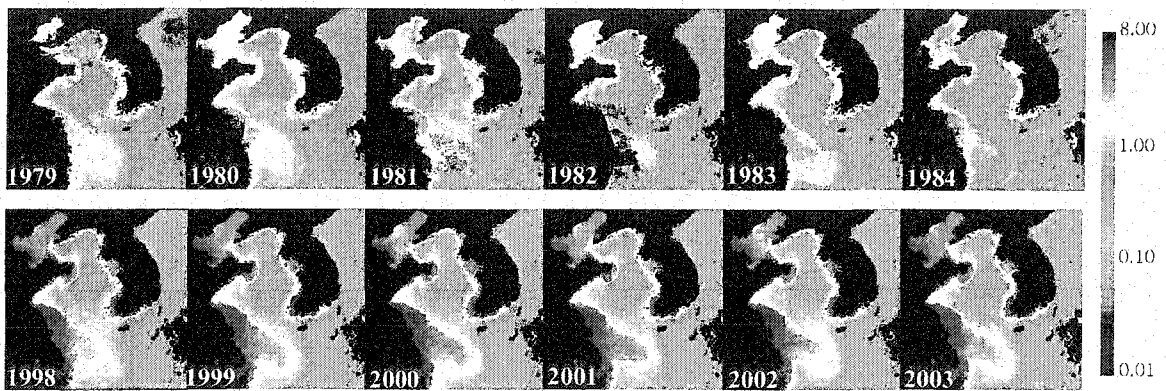


**Figure 2.2.** Results of applying the OC4 (SeaWiFS) chlorophyll algorithm (vertical axis) and the CZCS pigment algorithm (horizontal axis) to the original SeaBAM data of O'Reilly et al., (1998). The vertical dashed line marks the value pigment = 1.5 mg m<sup>-3</sup> where the CZCS algorithm switched from using the 443:550 radiance ratio to the 520:550 ratio. The dashed line is the relationship CHL = 0.8 PIG proposed by O'Reilly et al. (1998) that was subsequently used by Conkright and Gregg (2001).

(a) nLw443



(b) nLw555



(c) chlorophyll

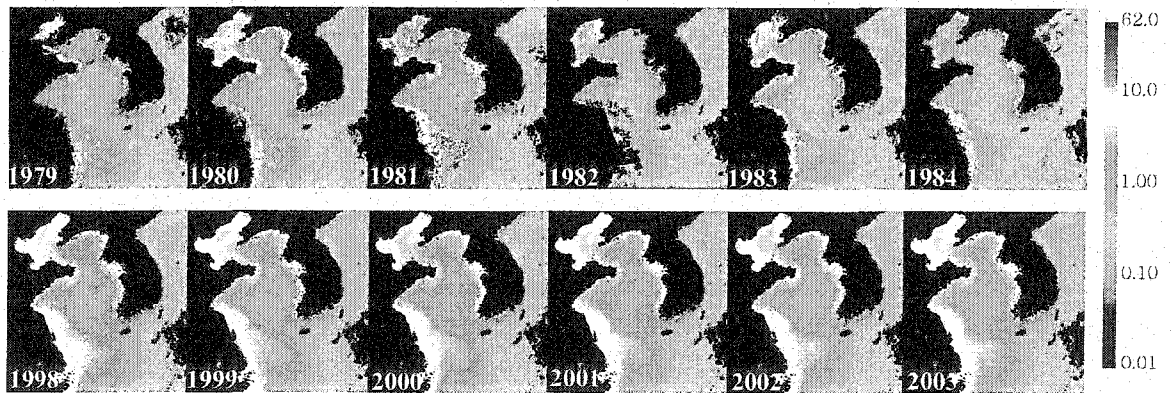


**Figure 2.3.** Yearly composite CZCS (1979-1984) and SeaWiFS (1998-2003) images of (a) nLw443, (b) nLw555 and (c) chlorophyll in the Yellow and East China Seas. The scales give water-leaving radiances in  $W/m^2/sr/nm$  and chlorophyll in  $mg/m^3$ .

Composite nLw443

CZCS (1979-1984)

SeaWiFS (1998-2003)

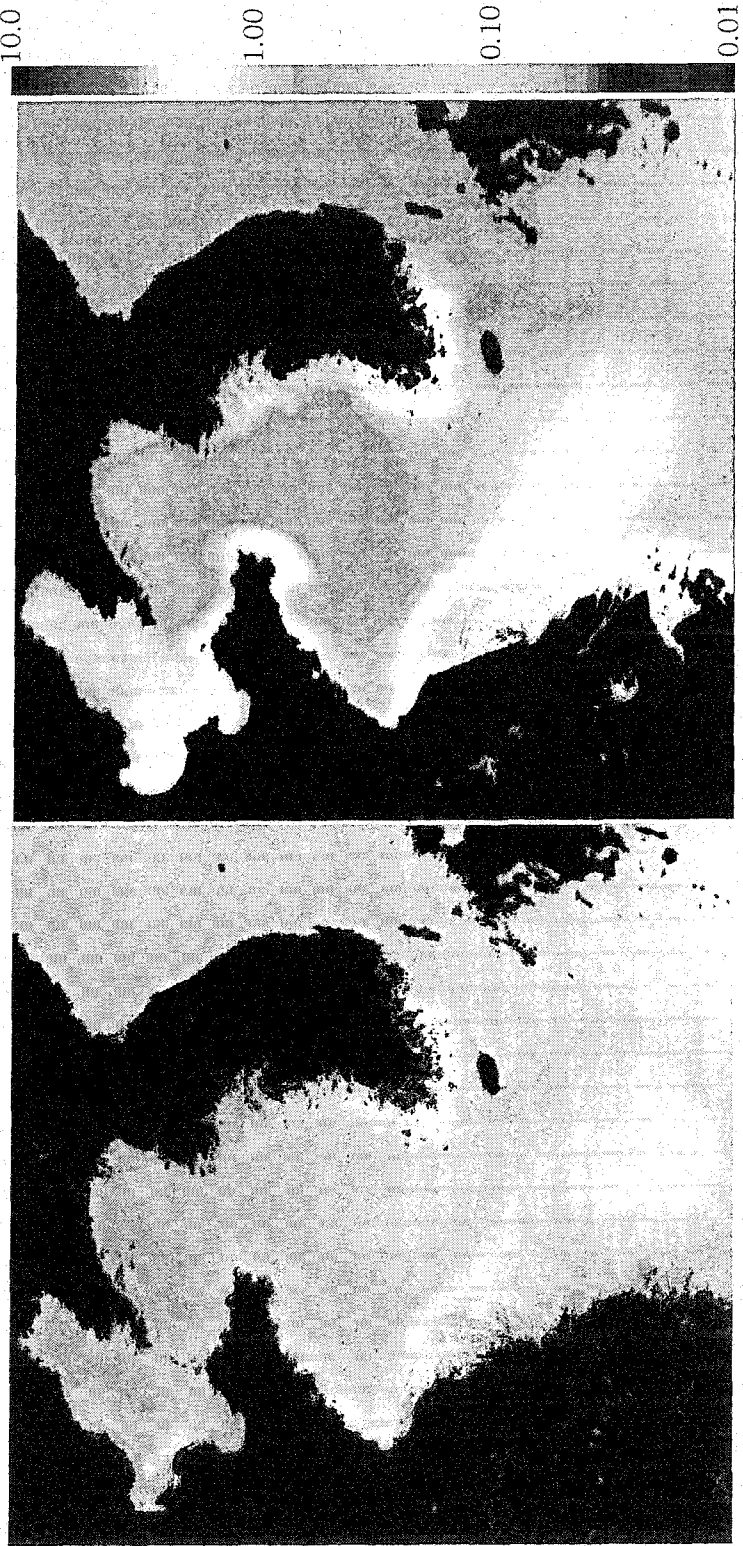


Figure 2.4. Long-term average of CZCS (1979-1984) and SeaWiFS (1998-2003) nLw443.



Composite nLw555

CZCS (1979-1984)

SeaWiFS (1998-2003)

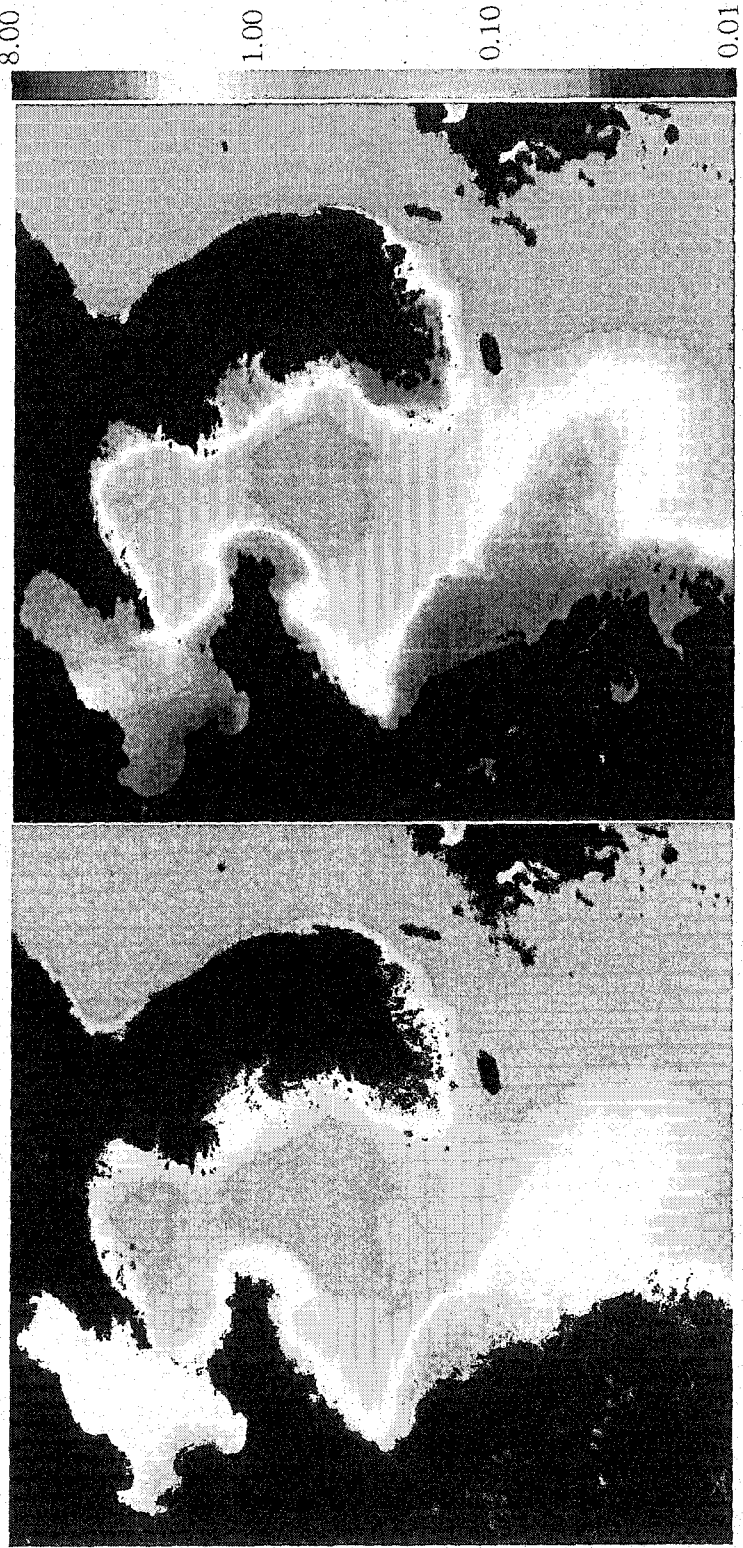
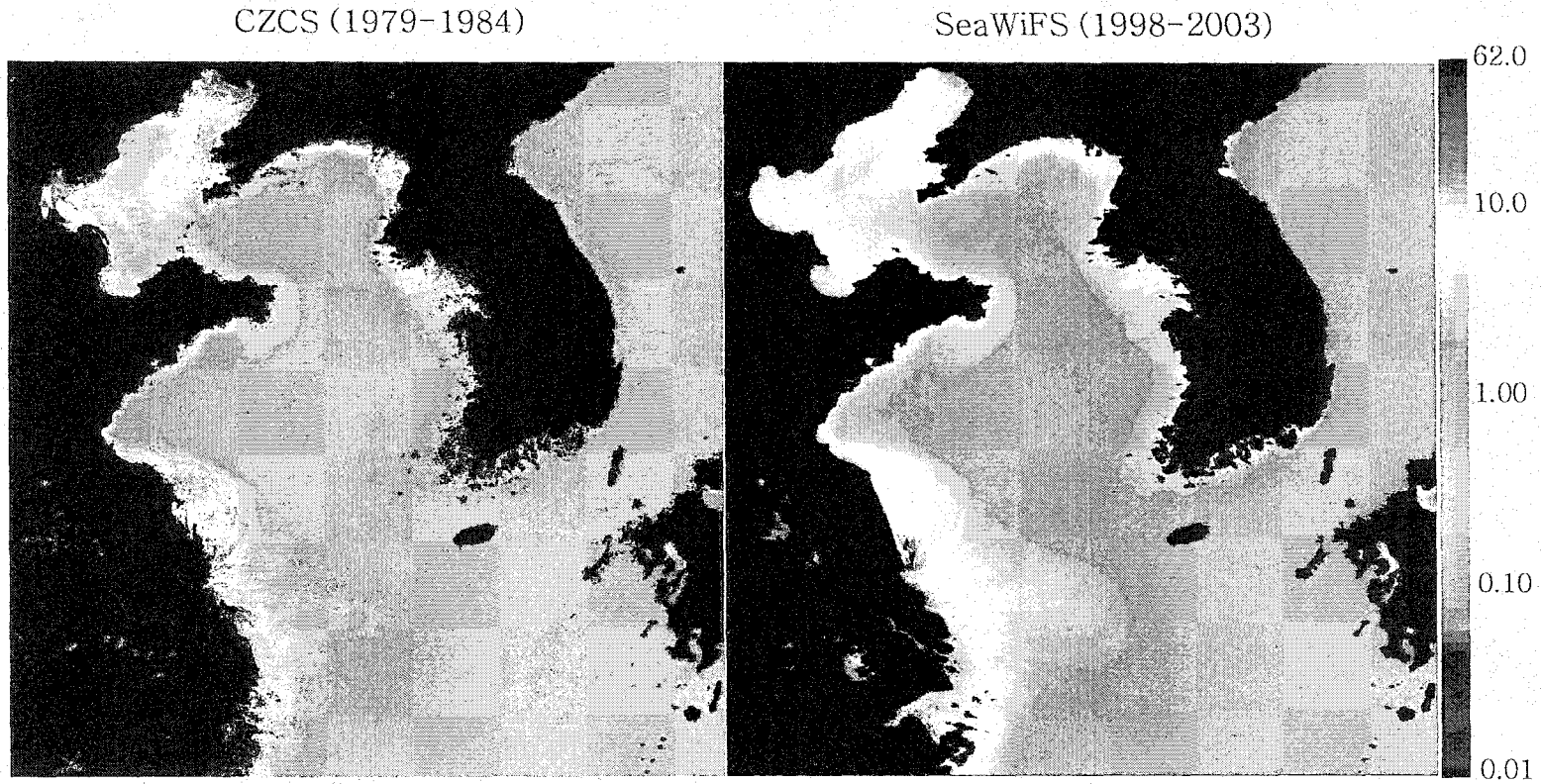
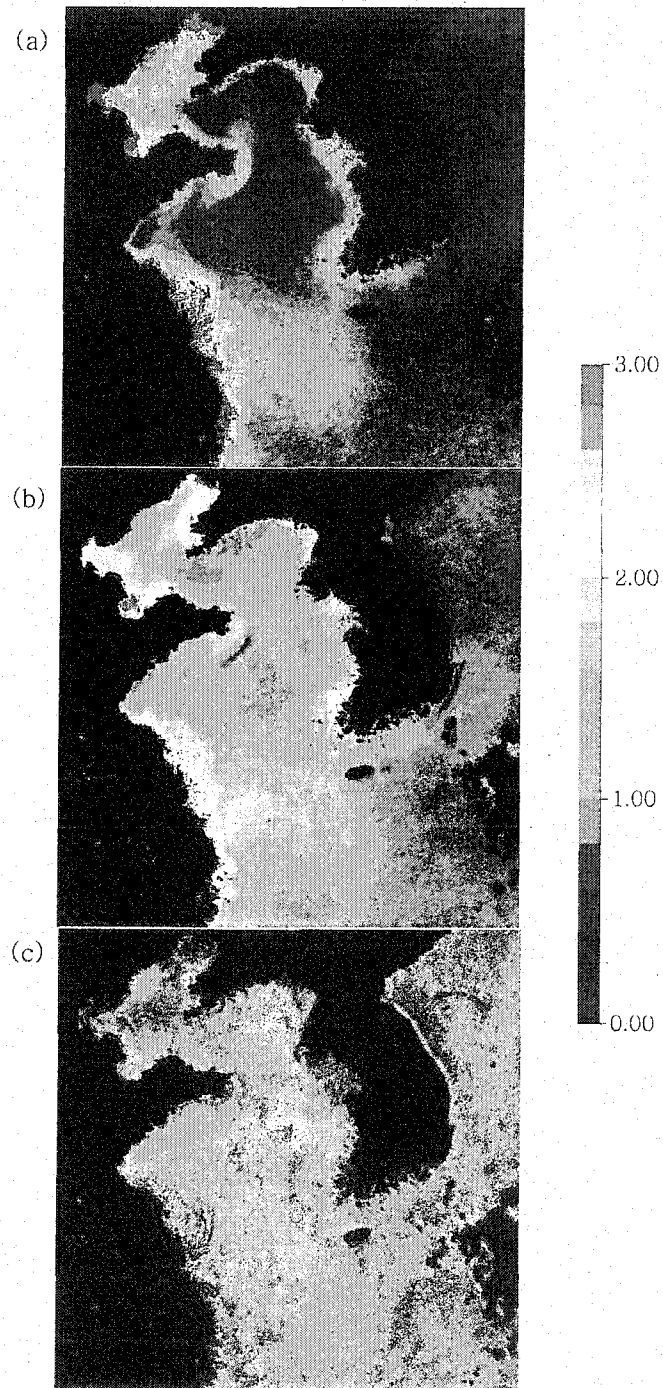


Figure 2.5. Long-term average of CZCS (1979-1984) and SeaWiFS (1998-2003) nLw555.

### Composite chlorophyll



**Figure 2.6.** Long-term average of CZCS (1979-1984) and SeaWiFS (1998-2003) chlorophylls.



**Figure 2.7.** Ratios of SeaWiFS-to-CZCS long-term means. (a)  $L_w(443)$ , (b)  $L_w(555)$  and (c) chlorophyll. Increases are shown in yellows and reds, decreases in greens and blues, and white indicates no change.

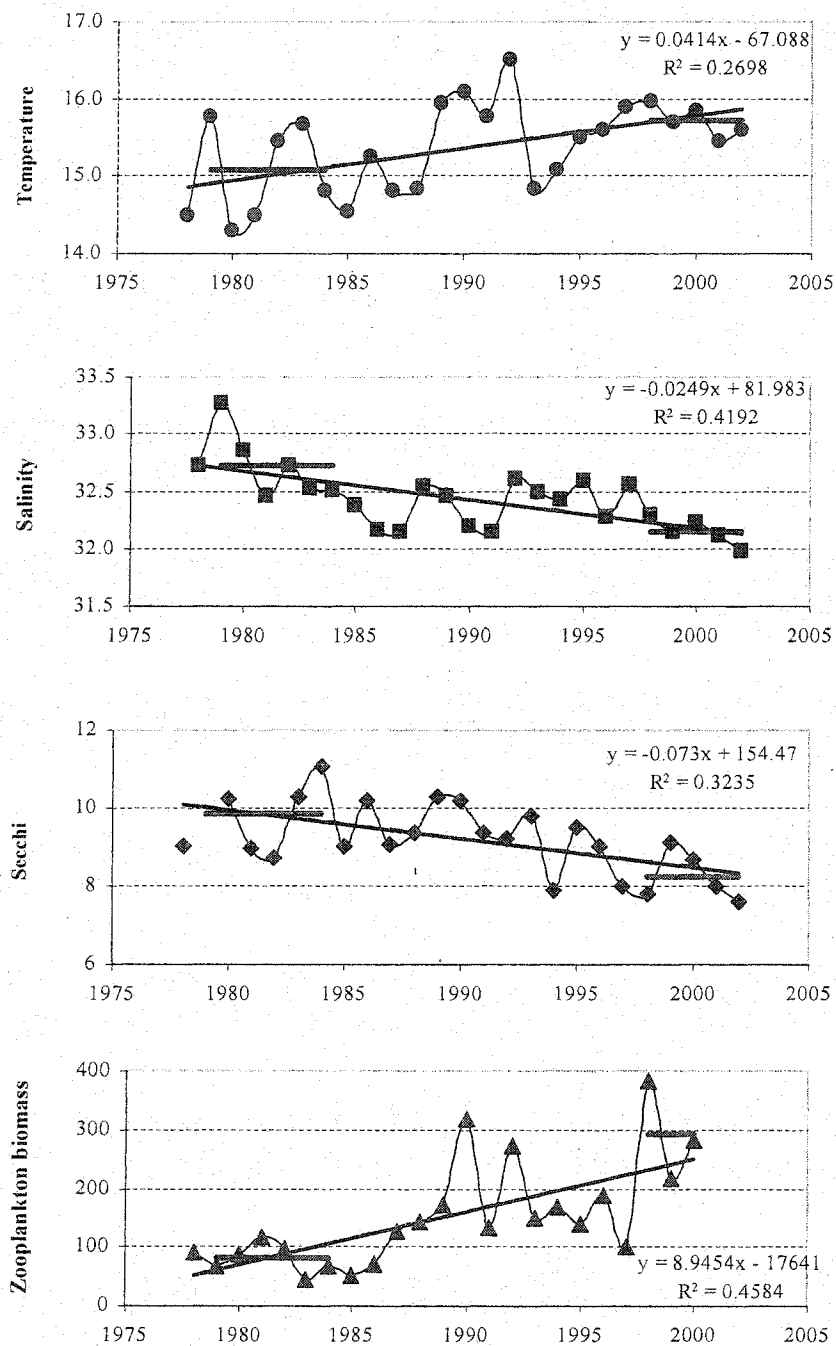


**Figure 2.8.** The year-to-year variations of temperature, salinity, and Secchi depth from 1978 to 2002, and zooplankton biomass from 1978 to 1996 at the 61 KODC stations in the Yellow Sea. Dashed lines are the trend lines and thick horizontal lines are the means values for the CZCS (1979-1984) and SeaWiFS (1998-2002) eras. The yearly averaged chlorophyll, nLw443, and nLw555 values of the CZCS (1979-1984) and the SeaWiFS (1998-2002) are also plotted.

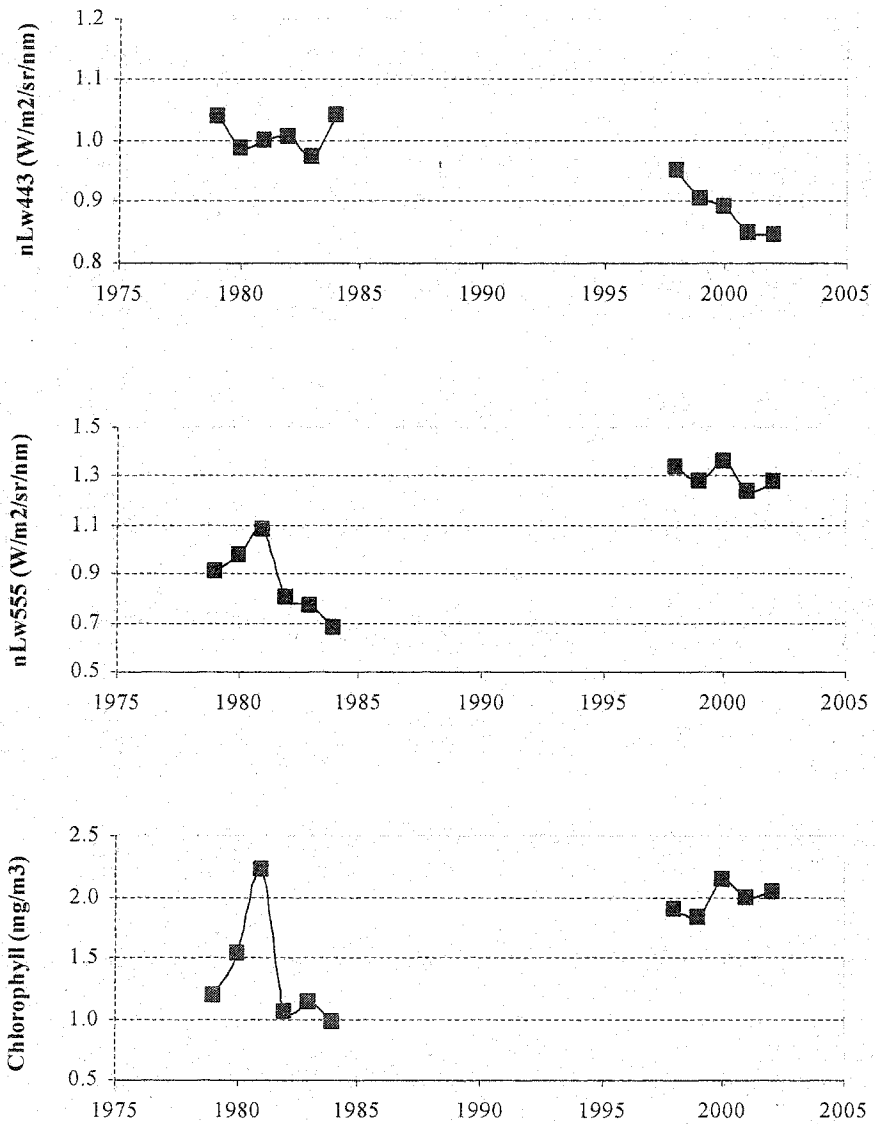
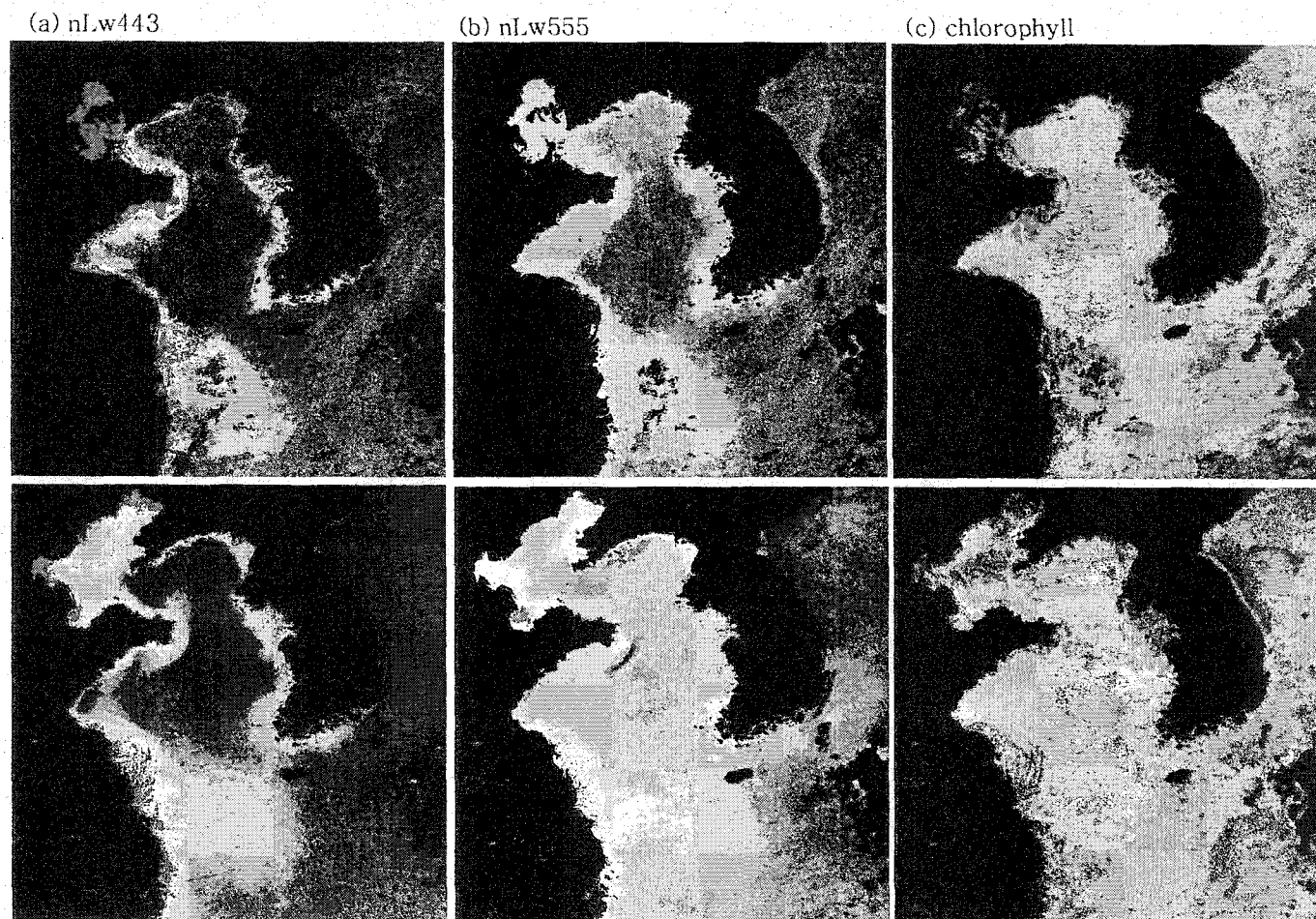


Figure 2.8. – continues -



**Figure 2.9.** Top row: Ratios of monthly composite SeaWiFS data for November 2003 derived by two atmospheric correction algorithms. The standard algorithm products are divided by those using a CZCS-like atmospheric correction algorithm (see text). Bottom row are the SeaWiFS-to-CZCS long-term means presented for comparison. (a)  $L_w(443)$ , (b)  $L_w(555)$  and (c) chlorophyll.

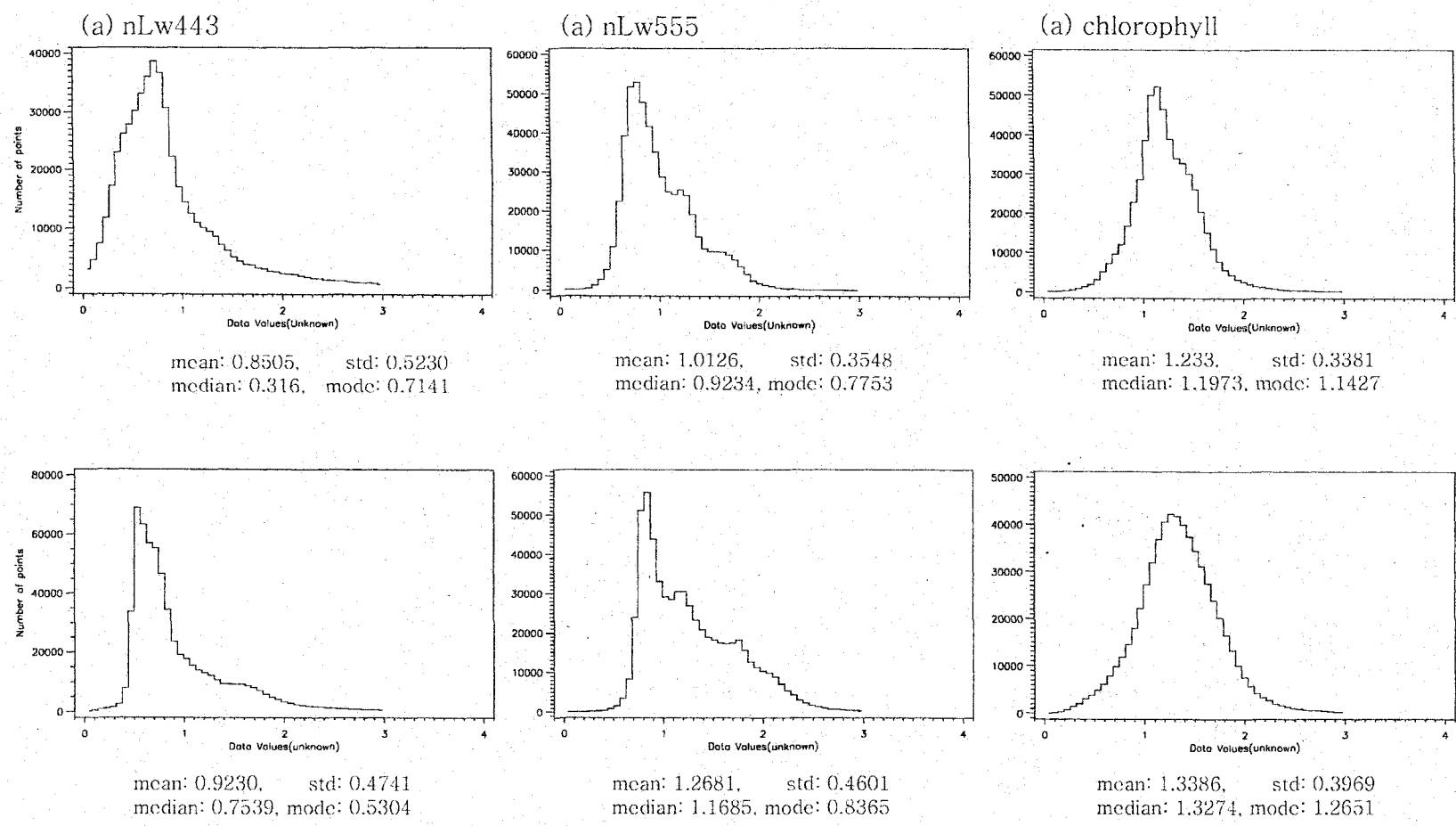


Figure 2.10. Histograms of the ratios shown in figure 2.9.

## Chapter 3

### Classification of Well-Mixed and Stratified Waters in the Yellow Sea

(To be submitted to *International Journal of Remote Sensing* by Seung-Hyun Son, Janet Campbell, Il-Ju Moon, Mark Dowell, and Sinjae Yoo)

#### ABSTRACT

Information on the vertical profile of phytoplankton biomass is important to estimate primary production using ocean color satellite data. As a first step, identification of well-mixed and stratified regions in the coastal ocean is needed. In this paper, the criterion of temperature difference between surface and bottom layer,  $|\Delta T| < 0.8^{\circ}\text{C}$ , and the Simpson-Hunter criterion,  $\log(H/U^3) < 2$ , (where  $H$  is the water depth and  $U$  is the depth-mean velocity of the tidal current), have been used to identify well-mixed waters in the Yellow Sea. A coupled ocean wave-circulation model and bathymetry data are used to derive the temperature difference between surface and bottom layer and  $\log(H/U^3)$ . Then model results were compared with remotely sensed sea surface temperature and water-leaving radiance at 667nm derived from the Moderate Resolution Imaging Spectroradiometer (MODIS) to develop a method to differentiate stratified and well-mixed waters using remote sensing data.



From the model results, the criterion based on surface-bottom  $\Delta T$  threshold ( $\Delta T < 0.8\text{C}$ ) proved to be a better criterion. The  $\log(H/U^3)$  criterion which applies only to mixing governed by tidal force is useful only during the summer season. In the winter, the Yellow Sea is vertically well mixed due to strong winds and surface cooling. Even in the summer, the  $H/U^3$  criterion does not work in the Chinese coasts because the buoyancy of freshwater plume from the Changjiang River discharge creates a strong halocline in the surface layer. Three-year (2000 to 2002) monthly composite images of MODIS SST and nLw667 were compared with the model-based  $\Delta T$  results in March to October to investigate whether the satellite data can be used as the criterion. The nLw667 threshold could be used reasonably along the southwest coast of Korea during the warmer months. Maps of the well-mixed area were derived from MODIS nLw667 using the relationship between the nLw667 and the model  $\Delta T$  in the southeastern Yellow Sea for the warmer months (April to September). The well-mixed area is located in the area where the nLw667 is higher than  $2\text{--}4 \text{ W}\cdot\text{m}^{-2}\cdot\text{nm}^{-1}\cdot\text{sr}^{-1}$  depending on the month.

### 3.1. INTRODUCTION

The Yellow Sea is strongly affected by tidal forces as well as fresh water discharge from the Changjiang (Yangtze) River. While the center of the Yellow Sea is thermally stratified from spring through fall, the coastal areas of the Yellow Sea are vertically well-mixed due to tides throughout the year. Tidal fronts appear in April with

surface heating by solar energy and become most clear in August. Then the fronts disappear in November with surface cooling (Seung et al., 1990). During winter months, most of the Yellow Sea is mixed due to surface cooling and strong winter winds. The southwestern part of the Yellow Sea is affected by the freshwater discharge from the Changjiang River. The annual mean freshwater discharge from the Changjiang River is about  $2.9 \times 10^4 \text{ m}^3 \text{ s}^{-1}$  with minimum of  $0.9 \times 10^4 \text{ m}^3 \text{ s}^{-1}$  in January and maximum of  $5.4 \times 10^4 \text{ m}^3 \text{ s}^{-1}$  in July (Riedlinger and Preller, 1995). The mid-western coast of Korea (Kyunggi Bay) is also affected by freshwater discharge from the Han River with the total annual mean is about  $1.0 \times 10^3 \text{ m}^3 \text{ s}^{-1}$  (Schubel et al., 1984).

Information on the vertical profile of phytoplankton biomass plays an important role in algorithms used to estimate ocean primary production within a water column using satellite-derived data. The biomass profile is generally dependent on the physical structure of the water column. Coastal and shelf seas are divided into stratified and well-mixed areas during the warmer months. The biomass profile in the tidally well-mixed area can be assumed as vertically uniform while there are deep chlorophyll maxima in the stratified areas. The vertically well-mixed area due to tidal forces has importance on phytoplankton growth and distribution. In addition, light limitation due to high turbidity caused by tidal mixing can inhibit the primary production. It has been reported that light transparency is an important factor governing primary production in the tidally mixed areas of the Yellow Sea (Kang, et al., 1992; Choi, 1991; Choi, et al., 1995; Yoo and Shin, 1995). Thus, it is important to identify well-mixed and stratified regions for estimation of primary production using the ocean color satellite data.

Simpson and Hunter (1974) proposed a criterion, based on  $H/U^3$ , where  $H$  is the water depth and  $U$  is the depth-mean velocity of the tidal current, to differentiate tidally mixed and stratified waters. They proposed a threshold value of  $\log(H/U^3)$  less than 2 for vertically well-mixed areas and a value greater than 2 for stratified areas. Yentsch and Garfield (1981) differentiated mixed and stratified waters in the Gulf of Maine using the criterion proposed by Simpson and Hunter (1974) in order to establish the magnitude of the productivity associated with well-mixed regions, and compared maps of  $\log(H/U^3)$  with infrared satellite imagery. They found a good agreement with the SST maps. Others have compared satellite infrared imagery and/or ship-measured temperature with this criterion in other regions (Pingree and Griffiths, 1978; Garrett et al. 1978; Bowman and Esaias, 1981; Baines and Fandry, 1983; Lie, 1989).

There were several attempts to predict the location of tidal fronts using the criterion,  $H/U^3$ , in the Yellow Sea (Beardsley et al., 1983; Lie, 1989; Naimie et al., 2001). These authors demonstrated that tidal fronts were located along the mid-Chinese coast and in Kyunggi Bay and Seohan Bay, and that visual comparison with satellite SST was reasonably consistent. However, the  $\log(H/U^3)$  threshold varied with regions: it was between 2.0 and 2.4 over the shallow Yangtze Bank (Beardsley et al., 1983) and between 1.0 and 1.4 in the region off the southwest coast of Korea (Lie, 1989).

The upper mixed layer is generally defined as the surface layer where the temperature differs by less than  $0.5^\circ\text{C}$  from the sea surface temperature (Obata et al., 1996; Monterey and Levitus, 1997). Recently, Kara et al. (2000) defined an optimal mixed layer depth (MLD) as the depth at the temperature difference of  $0.8^\circ\text{C}$ . In this

work, we regard the water column as vertically mixed if the temperature difference ( $\Delta T$ ) between surface and bottom is less than  $0.8^{\circ}\text{C}$ .

The main objectives of this study were to establish the stratified and well-mixed areas associated with monthly variations and to develop a method to differentiate those two areas using satellite observations. In the stratified water, there is commonly a deep chlorophyll maximum (DCM) at the base of the mixed layer that influences the vertical profile of productivity (Fig. 3.1). The primary production often peaks at the depth of DCM. In the mixed water where temperature and salinity are uniform, the chlorophyll profile is almost uniform and the primary production exponentially decreases with depth.

In this paper, the Yellow Sea was classified with the Simpson-Hunter criterion,  $H/U^3$ , and also the criterion based on the temperature difference between surface and bottom. Both criteria were calculated from the results of the coupled ocean wave-circulation model developed by Moon (2004). The classifications were then compared with *in-situ* and remote sensing data to develop a method to differentiate stratified and well-mixed waters using remote sensing data.

## 3.2. METHODS

### 3.2.1. Model data

A coupled ocean wave-circulation model for the Yellow and East China Seas was developed by Moon (2004), which considered the effects of tide, winds, heat flux, river

discharge from the Changjiang River, and the Kuroshio Current. Monthly three-dimensional temperature data were derived from the model. The temperature difference between surface and bottom layer ( $\Delta T$ ) was calculated from the model results to define the positions of the well-mixed and the stratified areas. The isoline  $\Delta T = 0.8^\circ\text{C}$  was then drawn as the boundary between well-mixed and stratified waters based on the “optimal” MLD definition of Kara et al. (2000).

In addition, mean values of velocity ( $U$ ) within the water column derived from the Moon (2004) model were used to compute the Simpson and Hunter’s criterion. The log ( $H/U^3$ ) was calculated using the  $U$ -values and bathymetry data. The bathymetry ( $H$ ) data were obtained from the National Geophysical Data Center.

The temporal resolution of the model results (temperature and  $U$ ) is monthly and the spatial resolution is  $1/6^\circ \times 1/6^\circ$  degree (about  $19.5 \times 15$  km). The vertical temperature from the model was divided into 11 layers. The spatial resolution of the bathymetry was the same as that of the temperature and  $U$ . Since the model was forced by climatological tide, winds, heat flux, river discharge, the model results represent average properties.

### ***3.2.2. Satellite data***

The Moderate Resolution Imaging Spectroradiometer (MODIS) products are available from the National Aeronautics and Space Administration (NASA) Goddard Distributed Active Archive Center (DAAC). Three-years (2000 to 2002) MODIS monthly Level-3 mapped products were obtained at a resolution of  $4 \times 4$  km. From each

MODIS product, data surrounding the Yellow Sea (32-42°N, 118-128°E) were extracted. The monthly MODIS data were averaged for each month. The water-leaving radiance at 667 nm (nLw667), SeaWiFS-analog chlorophyll concentration (Chla2), and the daytime sea surface temperature from the 11-12  $\mu\text{m}$  band were used for this study.

### ***3.2.3. Ship measurements***

Geographical map of the Yellow Sea is shown in Fig. 3.2. Chlorophyll and suspended sediment data were measured from the Large Marine Ecosystem cruise in the Yellow Sea from June 14–21 in 2000. Temperature, salinity, and chlorophyll fluorescence profiles were also measured using CTD SBE25 as well. The spatial distributions and vertical profiles of the parameters obtained from the cruise were compared with  $\log(H/U^3)$  and the difference of the model temperature between surface and bottom, and with the MODIS observations.

## **3.3. RESULTS**

### ***3.3.1. Difference between surface and bottom temperature***

The spatial distributions of well-mixed areas based on the  $\Delta T < 0.8^\circ\text{C}$  criterion are shown in Fig. 3.3. In the winter season (December, January, and February), most of the Yellow Sea is well mixed due to cooling at the surface and wind stirring. However,

$\Delta T$  is greater than  $0.8^{\circ}\text{C}$  in a small area of the central and southeastern Yellow Sea in January and December. All of the Yellow Sea is well mixed in February except the southeastern Yellow Sea deeper than 100 m that is influenced by the warm Kuroshio current. Large areas of the Yellow Sea are still well mixed in March, but the northern Yellow Sea (around  $38.5^{\circ}\text{N}$  and  $121\text{--}124^{\circ}\text{E}$ ) is becoming stratified. In April, the area of the well-mixed regions was significantly decreased compared with March. The vertically mixed regions are restricted to the coastal regions of the Yellow Sea: along the west coast of Korea except for the middle coast between  $36^{\circ}\text{N}$  and  $37^{\circ}\text{N}$ , along the southeastern coast of China (near the Changjiang River), along the southern coast of the Shandong Peninsula, and in the northeastern and the southwestern Bohai Sea.

The spatial distribution of the mixed area is similar from May to August although further reduced in size compared with April. The mixed area is smallest in July and August. The mixed regions in May to August are located along the southwest coast of Korea, and around the Kyunggi Bay and the Seohan Bay, along the Chinese coast ( $33\text{--}35^{\circ}\text{N}$ ,  $36\text{--}37^{\circ}\text{N}$ ), and in the northeastern and southwestern Bohai Sea. The mixed area around the Changjiang River in April disappeared, where there is a strong halocline caused by the input of freshwater from the Changjiang River. The amount of the freshwater discharge is biggest in summer (Riedlinger and Preller, 1995; Yang et al. 2002). The stratification is weakening in September as the surface cooling starts. The mixed areas are located along most of the coast of Korea and China, and the areas become larger. The water column in most of the Bohai Sea and around the Changjiang River becomes uniform in October. In November, the northern Yellow Sea above  $37^{\circ}\text{N}$

mixes and  $\Delta T$  is greater than  $0.8^{\circ}\text{C}$  only in the middle of the Yellow Sea deeper than about 70m.

### *3.3.2. Simpson and Hunter's criterion*

The distribution of a range of  $\log(H/U^3)$  criteria (values 1.5, 2.0 and 2.5) are shown for two summer months (June and August) and compared with the  $\Delta T = 0.8^{\circ}\text{C}$  isoline in Fig. 3.4. The distribution of  $\log(H/U^3)$  is similar in both months. Low values of the criterion less than 2.0 appeared around the southwest coast of Korea, the mid-west coast of Korea, the northeastern area of the Bohai Sea, and the mid-east coast of China, especially around the Changjiang River, while the values higher than 2.5 appeared in the central area of the Yellow Sea and the open seas of the East China Sea. The overall distribution is similar to the results of other studies (Lie, 1989; Naimie et al, 2001) although there are some discrepancies in the Bohai Sea.

The isoline line of  $\Delta T = 0.8^{\circ}\text{C}$  is also plotted on the map of  $\log(H/U^3)$ . The distribution of  $\Delta T$  is coincident with the spatial pattern of  $\log(H/U^3)$ , especially along the west coast of Korea and Bohai Sea where the isoline of  $\Delta T = 0.8^{\circ}\text{C}$  is between  $\log(H/U^3) = 1.5$  and 2.0. The most notable difference between the  $H/U^3$  and  $\Delta T$  criteria is in the area of the Changjiang River plume where the  $\Delta T$  isoline is not present, but  $\log(H/U^3) < 2.5$ . Clearly, the  $\log(H/U^3)$  criteria does not account for the effects of the freshwater discharge since it is only based on tidal mixing.



### *3.3.3. Satellite observations*

Three-year (2000 - 2002) averages of monthly composite images of MODIS SST and nLw667 in March to October are shown in figures 3.5 and 3.6, respectively. In March, the SST is higher in the central area of the Yellow Sea and decreasing toward the north (Fig. 3.5). All except the central areas of the Yellow Sea are well-mixed ( $\Delta T < 0.8^{\circ}\text{C}$ ). The SST ranges from about  $5^{\circ}\text{C}$  in the northern Yellow Sea and to less than  $10^{\circ}\text{C}$  in the middle of the Yellow Sea. In April and May, cooler SST appears in the Bohai Sea and the northern (above  $37^{\circ}\text{N}$ ) and mid-eastern Yellow Sea. The spatial distribution of SST is similar in June to September although the temperature ranges vary with months. The distribution is approximately coincident with the result of  $\Delta T$  and  $\log(H/U^3)$  in the eastern part of the Yellow Sea. Lower temperatures along the western coasts of Korea are indicative of vertical mixing appear, but the actual SST values in the well-mixed areas vary with months and regions. The SST off the east coasts of China and in the Bohai Sea, where the distributions of  $\Delta T$  indicate a vertically mixed water column, is not lower compared with adjacent offshore areas. Higher temperatures,  $>19^{\circ}\text{C}$  in June and  $>25^{\circ}\text{C}$  in August, were associated with the northeastern areas of Kyunggi Bay and Seohan Bay. These areas are regarded as well-mixed from the model results. These waters are warmer than the offshore waters due to their shallow depth and solar heating. In addition, lower SST appearing in the eastern area of the Bohai Sea differs from the model results. In October, the SST was decreased and more uniformly distributed spatially.

The MODIS nLw667 images show spatially similar patterns with months. While the nLw667 is comparatively low in the middle of the Yellow Sea, the value is much higher along the west coasts of Korea, Bohai Sea, and the east coast of China including the Changjiang River (Fig. 3.6). The images show a high nLw667 feature protruding offshore from near the Changjiang River (toward the east). However, nLw667 increases and the areas spread more offshore in March, April, and October. In April to September, the higher value regions are coincident with the model results ( $\Delta T = 0.8^\circ\text{C}$ ) in the western coast of Korea. In areas regarded as well-mixed along the Korean coasts, the seasonal variation of nLw667 was relatively small whereas that of the SST varied with months. The nLw667 values from April to September indicative of well-mixed waters were greater than  $2\text{--}4 \text{ W}\cdot\text{m}^{-2}\cdot\text{nm}^{-1}\cdot\text{sr}^{-1}$ . Off the eastern coast of China, especially in the summer months (May to September), high values of nLw667 extended farther offshore compared to the lines of  $\Delta T = 0.8^\circ\text{C}$  and  $\log(H/U^3) = 1.5 - 2.0$ . This may be caused by large amount of discharge from the Changjiang River in summer.

#### ***3.3.4. In situ measurements***

The distribution of *in situ* temperature, chlorophyll-a, and suspended sediment at the surface in the eastern Yellow Sea, which were measured from the LME cruise in June 14–21, 2000, as well as the contour line of  $\Delta T = 0.8^\circ\text{C}$ , are shown on the monthly composite MODIS images of SST, chlorophyll-a concentration, and nLw667 for June, 2000 (Fig. 3.7). Lower values of ship-measured temperatures appeared in the southwest

coastal area (around 34.5°N and 125–126°E) and mid-west coastal area (about 37°N and 126°E) of Korea. The overall distribution is similar both in *in situ* chlorophyll-a and suspended sediment: higher concentrations in the southwest coasts of Korea and Kyunggi Bay. However higher chlorophyll area is located slightly northerly in the southwest coast of Korea and higher suspended sediment appeared in the central area of the Yellow Sea as well. The stations of the *in situ* measurements were not located in the mixed area defined by  $\Delta T < 0.8^{\circ}\text{C}$ . However, the spatial patterns of *in situ* variables are approximately coincident with that of the criterion from the temperature difference in the southwest coast of Korea.

The spatial distribution of the MODIS images in June, 2000 is similar to that of the three-year composite MODIS images shown in Fig. 3.5 and 3.6. The overall distribution of *in situ* data was analogous to the satellite products although there is discrepancy in quantity and unit.

### ***3.3.5. Comparison between model result and satellite data***

As mentioned above, no significant horizontal gradient of MODIS SST was shown along the Chinese coast and some of the northwestern coast of Korea although the areas were well-mixed in the model result. This region seems to be homogeneous from bottom to surface due to the shallow bathymetry and solar heating. In addition, there is a large seasonal variability of the SST values. Thus satellite SST images are not as applicable as the criterion for the classification in the Yellow Sea. In the tidally well-

mixed and shallow waters, the concentration of suspended sediment would be higher by re-suspension from the bottom. The nLw667 has been used in single-band algorithms for suspended sediment concentration (Salisbury, 2003). Seasonal variability of the MODIS nLw667 is relatively small compared with the SST in the Yellow Sea. However, high values of nLw667 may also be affected by suspended sediments from the river discharges. The concentration of suspended sediments in the Chinese coasts would be affected not only by tidal mixing but also by fresh waters from the Changjiang River. Meanwhile, the Yellow Sea is totally well-mixed during the winter season due to strong winds and surface cooling. As stated, the satellite nLw667 provides a better criterion to differentiate the Yellow Sea into well-mixed and stratified areas, particularly on the Korean side and in warmer months.

To derive the threshold for the classification using satellite data, nLw667 and  $\Delta T$  were compared off the Korean coasts in April to September (Fig. 3.8). Bin averages of the composite MODIS nLw667 (2000–2002) were plotted against the model  $\Delta T$ . The relationship varies with months but there is no seasonal trend. The nLw667 values at  $\Delta T = 0.8^\circ\text{C}$ , which are derived from these relationships, range from  $2.1 - 4.1 \text{ W}\cdot\text{m}^{-2}\cdot\text{nm}^{-1}\cdot\text{sr}^{-1}$  depending on the month. The maps of well-mixed area ( $\Delta T < 0.8^\circ\text{C}$ ) were derived from the MODIS nLw667 images using the relationships between nLw667 and  $\Delta T$  in the southeastern Yellow Sea (Fig. 3.9). The location of the well-mixed area derived from nLw667 agrees with the model result (isoline of  $\Delta T = 0.8^\circ\text{C}$ ) in most of the months.

### 3.4. DISCUSSION

In the results presented, temperature difference between surface and bottom layer ( $\Delta T = 0.8^{\circ}\text{C}$ ) following Kara et al. (2000) was used as a criterion to differentiate the well-mixed and the stratified areas. The temperature differences were derived from the results of the coupled ocean wave-circulation model (Moon, 2004). The  $\Delta T$  criterion established well-mixed and stratified areas associated with monthly variations in the Yellow Sea. During the winter season, most of the Yellow Sea is totally well-mixed except for a small area in the middle of the Yellow Sea. The middle of the Yellow Sea is thermally stratified from spring through fall. The coastal areas of the Yellow Sea are vertically well-mixed year-around due to tidal force. This result is similar to that of Seung et al. (1990). However, the waters around the Changjiang River seem to be stratified during the warmer months (May to September) due to large input of freshwater from the Changjiang River. The amount of the freshwater discharge is biggest in summer (Riedlinger and Preller, 1995; Yang et al. 2002).

The Simpson and Hunter (1974) criterion,  $\log(H/U^3)$ , was compared with the distribution of  $\Delta T$ , where the  $U$  values have been derived from the Moon's model (Moon, 2004). The Simpson-Hunter criterion is based on the situation where tidal force is solely responsible for vertical mixing in shallow seas. Since tidal forces do not change appreciably with seasons in the Yellow Sea, the  $\log(H/U^3)$  criterion for winter months was nearly identical to that in the summer months. Therefore, this criterion is useful only during the summer season, but is not useful in winter when mixing is governed largely by

thermal convection and winds. Studies (Simpson and Hunter, 1974; Pingree and Griffiths, 1978; Bowman and Esaias, 1981) proposed a threshold value of  $\log(H/U^3)$  of 1.5 or 2 to differentiate vertically well-mixed areas from stratified areas. From our result, the isoline of  $\Delta T = 0.8^\circ\text{C}$ , which divides well-mixed and stratified areas, is located approximately between  $\log(H/U^3) = 1.5$  and 2.0 in the warmer months although it varies with regions. However, there is discrepancy in the east coast of China, especially around the Changjiang River. It is inferred that the difference is caused by the buoyancy of freshwater discharge plume from the Changjiang River which makes the strong halocline in the surface layer as mentioned above.

In the result of Lie (1989), the boundary between stratified and well-mixed area was expected to be  $\log(H/U^3) = 1.0 - 1.4$  in the southwest coastal water of Korea. This value was derived in a very small area and used observed tidal current data in a small island in the southwest of Korea. Thus the value may be different from our result due to the different temporal and spatial resolution. In addition, many tiny islands in that region were ignored in Moon's model.

Ideally, one should use a time-dependent model forced by real winds and ambient conditions at the same time as the satellite data used for estimating primary production. In our case, we used a climatological model and therefore results are only general for the Yellow Sea. We do not have coincident *in situ* information about the stratification to compare with the MODIS satellite imagery. However, we have compared the isolines of  $\Delta T = 0.8^\circ\text{C}$  with SST and normalized water-leaving radiance (nLw667) values from the monthly composite MODIS images averaged over three years (2000-2002). These

composite images should be comparable to the climatological model results. We believe that it is possible to base a criterion either on the SST or normalized water-leaving radiance in the red region. Cool temperatures would generally indicate vertical mixing. Yentsch and Garfield (1981) compared the Simpson-Hunter criterion with SST maps for the Gulf of Maine and found a reasonable correspondence with their criterion.

The distribution of cool inshore MODIS SST in summer months corresponded with the model results along the western coastal areas of Korea although the lower SST region extended more offshore compared with the results of  $\Delta T$ . Although mixing zones can generally be identified with the appearance of lower temperature, the inshore SST values in the Bohai Sea, the mid-east coast of China, and the northeastern area of Kyunggi Bay and Seohan Bay were higher than offshore values. It is possible that the shallow bathymetry in the Bohai Sea, the eastern coast of China, and the northeastern area of Kyunggi Bay and Seohan Bay make the water temperature homogeneously high from bottom to the surface by solar heating even though these areas are well mixed by tidal force in summer. In addition, the surface stratification due to the fresh water discharge from the Changjiang River occurs over the areas adjacent to the Changjiang River.

The nLw667 has been used by others in single-band algorithms for suspended sediment concentration (Salisbury, 2003). High sediment or turbidity would indicate shallow well-mixed regions, and thus a threshold for nLw667 could be used. The mixed waters in the Yellow and East China Seas are strongly affected by re-suspended sediment due to the vertical mixing and shallow depths. The distribution of MODIS nLw667 is

higher along most of the coastal areas while the values are comparatively low in the middle of the Yellow Sea. The visual comparison between the MODIS nLw667 image and the model results showed correlated patterns along the western coast of Korea. While SST values varied with months, seasonal variation of the nLw667 values in the areas regarded as well-mixed was relatively small in the Korean coasts. Therefore, it was concluded that the nLw667 data would be used as a better criterion for differentiating well-mixed and stratified areas. Meanwhile, high values of nLw667 may also be influenced by suspended sediments from the river discharges such as the Changjiang river for the southwest Yellow Sea and the Yellow (Hwang He) River for Bohai Sea. Thus, if a high turbidity criterion were used as indicated by nLw667, the extent of well-mixed waters off the regions near the rivers, especially in the Changjiang River Bank, would be larger than the actual reality.

Similar pattern was shown in comparisons among the model results, the LME cruise data in 14–21 June, 2000, and the monthly composite MODIS images of June, 2000 in the southeastern Yellow Sea although *in situ* data were spatially limited compared to model results. The areas of lower temperature and higher nLw667 from MODIS deviated from the threshold line of the model results toward offshore. This discrepancy may be caused by temporal resolution. The model results were based on the climatological data, so the year-to-year variation is not considered in this model. The satellite images and *in situ* data vary with time and regions. Thus, satellite data can be better way to identify the mixed water.



The maps of well-mixed area were derived from the MODIS nLw667 images using relationships between nLw667 and  $\Delta T$  in the southeastern Yellow Sea in warmer months. The location of the well-mixed area derived from the nLw667 images and the model result compared reasonably well although there is some discrepancy with regions and months. As mentioned, the discrepancy may be caused by the difference of temporal resolution. In addition, it is needed to point out that the model result has spatial resolution of  $1/6^\circ \times 1/6^\circ$  (about  $19.5 \times 15$  km), but that of the MODIS images is  $4 \times 4$  km and the *in situ* data is in a certain point. The model results are approximately 3.5 – 5 times coarser than the MODIS data. Lie (1989) reported that the discrepancy between SST and his model result was probably due to the coarse grid system of his model

### 3.5. CONCLUSION

Using the model-based criterion of temperature difference between surface and bottom layer ( $\Delta T = 0.8^\circ\text{C}$ ), we established well-mixed and stratified area associated with monthly variations in the Yellow Sea. This was a first step for estimating primary production using remote sensing data. Most of the Yellow Sea is vertically well-mixed during winter season. The middle of the Yellow Sea is thermally stratified from spring through fall. There is a rapid onset of stratification from March to April and breakdown of stratification from September to October. The coastal areas of the Yellow Sea remain vertically well-mixed year-around due to tidal forces. However, the area around the

Changjiang River would be stratified in the surface layer due to strong halocline by the input of freshwaters from the Changjiang River during the summer season. The  $\log(H/U^3)$  criterion for identifying tidally mixed areas is useful only during the summer season. However, this criterion does not work in the Chinese coasts because the buoyancy of the freshwater discharge from the Changjiang River creates a strong halocline in the surface layer.

The satellite data could be used as a criterion to discover the position of the well-mixed and the stratified areas. High sediment or turbidity would indicate shallow well-mixed regions, and thus a threshold for nLw667 might be used. However, since the Chinese coast is strongly influenced by the large input of freshwaters from the Changjiang River, the nLw667 threshold would work more reasonably along the Korean coasts, especially in the southwest coast of Korea. Maps of the well-mixed area were derived from MODIS nLw667 using the relationship between the nLw667 and the model  $\Delta T$  in the southeastern Yellow Sea for the warmer months (April to September). The well-mixed areas were located where nLw667 is higher than  $2-4 \text{ W}\cdot\text{m}^{-2}\cdot\text{nm}^{-1}\cdot\text{sr}^{-1}$  depending on the month. These results provide the basis for modeling vertical biomass profiles in estimating primary production using satellite data in the Yellow Sea.

#### **ACKNOWLEDGMENT**

This work was supported by a NASA MODIS Instrument Team investigation contract (NAS5-96063).

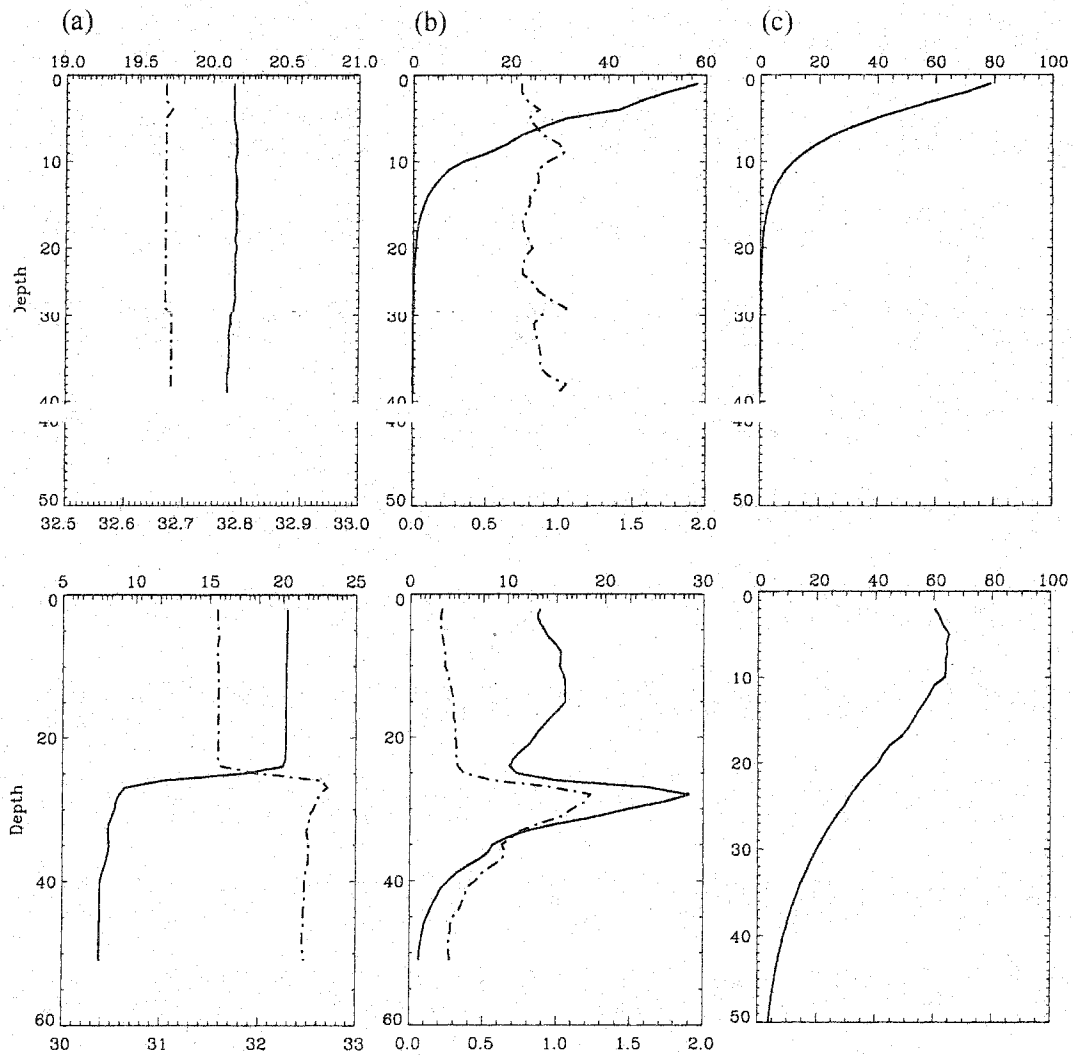


**Figure 3.1.** The profiles of (a) temperature (solid line) and salinity (dashed line), (b) primary production (solid line) and chlorophyll (dashed line), and (c) primary production divided by chlorophyll at a well-mixed area (126.0°E and 36.0°N; top figures) and at a stratified area (124.0°E and 36.0°E; bottom figures) in October, 1992. The data were obtained from Choi *et al.* (1995).

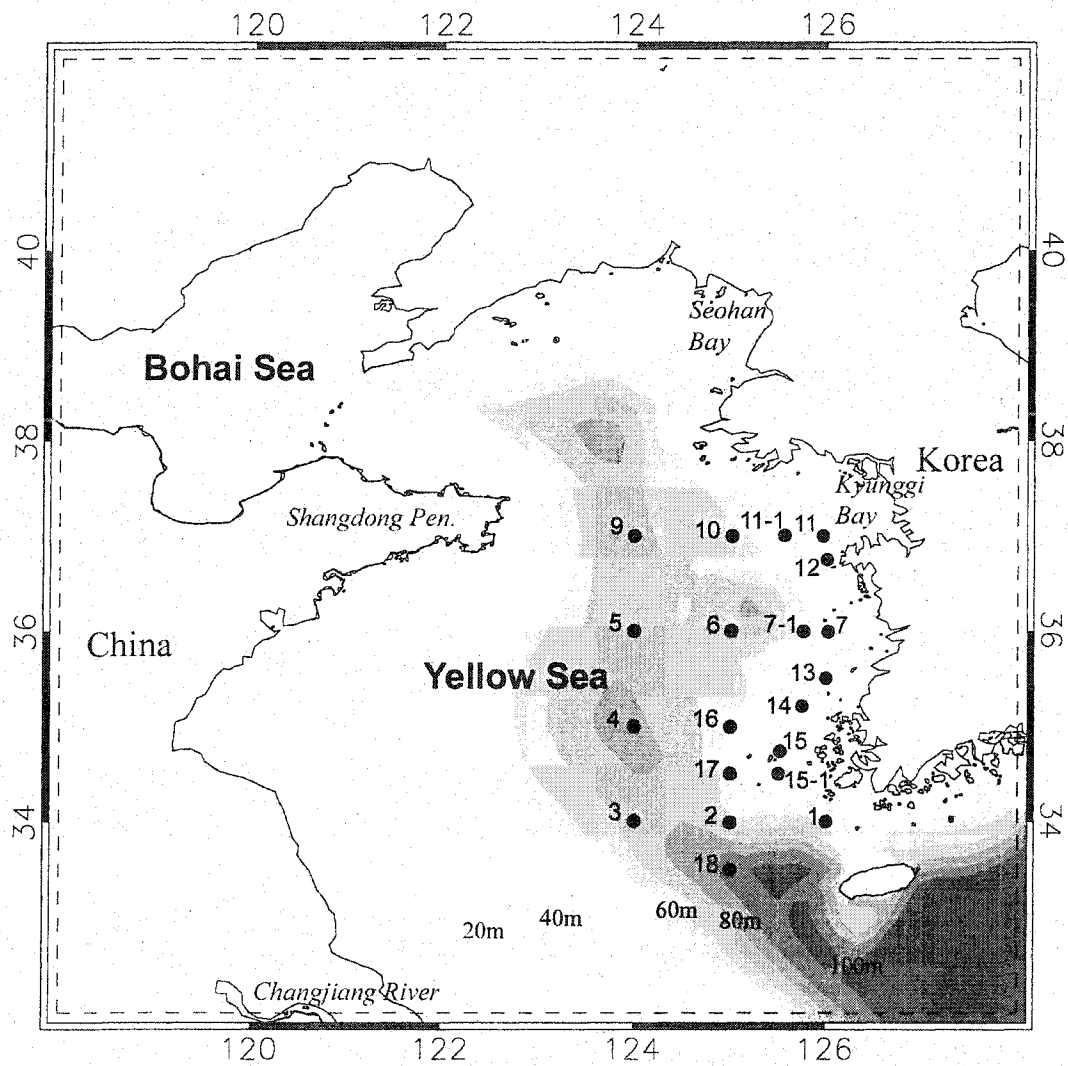


**Figure 3.2.** Study area and station maps with the bathymetry contours in the Yellow and East China Seas. The filled circles denote the stations observed in the Large Marine Ecosystem (LME) cruise in 14-21 June, 2000.

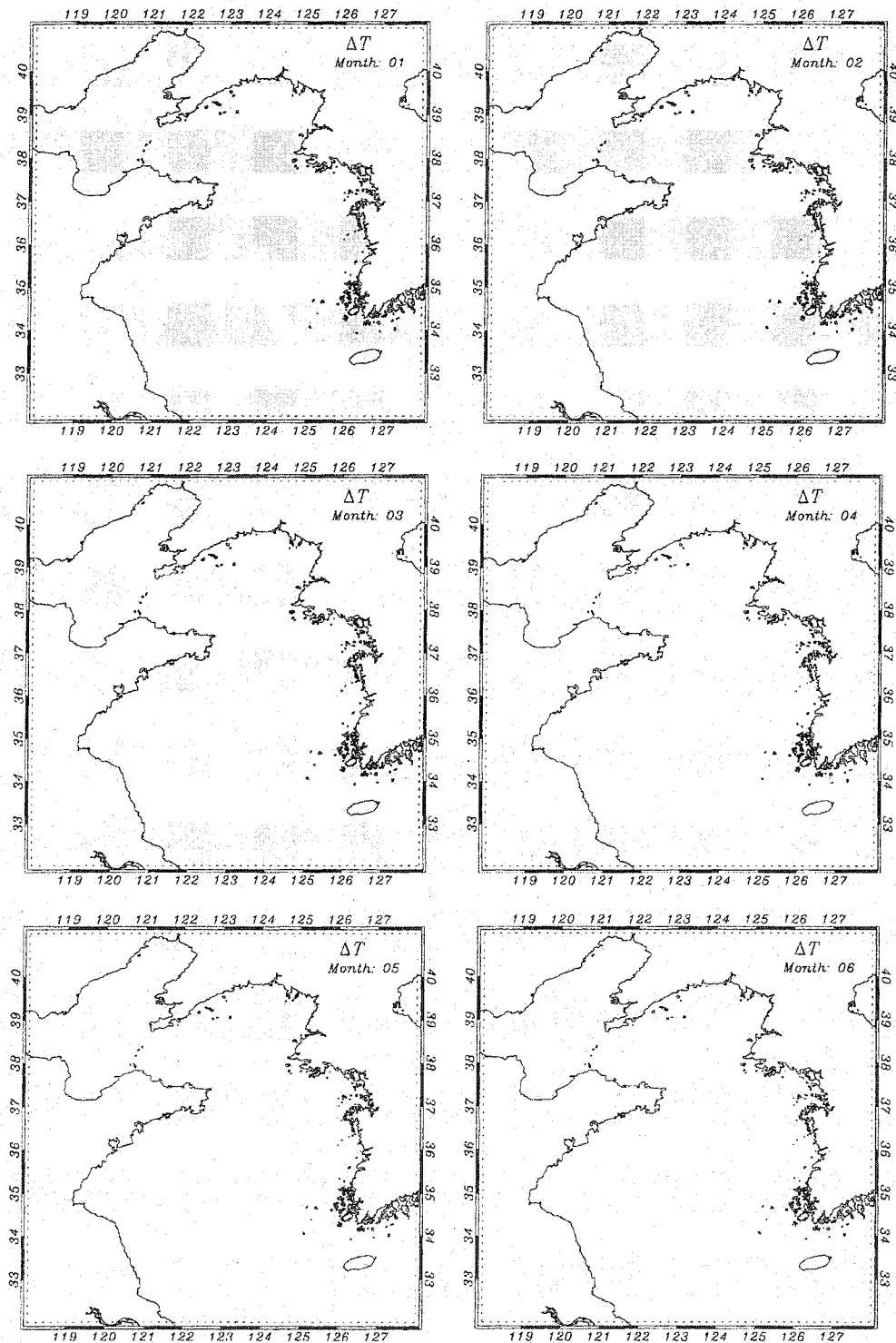


**Figure 3.3.** Distribution of well-mixed areas (filled gray) based on the temperature difference between surface and bottom ( $\Delta T < 0.8^\circ\text{C}$ ) from Moon's model for the 12 months from January to December.

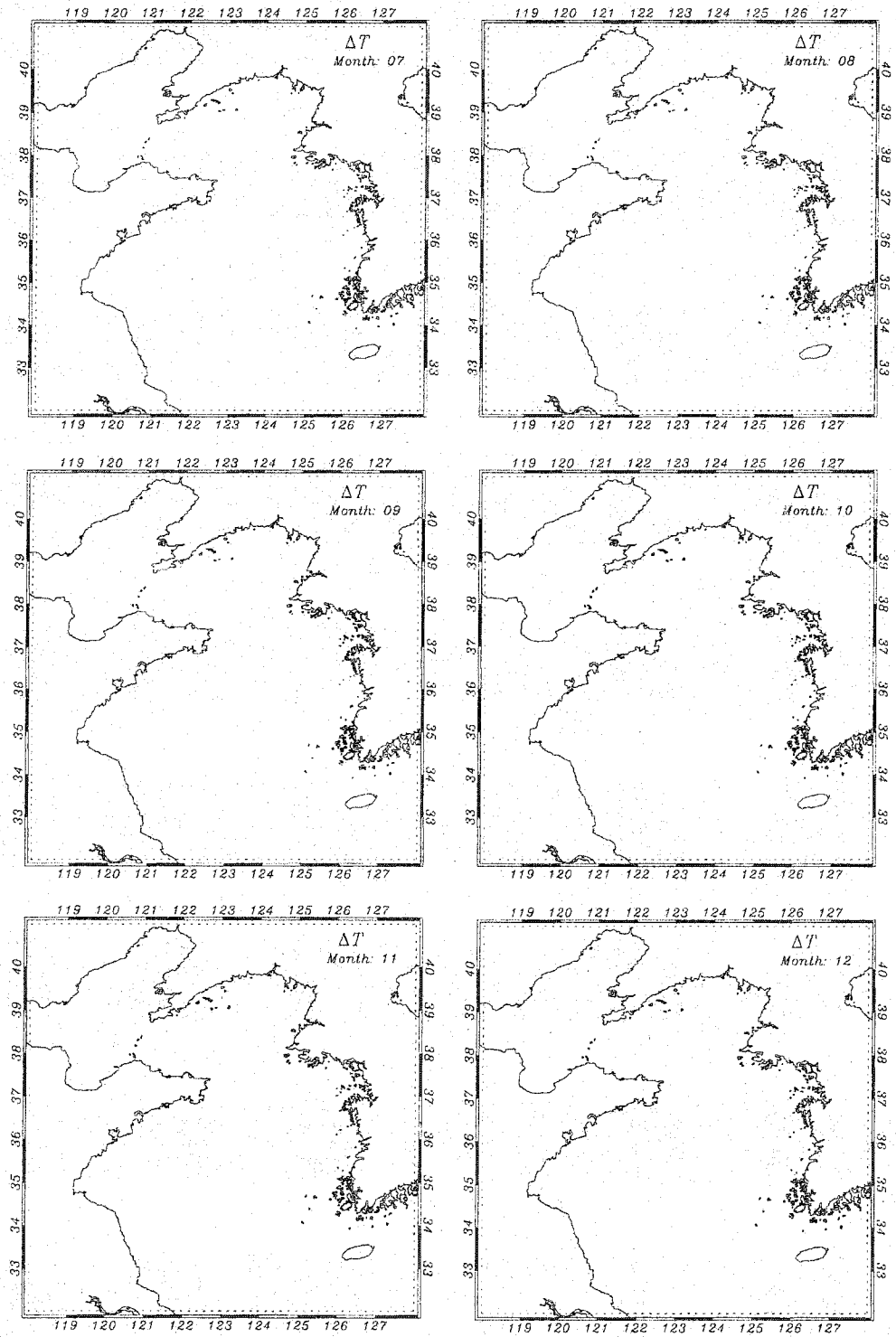
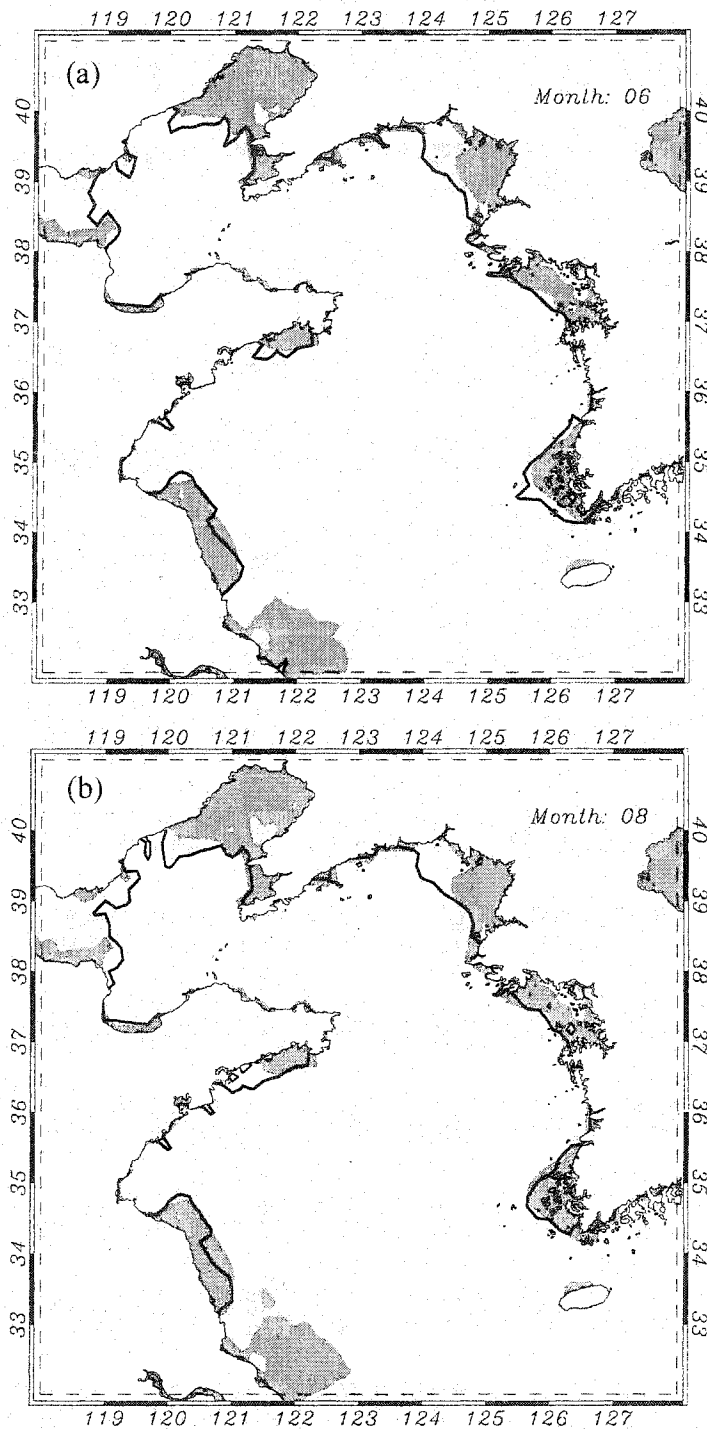
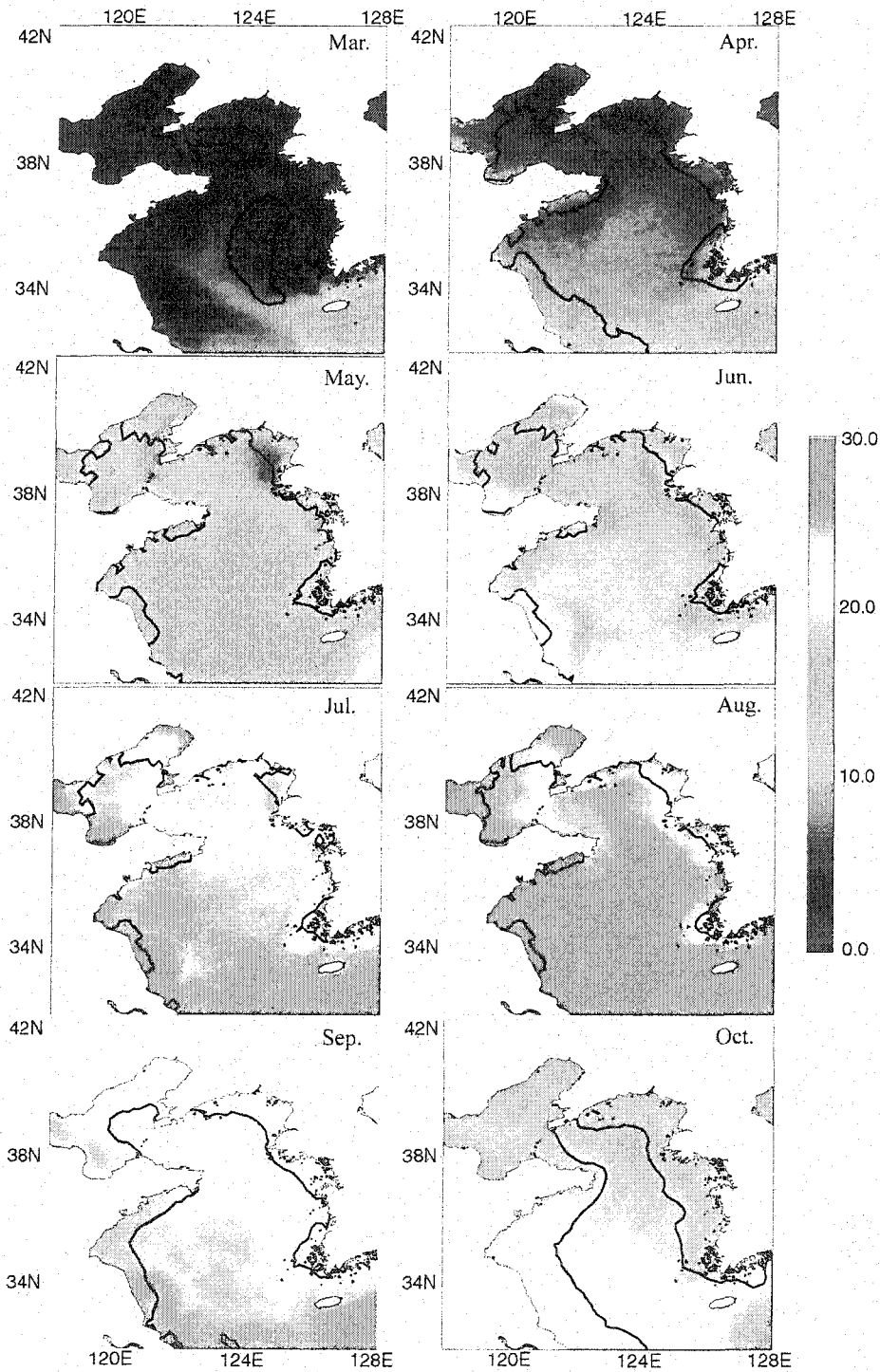


Figure 3.3. -- continued -



**Figure 3.4.** Contours of  $\log(H/U^3)$  in (a) June and (b) August in the Yellow and East China Seas. Filled contours denote  $\log(H/U^3) = 1.5, 2.0,$  and  $2.5$  (darker  $\rightarrow$  lighter shades) and the isoline of  $\Delta T = 0.8^\circ\text{C}$  is shown as solid black line.



**Figure 3.5.** Three-year (1998-2000) averaged monthly sea surface temperature images from MODIS for March to October with the isoline of  $\Delta T = 0.8^\circ\text{C}$  (black line). The scale shows SST in degrees Celsius ( $^\circ\text{C}$ ).



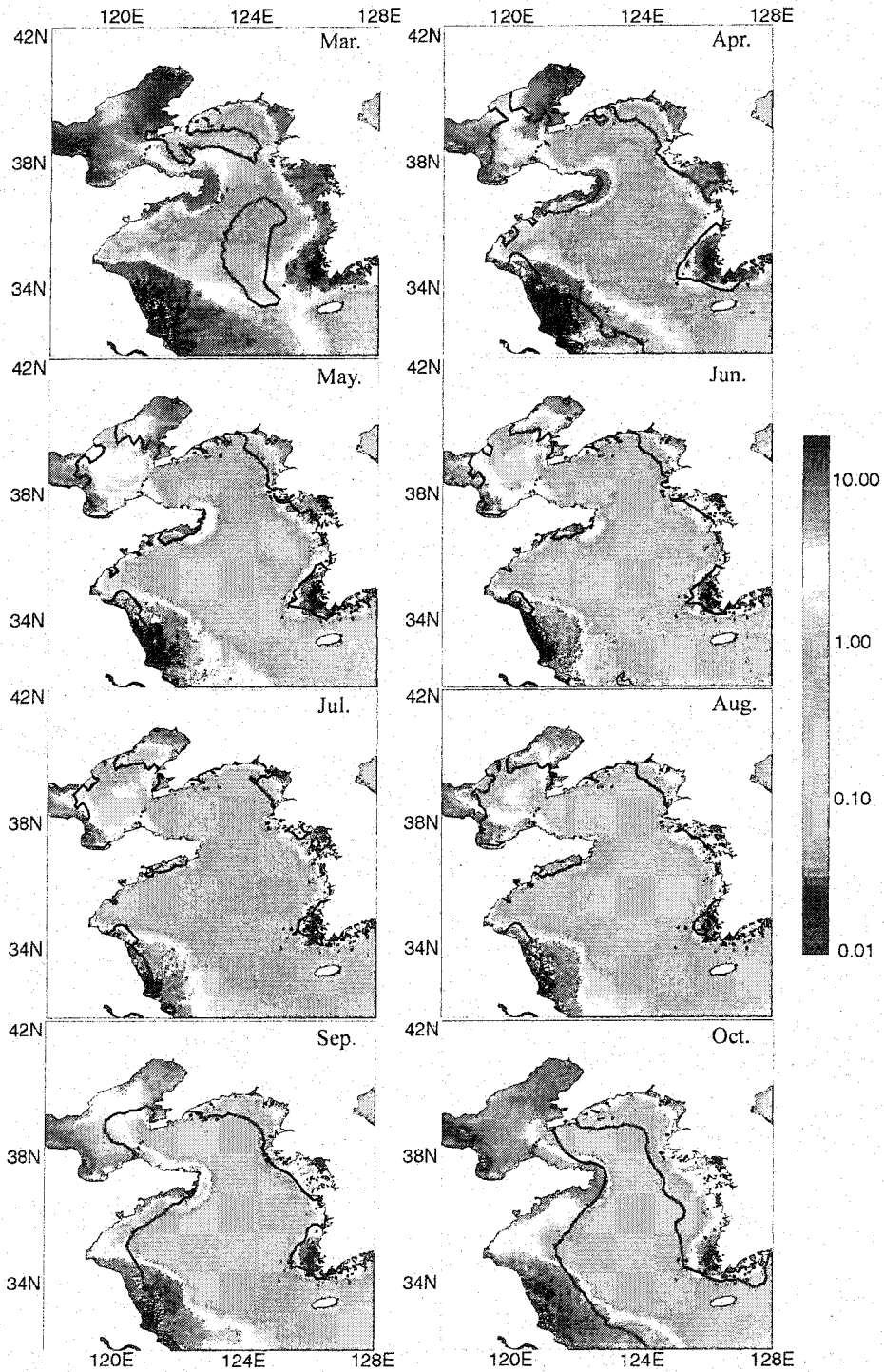


**Figure 3.6.** Three-year (1998-2000) averaged monthly 667-nm water-leaving radiance images from MODIS for March to October with the isoline of  $\Delta T = 0.8^\circ\text{C}$  (black line). The scales is  $nLw_{667}$  in units of  $\text{W}\cdot\text{m}^{-2}\cdot\text{nm}^{-1}\cdot\text{sr}^{-1}$ .

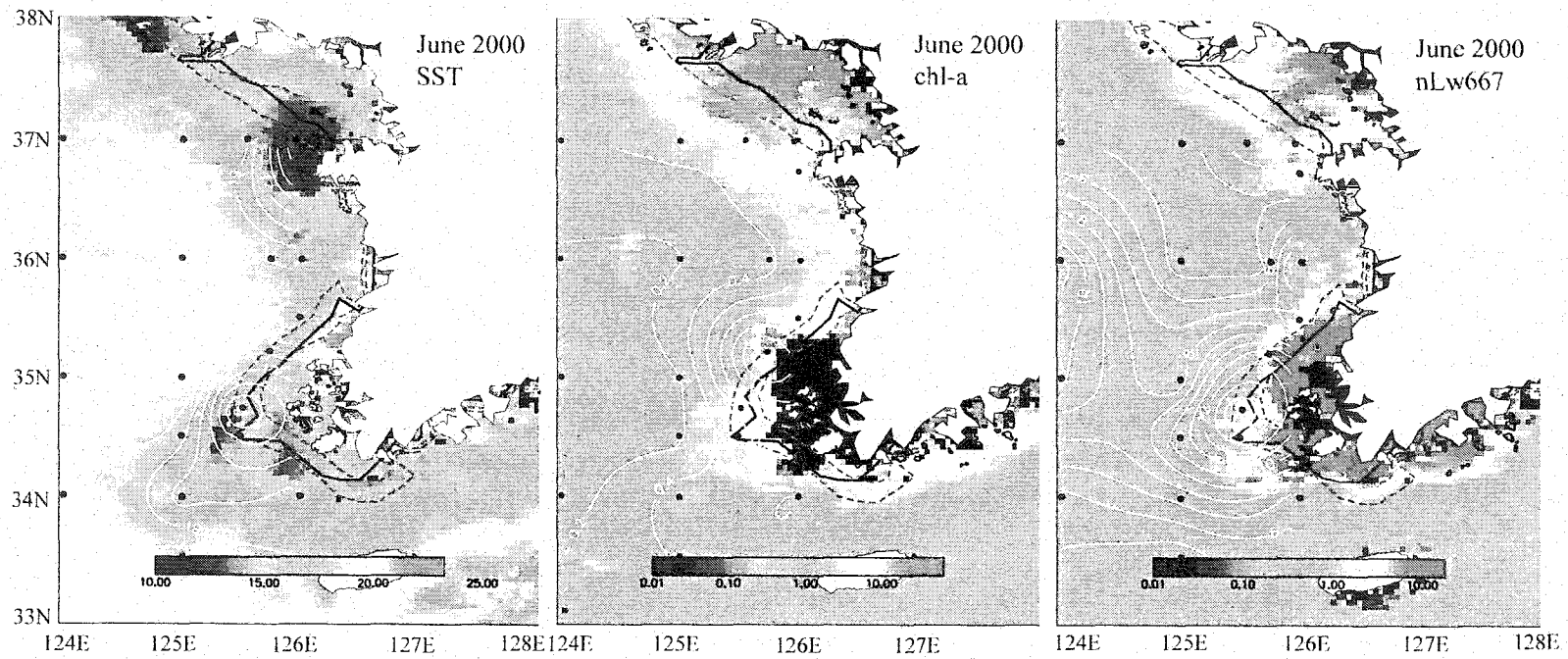


**Figure 3.7.** Contours of *in situ* measured (a) temperature, (b) chlorophyll-a, and (c) suspended sediment at the surface (white lines) in the southeastern Yellow Sea (June 14-21, 2000) superimposed on the monthly SST, chlorophyll-a, and nLw667 images from MODIS in June, 2000. Black line denotes the isoline of  $\Delta T = 0.8^\circ\text{C}$  and red dotted lines are the isolines of  $(H/U^3) = 1.5$  and 2.0.

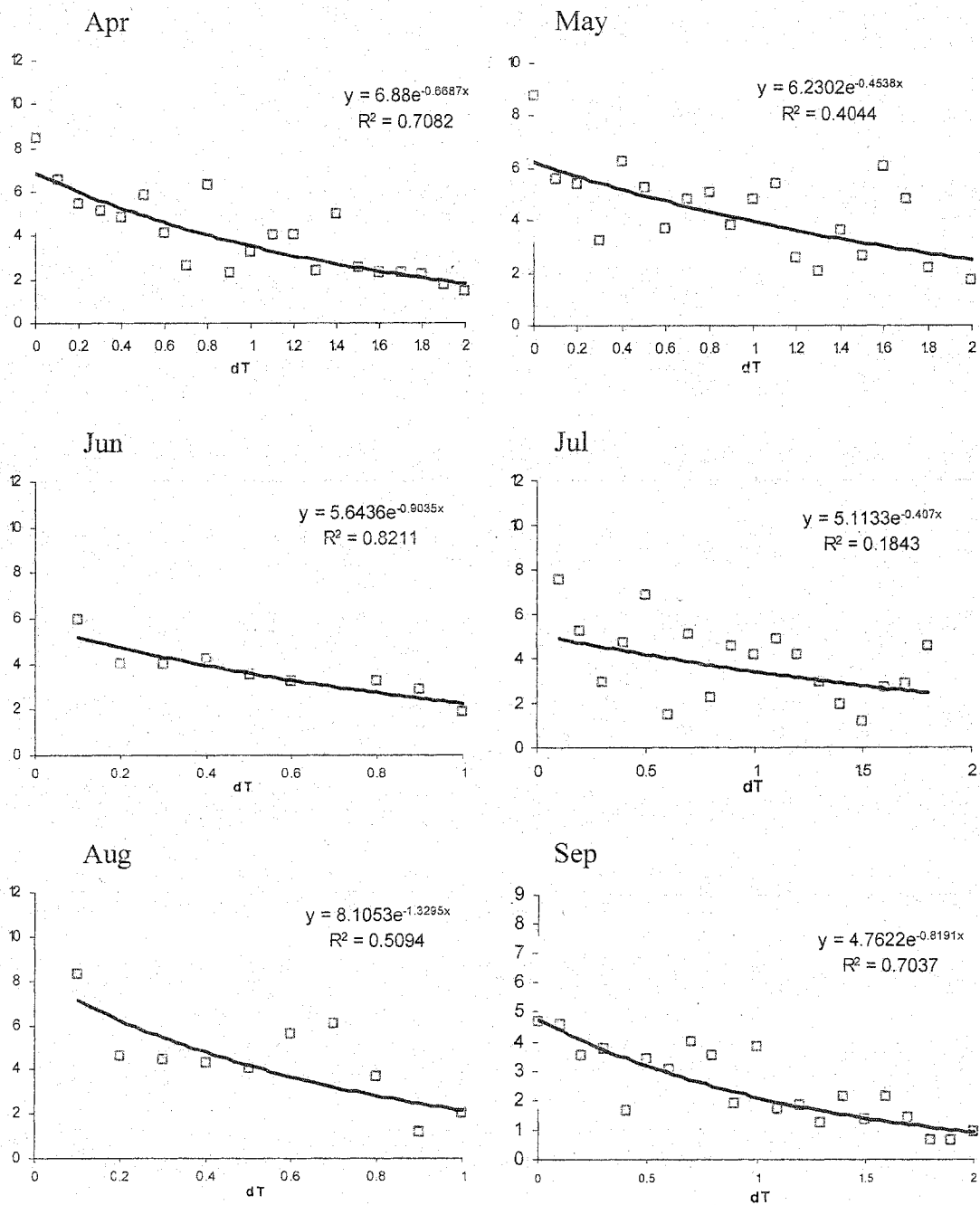


**Figure 3.8.** Bin averages of the composite (2000-2002) MODIS nLw667 are plotted against the model  $\Delta T$  with the error bar of one standard deviation in the southeast area of the Yellow Sea.

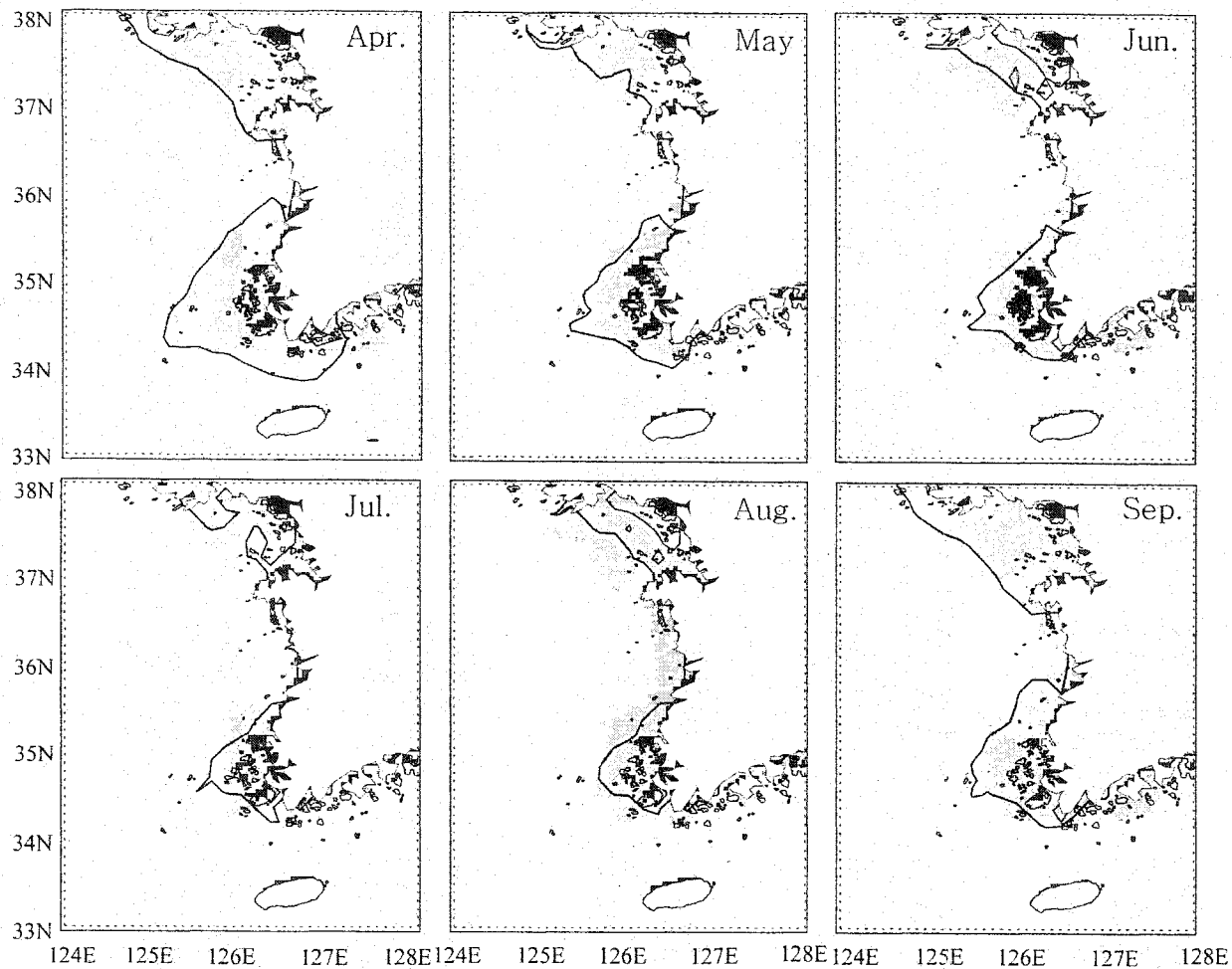


**Figure 3.9.** Map of well-mixed areas derived from MODIS nLw667 (gray filled) and isoline of the model  $\Delta T = 0.8^\circ\text{C}$  (solid black line).

## Chapter 4

### Primary Production by Ocean Color Remote Sensing in the Yellow Sea

(To be submitted to *Marine Ecology Progress Series* by Seung-Hyun Son, Janet Campbell, Mark Dowell, Sinjae Yoo, and Jae-Hoon Noh)

#### ABSTRACT

The Yellow Sea is a shelf sea surrounded by the Korean peninsula and the eastern coast of China. The bordering countries derive a substantial share of their food from fishing in these coastal waters. An existing primary production algorithm based on ocean color satellite data was used to derive the annual and daily rates of primary production in the Yellow Sea. The Yellow Sea was divided into three sub-areas: Chinese coastal waters, middle of the Yellow Sea, and Korean coastal waters. Sea-viewing Wide Field-of-view Sensor (SeaWiFS) data in 1998–2003 were processed after eliminating scenes on cloudy days. A local empirical chlorophyll algorithm was applied to derive more accurate chlorophyll concentration in the Yellow Sea. Diffuse attenuation was derived from a relationship between the SeaWiFS water-leaving radiance at 555nm and Secchi depth measured at more than 300 stations within  $\pm 1$  day of the satellite overpass.

Synoptic maps of water column integrated primary production were derived for the months of May and September because the only available *in situ* measurements were made in these two months. The middle of the Yellow Sea (MYS) was found to have higher levels of primary production in these months compared with the two shallower

(<50 m) coastal areas. The low primary production in the coastal areas is caused by high turbidity due to strong tides and shallow depths. Lower turbidity in the middle of the Yellow Sea allows the light energy for primary production to penetrate to a deeper depth. The mean daily rate of the integrated primary production in the middle of the Yellow Sea (MYS) was  $947 \text{ mgC m}^{-2} \text{ d}^{-1}$  in May and  $723 \text{ mgC m}^{-2} \text{ d}^{-1}$  in September. The mean values in Chinese coastal waters and Korean coastal waters were respectively 590 and  $589 \text{ mgC m}^{-2} \text{ d}^{-1}$  in May, and 734 and  $553 \text{ mgC m}^{-2} \text{ d}^{-1}$  in September. Our computation of daily total primary production for the entire the Yellow Sea is  $19.7 \times 10^4 \text{ tonC d}^{-1}$  in May and  $15.8 \times 10^4 \text{ tonC d}^{-1}$  in September.

By making assumptions regarding the vertical distribution of biomass and the photosynthetic parameters in other months, we computed annual primary production for each year from 1998 to 2002. The average daily rate was  $584.2 \text{ mgC m}^{-2} \text{ d}^{-1}$ , and the annual production ranged from  $47.8 \times 10^6 \text{ tonC y}^{-1}$  in 2000 to  $53.3 \times 10^6 \text{ tonC y}^{-1}$  in 1998, with an average annual production of  $50.1 \times 10^6 \text{ tonC y}^{-1}$ .

#### 4.1. INTRODUCTION

Coastal waters play an important role as food resource. While the coastal ocean occupies 8% of the ocean surface, about 90% of world commercial fish is caught in coastal waters (Pernetta and Milliman, 1995). Primary production has an importance as the basis of marine food webs and as a mediator of carbon flux in the ocean. It is

reported that the coastal primary production contributes 14~25% of the global oceanic primary production (Longhurst et al., 1995; Pernetta and Milliman, 1995).

The Yellow Sea is a shelf sea surrounded by the Korean peninsula and the eastern coasts of China, with a mean depth of 44 m and maximum depth of 103 m. The Yellow Sea is affected by strong tidal currents and discharges of the fresh waters from the Changjiang (Yangtze) River which is the largest river in Asia. The Kuroshio Current characterized as comparatively high temperature and saline waters also influences the southeastern area of the Yellow Sea.

There have been many studies of phytoplankton primary production based on field measurements in the Yellow Sea (Choi and Shim, 1986; Choi, 1991; Kang et al., 1992; Choi et al., 1995; Wu et al., 1995; Yoo and Shin, 1995). However, these studies were temporally and spatially restricted, so it is not possible to estimate primary production for the entire Yellow Sea based on these measurements alone. Ocean color data now provide the only means to determine the basin- to global-scale phytoplankton chlorophyll-a even though there are still problems to be solved (Balch et al., 1992; Sathyendranath and Platt, 1993). The model studies based on the remotely-sensed chlorophyll-a concentration allow estimating the basin and global scale ocean primary productivity (Platt et al., 1991; Balch et al., 1992; Longhurst et al., 1995; Antoine et al., 1995; Antoine and Morel, 1996; Behrenfeld and Falkowski, 1997; Hoepffner et al., 1999).

The standard algorithms for primary production rely on the remotely-sensed chlorophyll-a concentration, light attenuation, surface irradiance, and/or sea surface temperature. For the selection of the model for primary production at a local scale, there are other requirements such as vertical distribution of phytoplankton biomass and

photosynthetic parameters to be considered. To handle non-uniformity of the chlorophyll profile in the thermally stratified waters, it has been customary to extrapolate from the remotely sensed pigment at the surface to the vertical profile of phytoplankton biomass (Lewis et al., 1983; Platt et al., 1988b; Morel and Berthon, 1989). The shifted Gaussian distribution was proposed to derive the biomass profiles (Lewis et al., 1983; Platt et al., 1988b).

There are two main approaches to achieve the photosynthetic parameters although both methods have weakness (Platt et al., 1995). One is to derive the required parameter as a function of environmental variables such as sea surface temperature (Behrenfeld and Falkowski, 1997; Gong and Liu, 2003). The other is to assign the parameters based on their location and season from an existing database prescribed for biogeochemical provinces (Platt and Sathyendranath, 1988a; Sathyendranath et al., 1995; Longhurst et al., 1995; Hoepffner et al., 1999). The latter approach was applied to the Yellow Sea in this study.

We used the existing productivity algorithm of Platt and Sathyendranath (1988a) to estimate phytoplankton primary production in the Yellow Sea. We first partitioned the Yellow Sea into three subregions based on the bathymetry and physical features, and used *in situ* measurements from these subregions made in May and September to parameterize the algorithm. We explored several ways of estimating the diffuse attenuation coefficient,  $K_d$ , and investigated whether it was necessary to model the vertical biomass profile. Finally, the algorithm was applied to derive the primary production in the Yellow Sea. The resulting maps of primary production calculated from



the remotely sensed data provide the first synoptic views of primary production in the Yellow Sea.

## **4.2. DATA and Methods**

### **4.2.1. *in situ* data**

The information on ship-measured data for phytoplankton biomass and primary production in the Yellow Sea (within 32-37°N and 122-127°E) is summarized in Table 4.1. There were 141 photosynthesis-light (P versus E curve) parameters measured from six different cruises between 1992 and 1998. Of the parameters, 93 P-E parameters were obtained at the surface, 37 were between 10 and 30 meters, and 11 were between 40 and 75 meters. All measurements of the P-E parameters were based on C-14 methods (Steemann Nielsen, 1952). Water samples were incubated for 2 hours on the deck of the ship under screened lights simulating 0 to 100% of the surface PAR with 9 to 10 levels. The P-E data were then fitted as described by Platt et al. (1980). For more details, see Park (2000) and Choi et al. (1995).

Chlorophyll-a fluorescence profiles were measured using CTD-SBE 25. There were 86 fluorescence profiles available for this study. The chlorophyll fluorescence was calibrated with discrete chlorophyll-a which was measured fluorometrically (Turner Design Inc.).

All *in situ* data were distributed in two months, May and September. Estimates of daily water column primary production were made only at 37 stations from the

September 1992 cruise of Choi et al. (1995) (Fig. 4.1(b)). Column integrated primary production could not be estimated at the other stations because there was no information on the light profile or diffuse attenuation at those stations. The daily water column primary production at these 37 stations was compared with satellite-based primary production although the satellite data were not coincident in time with the *in situ* data.

Ship-measured transparency (Secchi depth) data for the southeastern area of the Yellow Sea was obtained from the Korea Oceanographic Data Center (KODC) and compared with the SeaWiFS water-leaving radiance at 555 nm to explore a means of estimating the diffuse attenuation. The serial oceanographic observations were carried out bimonthly (February, April, June, August, October, and December) in Korean waters by the National Fisheries Research and Development Institute (NFRDI). Transparency data for 71 stations in the Yellow Sea from 1998 to 2002 were used (Fig. 4.1(a)).

#### **4.2.2. Satellite data**

SeaWiFS level-1a version-4 data from 1998 and 2003 for the Yellow Sea were obtained from the NASA Goddard Space Flight Center (GSFC). The daily SeaWiFS data with spatial resolution of  $1 \times 1 \text{ km}^2$  were processed from level 0 to level 2 and remapped using the SeaWiFS Data Analysis System (SeaDAS) version 4.4 software offered by NASA GSFC. The standard algorithms in SeaDAS were used for SeaWiFS atmospheric corrections. After eliminating images on cloudy days, more than 1350 individual

SeaWiFS scenes from 1998 to 2003 were used to derive primary production, and then the SeaWiFS products and primary production images were averaged monthly.

The standard algorithm of the remotely-sensed chlorophyll-a concentration is based on Case 1 waters, which are defined as those waters where phytoplankton pigments are the primary factor determining the color of the water (Morel and Prieur, 1977). In coastal waters (Case 2 waters), the water color is affected by suspended sediments and/or colored dissolved organic matter as well as chlorophyll-a concentration. Thus, the standard algorithms do not provide accurate chlorophyll concentrations in Case 2 waters.

Large areas of the Yellow Sea are recognized as Case 2 waters due to their shallow depth, strong tidal mixing, and river discharges while the middle of the Yellow Sea is characterized as Case 1 waters in the warm seasons (spring to fall). Here we used a local empirical algorithm of chlorophyll-a concentration for the Yellow Sea developed by Ahn (2004) as follows:

$$Chl - a = 1.30 \times \left[ \frac{Rrs490}{Rrs555} \right]^{-1.90} \quad (4.1)$$

where,  $Rrs490$  and  $Rrs555$  are remote-sensing reflectance at 490 and 555nm. The algorithm was developed using measured remote sensing reflectance from the Dual UV/VNIR spectroradiometer at about 200 stations in the Korean Seas as well as measured chlorophyll concentrations. Although this is still a case-1 algorithm (since it doesn't account for other independently varying materials) its accuracy was improved for the Yellow Sea (RMS error =  $0.34 \text{ mg m}^{-3}$ ) compared with the standard algorithms (RMS errors were  $0.618 \text{ mg m}^{-3}$  for OC2 ver. 3 and  $0.663 \text{ mg m}^{-3}$  for OC4).

### 4.2.3. Parameterization of primary production model

#### 4.2.3.1. Primary production model

Since there are no available spectral light or phytoplankton absorption measurements from the cruises, a non-spectral primary production model was used (Platt and Sathyendranath, 1988a) for estimating primary production in the Yellow Sea. Daily depth integrated primary production (IPP) was derived using the following equation:

$$IPP = \int_{t_1}^{t_2} \int_0^{z_{cu}} \frac{B(z) \cdot \alpha^B \cdot E(z,t)}{\sqrt{1 + (\alpha^B \cdot E(z,t) / P_m^B)^2}} dz \cdot dt, \quad (4.2)$$

where  $B(z)$  is the chlorophyll-a concentration at depth  $z$ ;  $\alpha^B$  is the initial slope of the  $P^B$  vs  $E$  curve;  $E(z,t)$  is the irradiance at depth  $z$  and time  $t$ ;  $P_m^B$  is the assimilation number;  $t_1$  and  $t_2$  are the times of sunrise and sunset; and  $Z_{cu}$  is the euphotic depth. The vertical PAR profile is given by  $E(z,t) = E(0,t) \cdot \exp(-K_d \cdot z)$  where  $E(0)$  is PAR incident on the surface, and  $K_d$  is the diffuse attenuation coefficient for PAR. The input parameters used in the primary production model (eq. 4.2) are described in the following sections.

#### 4.2.3.2. Biomass profile (DCM model)

The Yellow Sea was classified as well-mixed and stratified waters. To differentiate two waters, the method proposed in the previous chapter with the SeaWiFS

water-leaving radiance at 670nm was used. We assumed that the biomass profile was uniform in the well-mixed waters and non-uniform in the stratified waters. Chlorophyll-a concentration was taken as the biomass index.

In order to generalize the biomass profile and to obtain four parameters for the stratified waters, the shifted Gaussian distribution model (Platt et al., 1988b; Sathyendranath and Platt, 1989) was fitted to the 86 chlorophyll profiles. The biomass profile was parameterized as follows:

$$B(z) = B_0 + \frac{h}{\sigma\sqrt{2\pi}} \exp\left[-\frac{(z-z_m)^2}{2\sigma^2}\right] \quad (4.3)$$

where  $B_0$  is a background biomass ( $\text{mg m}^{-3}$ );  $z_m$  is the depth of the chlorophyll maximum (m);  $\sigma$  is a measure of the thickness or vertical spread of the peak (m);  $h$  is the total biomass above the background ( $\text{mg m}^{-2}$ ), and the peak height above the baseline is given by  $H = h/(\sigma\sqrt{2\pi})$ .

#### 4.2.3.3. PAR profile

The photosynthetically available radiation (PAR) product of SeaWiFS was used for the incident surface light,  $E(0,t)$ , and the PAR profile was  $E(z,t) = E(0,t) \cdot \exp(-K_d \cdot z)$ . We still needed a way to estimate the diffuse attenuation coefficient,  $K_d$ . Unfortunately, there were very few available light measurements in the Yellow Sea for this study. Since large areas of the Yellow Sea are affected by colored dissolved organic matter and

suspended sediments, the diffuse attenuation model of Sathyendranath and Platt (1988) which is for Case 1 waters (i.e., based on chlorophyll) was not applicable for the Yellow Sea.

The Secchi depth data obtained from the serial oceanographic observations by the NFRDI provided the best source of information about light extinction in these coastal Korean waters. In addition, we had data from 17 stations where  $K_d$  and Secchi depth had been measured at the same time in the Yellow Sea. The  $K_d$  values were derived from measurements by a PAR sensor attached to the CTD SBE25. The relationship between Secchi depth and  $K_d$  for these stations is shown in figure 4.2. Also shown is the relationship  $K_d = 1.44/SD$  (Kirk, 1994), which appears to be in reasonable agreement with the data. Therefore, we used this relationship to derive  $K_d$  from the NFRDI Secchi depth data.

The Secchi depth (S.D.) data obtained from KODC in the period between 1998 and 2002 in the eastern part of the Yellow Sea were matched with SeaWiFS data. About 300 of 2100 Secchi depth measurements were matched up with SeaWiFS data acquired from one day before to one day after (one day before – 89 stations, same day – 149 stations, and one day after – 62 stations).

We compared the SeaWiFS K490 and nLw555 products with the match-up Secchi depth (SD) measurements (Fig. 4.3 and 4.4). The SeaWiFS K490 with  $r^2 = 0.5$  (Fig. 4.3) was not well correlated to Secchi depth. However, the nLw555 with  $r^2 = 0.78$  (Fig. 4.4) was well correlated to the Secchi depths. Therefore, we used the derived relationship  $SD = 6.4023 \times (nLw555)^{-0.7269}$  to estimate Secchi depth, which was then converted to diffuse attenuation coefficient by the relationship,  $K_d = 1.44/SD$  (Kirk, 1994).

The euphotic depth ( $Z_{eu}$ ) was defined as the depth at which PAR is 1 % of the surface PAR. Accordingly, the euphotic depth is given by  $4.6/K_d$  with the assumption that  $K_d$  is approximately constant with depth (Kirk, 1994). Given the relationship with Secchi depth, the euphotic depth was then derived by  $Z_{eu} = 3.2 \times SD$ .

#### 4.2.3.4. *Photosynthetic parameters*

Two approaches to estimate the photosynthetic parameters for primary production were mentioned above. To consider the first approach, we investigated the relationship between sea surface temperature and the photosynthetic parameter ( $P_m^B$ ) (Behrenfeld and Falkowski, 1997). There was no apparent relationship in our data set from the Yellow Sea (Fig. 4.5). Thus, we chose to use the second approach whereby parameters are assigned based on a partitioning of the ocean into biogeochemical provinces (Longhurst et al. 1995; Platt et al. 1995; Sathyendranath et al. 1995).

To interpolate and extrapolate the measured parameters for estimating the primary production, which is spatially and temporarily limited in this study, to the scale of the satellite observations, the Yellow Sea between 32°N and 37°N latitude and between 122°E and 127°E longitude was divided into 3 sub-regions based on bathymetry and physical oceanographic features such as current system (Fig. 4.1(b)): the Chinese Coastal Waters (CCW) and the Korean Coastal Waters (KCW) which are regions shallower than 50 meters, and the Middle of the Yellow Sea (MYS) deeper than 50 meter. Ning *et al.*

(1998) did a similar partitioning of the major water masses in the Yellow Sea. Measured parameters within each region were averaged and these averages used in the algorithm.

#### 4.2.4. Oceanographic sub-regions

The two coastal regions, CCW and KCW, are affected by strong tidal mixing. The area around the Changjiang River is also strongly influenced by freshwater discharge which causes surface layer stratification. The annual mean of freshwater discharge from the Changjiang River is about  $2.9 \times 10^4 \text{ m}^3 \text{ s}^{-1}$  (Riedlinger and Preller, 1995). The KCW region is affected by freshwater discharge from the Han River and Keum River with mean annual discharge of about  $1.0 \times 10^3 \text{ m}^3 \text{ s}^{-1}$  (Schubel et al., 1984). The southern part of the KCW region is the strongest tidal mixing area all year round. The Korean Coastal Current flows southward along the southern edge of the Korean Peninsula year round (Mask et al., 1998). In the CCW, the Yellow Sea Cold Water flows southward year round along the Chinese coast, and the Changjiang Coastal Current, related to the Changjiang discharge, flows southward along the Chinese coast in winter and eastward in summer (Beardsley et al., 1983, 1985; Mask et al., 1998; Su, 1998).

In MYS, the Yellow Sea Warm Current, which is a branch of the Kuroshio Current, flows northward through the central area of the Yellow Sea. The southern part of the central Yellow Sea deeper than 50 m is more affected by the warm and saline waters of the Kuroshio Current. In the northern part of the MYS, the Yellow Sea Cold Water, which is formed by strong vertical mixing in winter, exists during the summer.



### 4.3. RESULTS

The means and standard deviations of the photosynthetic parameters for the three sub-regions in May and September are listed in Table 4.2 and are shown in Fig. 4.6. The means of assimilation number ( $P_m^B$ ) in September (5.49 – 6.69 mgC (mg Chl-a)<sup>-1</sup> hr<sup>-1</sup>) are higher than those in May (3.90 – 6.50 mgC (mg Chl-a)<sup>-1</sup> hr<sup>-1</sup>) over the regions. Mean values of  $P_m^B$  in the KCW (6.50 mgC (mg Chl-a)<sup>-1</sup> hr<sup>-1</sup>) was much higher than in the CCW (3.90 mgC (mg Chl-a)<sup>-1</sup> hr<sup>-1</sup>) and the MYS (3.99 mgC (mg Chl-a)<sup>-1</sup> hr<sup>-1</sup>) in May. The pattern was similar (highest in KCW) in September, but the variation was smaller. The means of light utilization efficiency ( $\alpha^B$ ) in September (0.0233 – 0.0293 mgC (mg Chl-a)<sup>-1</sup> hr<sup>-1</sup> [ $\mu\text{Eins m}^{-2} \text{s}^{-1}$ ]<sup>-1</sup>) are higher than those in May (0.0176 – 0.0221 mgC (mg Chl-a)<sup>-1</sup> hr<sup>-1</sup> [ $\mu\text{Eins m}^{-2} \text{s}^{-1}$ ]<sup>-1</sup>) as like  $P_m^B$ . The mean value is slightly higher in the MYS than in the coastal regions in May and September. Error bars shown in figure 4.6 are the 95% confidence intervals. While the error bars for both  $P_m^B$  and  $\alpha^B$  are reasonably small in MYS, those in the coastal regions are very high, especially in the KCW, due to the small number of observations in those locations.

The Gaussian parameters derived from fitting equation (4.3) to the measured chlorophyll profiles were averaged within each month in the 3 subregions. The mean vertical profiles of biomass in the sub-regions of the Yellow Sea are shown in figure 4.7. The chlorophyll profiles in the coastal waters have higher chlorophyll, a shallower  $z_m$ , and smaller  $h$  and  $\sigma$  compared with the profiles in the MYS in both May and September.

In the KCW and MYS, the mean  $z_m$  is deeper in May (17 m in KCW and 30 m in MYS) than in September (7.8 m in the coastal regions and 24 m in MYS) whereas in the CCW the mean of  $z_m$  is similar in both months. The mean of the chlorophyll concentration at surface is higher in May (0.79–1.76 mg m<sup>-3</sup>) than in September (0.44–0.96 mg m<sup>-3</sup>) and  $h$  is much higher in May (19–23 mg m<sup>-2</sup>) than in September (4.4–12.4 mg m<sup>-2</sup>). There is a large variability in the values of DCM parameters in the coastal regions.

To test the effect of the non-uniform biomass profile on primary production, we compared primary production calculated using a uniform biomass profile (equal to the surface chlorophyll) with the integrated primary production based on non-uniform biomass profiles measured at the 37 stations in September, 1992 (Choi et al. 1995). Except for the biomass profile,  $B(z)$ , the same measured variables were used in both calculations to derive the primary production according to equation (4.2). The scatter plot of uniform-biomass primary production (PP1) versus non-uniform-biomass primary production (PP2) is shown in figure 4.8. Using uniform biomass profiles, the primary production is underestimated by an average of 15.6% in regions deeper than 50 m (with maximum of 39%). In the shallower waters (< 50 m), error between two primary productions was about 7%.

#### 4.3.1. Satellite-derive primary production

Monthly primary production was calculated for May and September because the input parameters ( $P_m^B$ ,  $\alpha^B$  and DCM parameters) were based on measurements made only in May and September (Table 4.1). The monthly composite images of PAR,  $K_d$ ,

chlorophyll, and primary production in 1998 – 2003 in May and September, as well as the 6-year average monthly composite images for these months, are shown in figures 4.9 and 4.10. In addition, the year-to-year variations of the mean values in each area are shown in figure 4.11.

The overall spatial distribution of PAR is uniform in May, but is increasing from south to north in September. On average, PAR was 26% higher in May (6-year mean of 58.3 – 58.6 Ein m<sup>-2</sup> d<sup>-1</sup>) than in September (6-year mean of 45.9 – 46.6 Ein m<sup>-2</sup> d<sup>-1</sup>). The PAR values varied interannually from 1998 to 2003. Lower values of PAR appeared in 1999 and 2003 in both months. PAR in September was higher in the Chinese coasts than in the Korean coasts since 2000.

The  $K_d$  images were derived from the SeaWiFS nLw555 image using the procedure described above. The spatial distribution of the 6-year average  $K_d$  in May and September are similar. High values of  $K_d$  were found near the Kyunggi Bay, the southwestern coastal regions of Korea, the Shangdong peninsula, and the Changjiang River in both months, while  $K_d$  was lower in the middle of the Yellow Sea. However, a comparatively high  $K_d$  patch appears in the middle of the Yellow Sea in May. The mean value of  $K_d$  based on the 6-year composite images for May ranged from 0.33 to 0.38 m<sup>-1</sup> in the coastal regions (CCW and KCW) to 0.13 m<sup>-1</sup> in the central regions of the Yellow Sea (MYS). The mean value of  $K_d$  in September in the central regions of the Yellow Sea are similar to those in May (0.12 m<sup>-1</sup>), but September values are slightly smaller in the coastal regions (0.30 m<sup>-1</sup>) compared to May. The interannual variability of  $K_d$  in the MYS is small while that in the coastal areas is comparatively strong.

The spatial patterns of chlorophyll are similar in both months. Higher chlorophyll appeared in coastal areas and near the Changjiang River, and relatively low values in the central area of the Yellow Sea. However, in May, a patch of significantly increased chlorophyll appeared in the middle of the Yellow Sea, located around a Korean dump site that has been used since 1992. The 6-year mean chlorophyll is slightly higher in May ( $0.95 \text{ mg m}^{-3}$ ) than in September ( $0.93 \text{ mg m}^{-3}$ ), and the chlorophyll is slightly higher in the Korean coastal waters ( $1.74$  in May and  $1.81 \text{ mg m}^{-3}$  in September) than in the Chinese coastal waters ( $1.61$  in May and  $1.46 \text{ mg m}^{-3}$  in September). The chlorophyll in May ( $0.70 \text{ mg m}^{-3}$ ) is slightly lower than in September in MYS ( $0.77 \text{ mg m}^{-3}$ ). The high chlorophyll patch in the middle of the Yellow Sea is shown in every year although its area and concentration varies. The patch spread widely in 1999 and is highest in 2001. The mean chlorophyll of May in all regions was highest in 2002, but that in September varied with regions. Interannual variability is stronger in September than in May.

The depth-integrated daily primary production of May and September in the Yellow Sea is shown in figure 4.10, and the means and the standard deviations of the primary production calculated for each sub-region are given in Table 4.3. The spatial distribution of the primary production in the 6-year composite images is similar in both months, with lower primary production along the southwest coast of Korea, near the Kyunggi Bay, near the Shandong Peninsula and near the Changjiang river, and with higher primary production in the middle of the Yellow Sea. The primary production in the middle of the Yellow Sea is more uniform in May while the primary production is comparatively higher in the eastern area of the mid-Yellow Sea. The values of primary production overall the Yellow Sea are higher in May than in September. The mean of

primary production in the middle of the Yellow Sea (MYS) is  $947 \text{ mgC m}^{-2} \text{ d}^{-1}$  in May and  $723 \text{ mgC m}^{-2} \text{ d}^{-1}$  in September. The mean of the primary production in the coastal regions varies from 508 to  $734 \text{ mgC m}^{-2} \text{ d}^{-1}$  in May and from 554 to  $589 \text{ mgC m}^{-2} \text{ d}^{-1}$  in September. In May, the highest mean primary production levels in the middle of the Yellow Sea appeared in 2002 and the lowest levels in 2000. The high primary production patch in the middle of the Yellow Sea was significantly higher 1999. The mean IPP in both coastal regions, CCW and KCW, is highest in 1998 and lowest in 2003. In September, the highest IPP in the middle of the Yellow Sea appeared in 2003 and the lowest in 1999. While the variability pattern and values of IPP in May are similar in both coastal regions, those in September are significantly different in 2001 and 2002. The daily primary production estimated for the entire Yellow Sea is  $19.7 \times 10^4 \text{ tonC d}^{-1}$  in May and  $15.8 \times 10^4 \text{ tonC d}^{-1}$  in September.

We have *in situ* IPP measurements only in September, 1992 for the Yellow Sea. Thus there are no coincident measurements of primary production to validate the satellite-based primary production. However, we compared the measured IPP at 37 stations in September, 1992 to the range of values at the same locations in the monthly-composite satellite data from 1998 to 2003 (Fig. 4.12). At about two-thirds of the stations, the measured-measured IPP falls within the range of the satellite-derived values. Exceptions occurred along the C-line (Fig. 4.1b) where the satellite values were much higher than the measured IPP. In contrast, the measured IPP was significantly higher than the satellite values at station F07.

The input parameters such as  $P_m^B$ ,  $\alpha^B$ , and DCM parameters for the primary production were based on *in situ* measurements made only in May and September. To

estimate annual primary production in the Yellow Sea required several assumptions about seasonal variability based on this limited information. From the results presented in Chapter 2, the Yellow Sea was regarded as totally well-mixed waters from November to March, and the average values of P-E parameters in May and September were used for the primary production. The input parameters based on *in situ* measurements in May were used for the primary production in May to August, and the values for September were used for April, September, and October. Primary production was then estimated from all the SeaWiFS data between 1998 and 2002. Monthly composites were formed and then annual composites were produced by averaging the individual monthly composites (Table 4.4 and Fig. 4.13). The average daily rate was  $584.2 \text{ mgC m}^{-2} \text{ d}^{-1}$ , and the annual production ranged from  $47.8 \times 10^6 \text{ tonC y}^{-1}$  in 2000 to  $53.3 \times 10^6 \text{ tonC y}^{-1}$  in 1998, with an average annual production of  $50.1 \times 10^6 \text{ tonC y}^{-1}$ .

#### **4.4. DISCUSSION and CONCLUSION**

In this study, primary production using uniform biomass profile was underestimated by 15% with maximum of 40% in the deeper waters (>50m). However, error between primary production using uniform and non-uniform biomass profile was relatively small (mean of 7%) in the coastal waters (<50m). This result is similar to others in different seas. The integrated primary production using uniform biomass profile was underestimated by about 20% compared with the primary production based on the vertically non-uniform biomass algorithm in the North Atlantic (Platt et al., 1991).

Primary production derived from the uniform profile (wavelength-integrated) model was underestimated by 20 – 35 % in Kuroshio and the frontal regions of the East China Sea (Siswanto, et al., 2004).

Following Platt et al. (1988b), measurement technique cannot do better than  $\pm 5\%$  for  $P_m^B$  and  $\pm 20\%$  for  $\alpha^B$ . Another error is related to the aggregation of the parameters within provinces (Platt et al. 1995). The natural variability within each province is reflected in the 95% confidence intervals for the mean, which were in the range of  $\pm 12\%$  (MYS) to  $\pm 54\%$  (KCW) for  $\alpha^B$  and in the range of  $\pm 13\%$  (MYS) to  $\pm 44\%$  (KCW) for  $P_m^B$ . Some uncertainty in the coastal regions comes from the small number of data points. It is reported that the computed primary production is more sensitive to changes of the P-E parameters than chlorophyll–profile parameters in the North Atlantic (Sathyendranath, et al., 1995). Thus, more information on the distribution of P-E parameters would be required to improve estimations of primary production.

Spectrally– and depth–resolved primary production algorithms have been considered as benchmarks in estimating primary production (Platt et al., 1991; Kyewalyanga et al., 1992). Most of the studies were in open ocean waters and used a spectral model for the light field in the water column based on Case 1 waters. The Case 1 spectral model is not applicable in the Yellow Sea because large areas of the Yellow Sea are Case 2 waters. Son et al. (2001) showed values of diffuse attenuation based on a Case 1 (chlorophyll-dependent) model underestimated  $K_d$  in case-2 waters by a factor of 2 to 4. We had very few light measurements in our data base. From 17 coincident measurements of Secchi depth and  $K_d$ , we found that  $K_d = 1.44/SD$  (Kirk, 1994) was a reasonable relationship to use. Using this relationship and an empirical relationship

between measured Secchi depth and satellite water-leaving radiances at 555 nm, we derived an algorithm for estimating  $K_d$ . We considered using the SeaWiFS K490 product, but its comparison with Secchi depth did not prove to be consistent in the Yellow Sea. The standard algorithm of the SeaWiFS K490 produces large uncertainty in turbid water, especially where K490 is greater than  $0.25 \text{ m}^{-1}$  (O'Reilly et al., 2000b). Thus the K490 product is not applicable in the Yellow Sea. The fitting of Secchi depth and the SeaWiFS nLw555 at about 300 stations in the southeastern Yellow Sea showed a good relationship with  $r^2 = 0.78$ .

The mean  $K_d$  derived from the nLw555 was about  $0.12 \text{ m}^{-1}$  in the central area and varied from  $0.3$  to  $0.38 \text{ m}^{-1}$  with maximum value of  $0.76 \text{ m}^{-1}$  in the coastal waters of the Yellow Sea. These values are similar to results of Son et al. (2001), where mean of  $K_d$  was  $0.20 \text{ m}^{-1}$  with minimum of  $0.09 \text{ m}^{-1}$  and maximum of  $0.74 \text{ m}^{-1}$  in the Yellow Sea.

Errors of the chlorophyll concentration derived from the ocean color satellites range from 50 to 100 % or more in the turbid waters found in the near-shore areas of the Northeastern Atlantic (Hoepffner et al., 1999). Since a large part of the Yellow Sea is characterized as Case 2 waters, the current standard chlorophyll algorithm overestimates the chlorophyll concentrations and consequently the primary production. Therefore, we chose a local empirical algorithm for chlorophyll-a concentration with lower RMS errors (Ahn, 2004). The SeaWiFS standard algorithms (OC2 and OC4) were compared with *in situ* measurements in the Korean waters (Ahn, 2004; Moon et al., 2002). The results showed that the SeaWiFS standard algorithms are suitable in the Sea of Japan and the Kuroshio waters which are characterized as Case 1 waters, but are not applicable for Case 2 waters such as the Yellow and East China Seas (RMS errors were  $0.618 \text{ mg m}^{-3}$  for



OC2 ver. 3 and  $0.663 \text{ mg m}^{-3}$  for OC4). Use of the empirical chlorophyll algorithm developed by Ahn (2004) was more reasonable for the estimation of the primary production in the Yellow Sea. Its accuracy was improved (RMS error =  $0.34 \text{ mg m}^{-3}$ ), although it is still a Case-1 algorithm since it does not account for variability in other optically active constituents.

In this study, we present monthly primary production only for two months, May and September, because input data such as photosynthetic and the vertical biomass distribution parameters were available only for these months. The estimate of primary production in the Yellow Sea includes new and regenerated production. In May, the IPP varied from 590 to 947 (with the overall mean of  $836 \text{ mgC m}^{-2} \text{ d}^{-1}$ ), and in September it varies from 554 to 723 (with the overall mean of  $672 \text{ mgC m}^{-2} \text{ d}^{-1}$ ). In both months, the primary production was lower in the coastal waters and higher in the middle of the Yellow Sea. This pattern was caused by higher turbidity and shallow depth in the coastal regions. The overall mean of primary production was 24% higher in May than in September, largely due to the fact that PAR was 26% higher in May than September. Thus the seasonal variation of light may be the important factor in determining variations in primary production.

There was higher primary production in the middle of the Yellow Sea (MYS) in May and September than in the coastal regions. There are only two studies describing the distribution of chlorophyll and primary productivity over all the Yellow Sea (Choi et al., 1995; Wu et al., 1995). Both were based on cruises made in September, 1992. The result of Choi et al. (1995) showed the mean primary production to be  $740 \text{ mgC m}^{-2} \text{ d}^{-1}$  which is similar to our result. Wu et al. (1995) reported a much lower mean primary production

(331 mgC m<sup>-2</sup> d<sup>-1</sup>) for the same month and year and similar stations. The large differences between these primary production estimates may be because they used different methods to derive the depth-integrated primary production. Choi et al. (1995) measured primary productivity using C-14 methods and estimated depth-integrated primary production with the formula of Platt et al. (1980). Wu et al. (1995) also measured primary production using a C-14 method, but used Cadee and Hegeman's (1974) formula to estimate depth-integrated primary production. In addition, they found very different chlorophyll levels (0.16 to 3.20 µg·l<sup>-1</sup> with mean of 0.69 µg·l<sup>-1</sup> – Choi et al.; 0.43 to 17.43 mg·m<sup>-3</sup> with mean of 1.362 mg·m<sup>-3</sup> – Wu et al.), which were curiously opposite in magnitude to the primary productivity differences. In this study, our primary production model is based on Platt et al. (1988), and we used the data measured by Choi et al. (1995) as input data for our algorithm. Thus, our result may be more comparable to that of Choi et al. (1995). In their results, the average primary production was 702 mgC m<sup>-2</sup> d<sup>-1</sup> in off-shore stratified waters and 620 mgC m<sup>-2</sup> d<sup>-1</sup> in the Korean coastal waters. Others reported that the primary production in the Kyunggi Bay was about 647 mgC m<sup>-2</sup> d<sup>-1</sup> in September (Chung and Park, 1988). The mean values are similar to our estimates; 740 mgC m<sup>-2</sup> d<sup>-1</sup> in the middle of the Yellow Sea and 684 mgC m<sup>-2</sup> d<sup>-1</sup> in the Korean coastal waters.

The mean daily rate of the integrated primary production in the middle of the Yellow Sea (MYS) was 947 mgC m<sup>-2</sup> d<sup>-1</sup> in May and 723 mgC m<sup>-2</sup> d<sup>-1</sup> in September. The mean values in Chinese coastal waters and Korean coastal waters were 590 and 734 mgC m<sup>-2</sup> d<sup>-1</sup>, respectively, in May, and 589 and 554 mgC m<sup>-2</sup> d<sup>-1</sup> in September. Our computation of daily primary production for the entire Yellow Sea is  $19.7 \times 10^4$  tonC d<sup>-1</sup> in May and  $15.8 \times 10^4$  tonC d<sup>-1</sup> in September.

Choi et al. (2004) measured primary production in the southeastern area of the Yellow Sea in five months of 1997. However, there is no measurement in May and September, but in February, April, August, October and December. It is not possible to compare their results with our estimates quantitatively. However, the spatial distributions of primary production are similar: lower primary production in the Kyunngi Bay and the southwestern coastal waters of Korea, and higher levels in the central waters of the Yellow Sea. The low primary production in the coastal areas is caused by the high turbidity caused by strong tides and shallow depths. Lower turbidity in the middle of the Yellow Sea allows for the penetration of light to greater depths.

We do not have any measured primary production data to validate the model primary production. However, we compared the primary production measured at 37 stations in September, 1992 with the satellite-based monthly composite primary production in September from 1998 to 2003. The values of the measured IPP generally fall in the range of the satellite-derived IPP from 1998 to 2003 although about one third of the measured IPP was much lower than the satellite values. As mentioned above, we do not have *in situ* measured primary production that are coincident in time with the satellite data. However, from the results, estimates of the primary production seem to be reasonable.

Our calculation showed that the annual total primary production in the Yellow Sea varied from  $47.8$  to  $53.3 \times 10^6$  ton C yr<sup>-1</sup> with a mean of  $50.13 \times 10^6$  ton C yr<sup>-1</sup>. The input parameters such as P-E and DCM parameters in May and September were used for the primary production in the other months. Thus, for more accurate estimates of the primary production in the Yellow Sea, obtaining more data is indispensable. However

crude, our results provide the first synoptic maps of primary production in the Yellow Sea.

### **Acknowledgements**

This work was supported by a NASA MODIS Instrument Team investigation contract (NAS5-96063) and the International Ocean Color Coordinating Group (IOCCG) Visiting Fellowship.

**Table 4.1.** Sources of data for the chlorophyll profiles and P-E parameters in the Yellow Sea (32-37°N and 122-127°E). Total number is 141 stations.

Cruise name	Source	Period	No. of P-E parameters	No. of chl. profiles
YS-9210	Choi et al. (1992)	17 Sep – 2 Oct, 1992	38	38
COPEX <sup>(1)</sup>	KORDI <sup>(3)</sup>	29 Aug – 5 Sep, 1994	11	10
COPEX	KORDI	26 Apr – 6 May, 1995	24	9
LME <sup>(2)</sup>	KORDI	20-24 May, 1996	12	11
LME	KORDI	20-31 May, 1997	36	14
LME	KORDI	15-19 May, 1998	20	4
Total			141	86

(1) The Coastal Ocean Process Experiment cruise

(2) The Yellow Sea Large Marine Ecosystem cruise

(3) Korea Ocean Research and Development Institute, South Korea

**Table 4.2.** P-E parameters for the 3 regions of the Yellow Sea.

Sub-regions		$\alpha^B$		$P_m^B$		no
		mean	stdev	mean	stdev	
May	CCW	0.0176	0.0062	3.90	1.52	8
	MYW	0.0221	0.0141	3.99	2.52	75
	KCW	0.0204	0.0096	6.50	3.46	9
Sep.	CCW	0.0268	0.0068	6.24	1.99	14
	MYW	0.0293	0.0097	5.49	2.01	31
	KCW	0.0233	0.0079	6.69	1.87	4
Total		0.0239	0.0122	4.78	2.54	141

**Table 4.3.** Primary production in the 3 regions of the Yellow Sea.

Sub-region	Area $\times 10^3$ $\text{km}^2$	Mean Primary Production Rate			
		$\text{mgC m}^{-2} \text{d}^{-1}$		$\times 10^4 \text{ tonC d}^{-1}$	
		May	Sep	May	Sep
<b>CCW</b>	58.9	590.3	589.3	3.5	3.5
<b>MYW</b>	147.4	946.5	722.6	13.9	10.6
<b>KCW</b>	28.9	734.2	553.7	2.1	1.6
<i>mean</i>		835.6	672.4		
<i>total</i>	235.2			19.7	15.8

**Table 4.4.** Annual total primary production in the Yellow Sea.

Year	Area $\times 10^3 \text{ km}^2$	Daily mean PP	Annual total PP
		$\text{mgC m}^{-2} \text{d}^{-1}$	$\times 10^6 \text{ ton C yr}^{-1}$
<b>1998</b>		612.9	53.3
<b>1999</b>		559.6	48.0
<b>2000</b>	235.2	557.7	47.8
<b>2001</b>		586.2	50.3
<b>2002</b>		595.5	51.1
<i>mean</i>		584.2	50.1

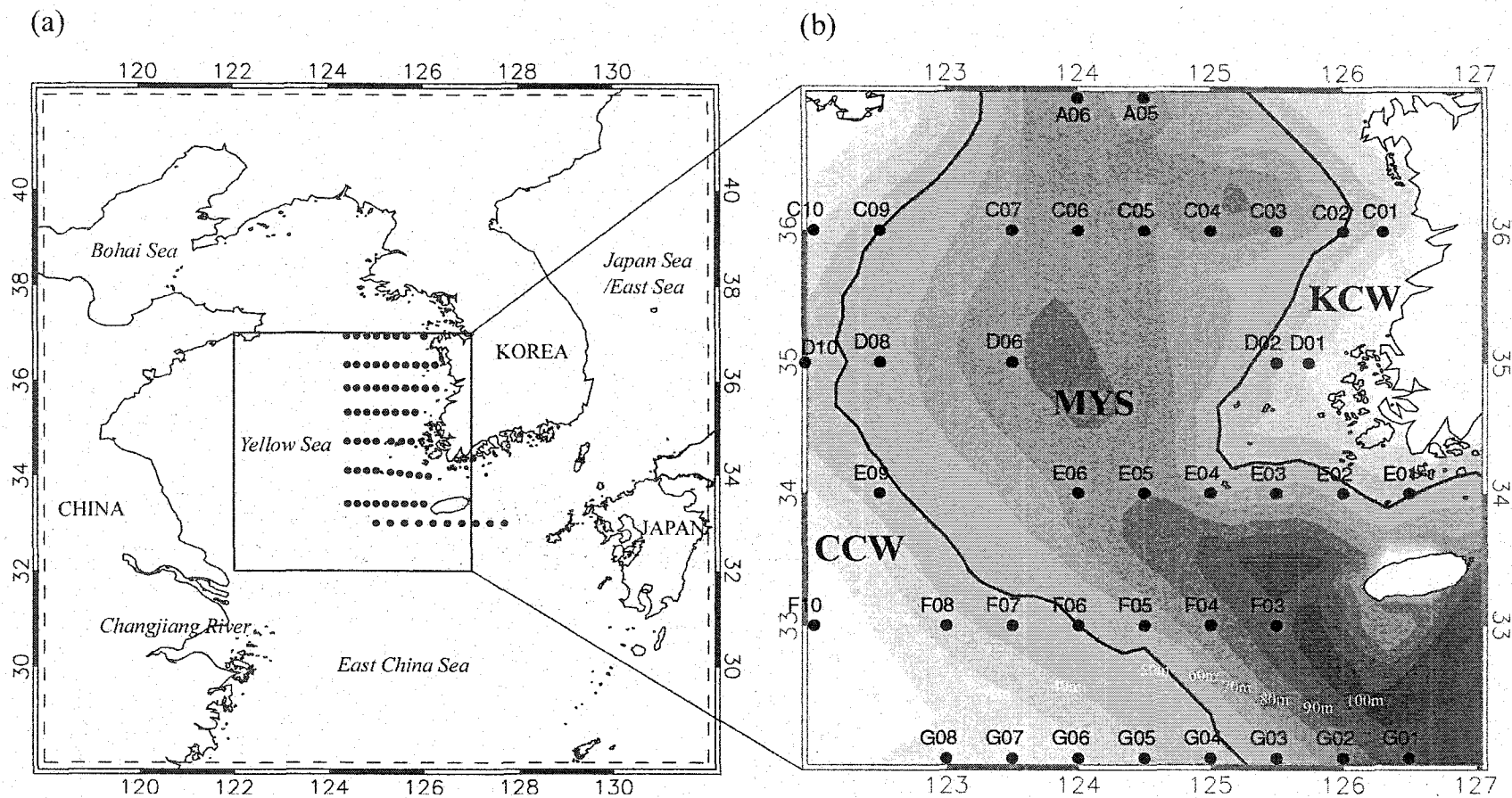


**Figure 4.1.** Geography of the study area. The Yellow Sea was divided into 3 sub-regions using bathymetry and physical features (CCW: Chinese Coastal Waters, MYS: Mid-Yellow Sea, and KCW: Korean Coastal Waters) in (b). The serial oceanographic stations of KODC for Secchi depth data are shown in (a) and the observatory stations for primary production of the Yellow Sea cruise in September, 1992 (Choi et al., 1995) are shown in (b).



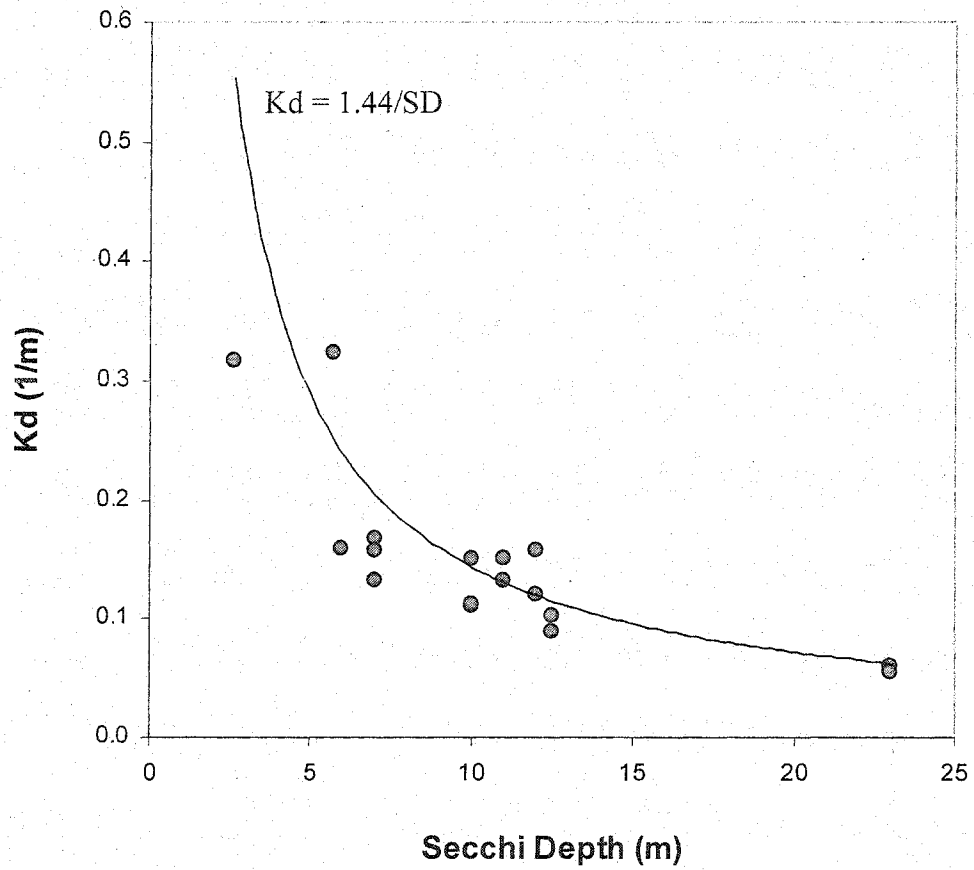


**Figure 4.2.** Scatter plots of measured diffuse attenuation derived from PAR in the water column versus measured Secchi depth (SD) at 17 stations in the Yellow Sea. The line of  $K_d = 1.44/SD$  is also drawn on the scatter plots.

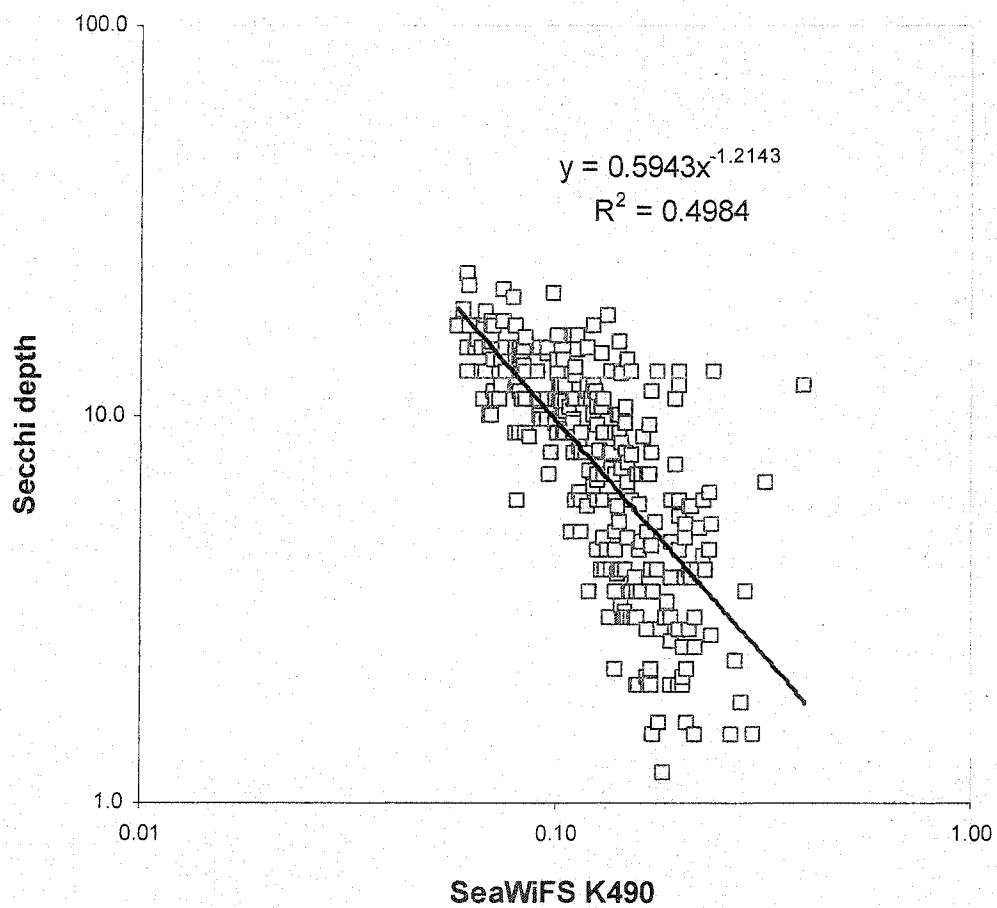


**Figure 4.3.** Secchi depth data obtained in the southeastern Yellow Sea from KODC were plotted against the SeaWiFS K490 in 286 stations during the periods of 1998 to 2002 (match up data is one day before to one day after).

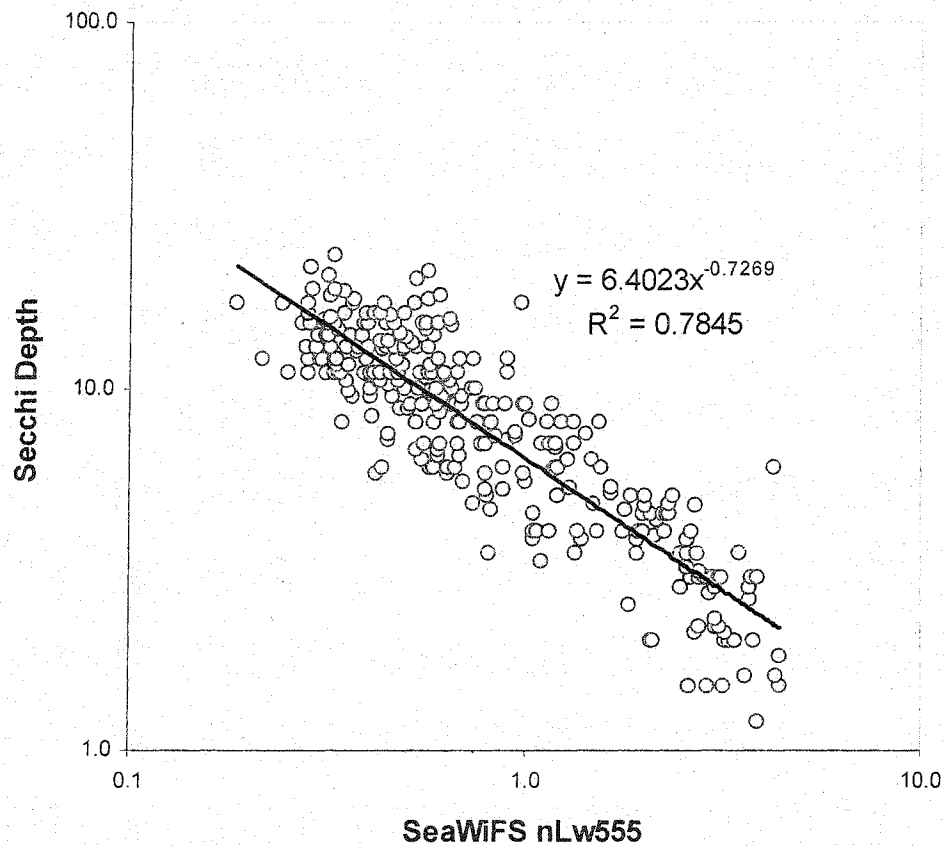


**Figure 4.4.** Secchi depth data obtained in the southeastern Yellow Sea from KODC were plotted against the SeaWiFS water-leaving radiances at 555nm in 286 stations during the periods of 1998 to 2002 (match up data is one day before to one day after).

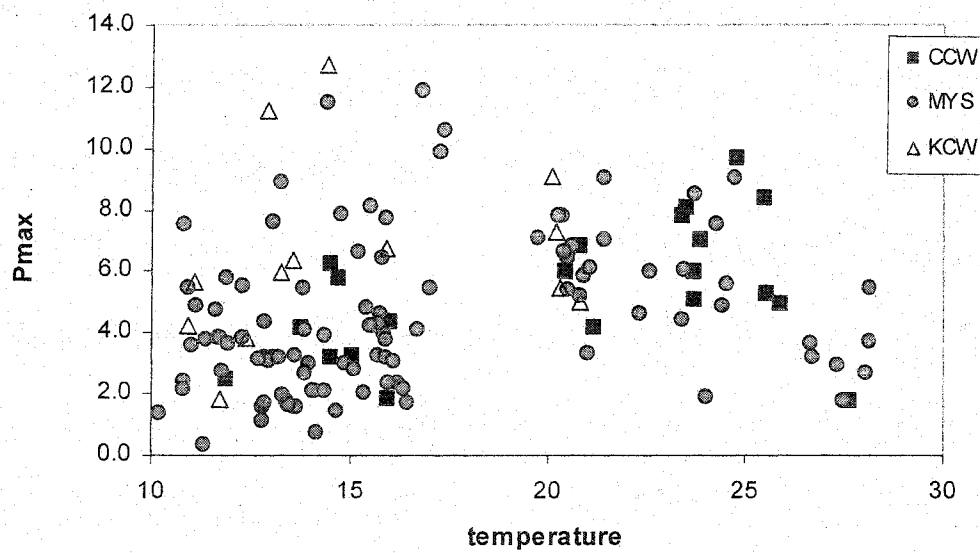


**Figure 4.5.** Scatter plots of temperature and  $P_m^B$  in three different regions (CCW: Chinese Coastal Waters, MYS: Middle of Yellow Sea waters, and KCW: Korean Coastal Waters) in the Yellow Sea.

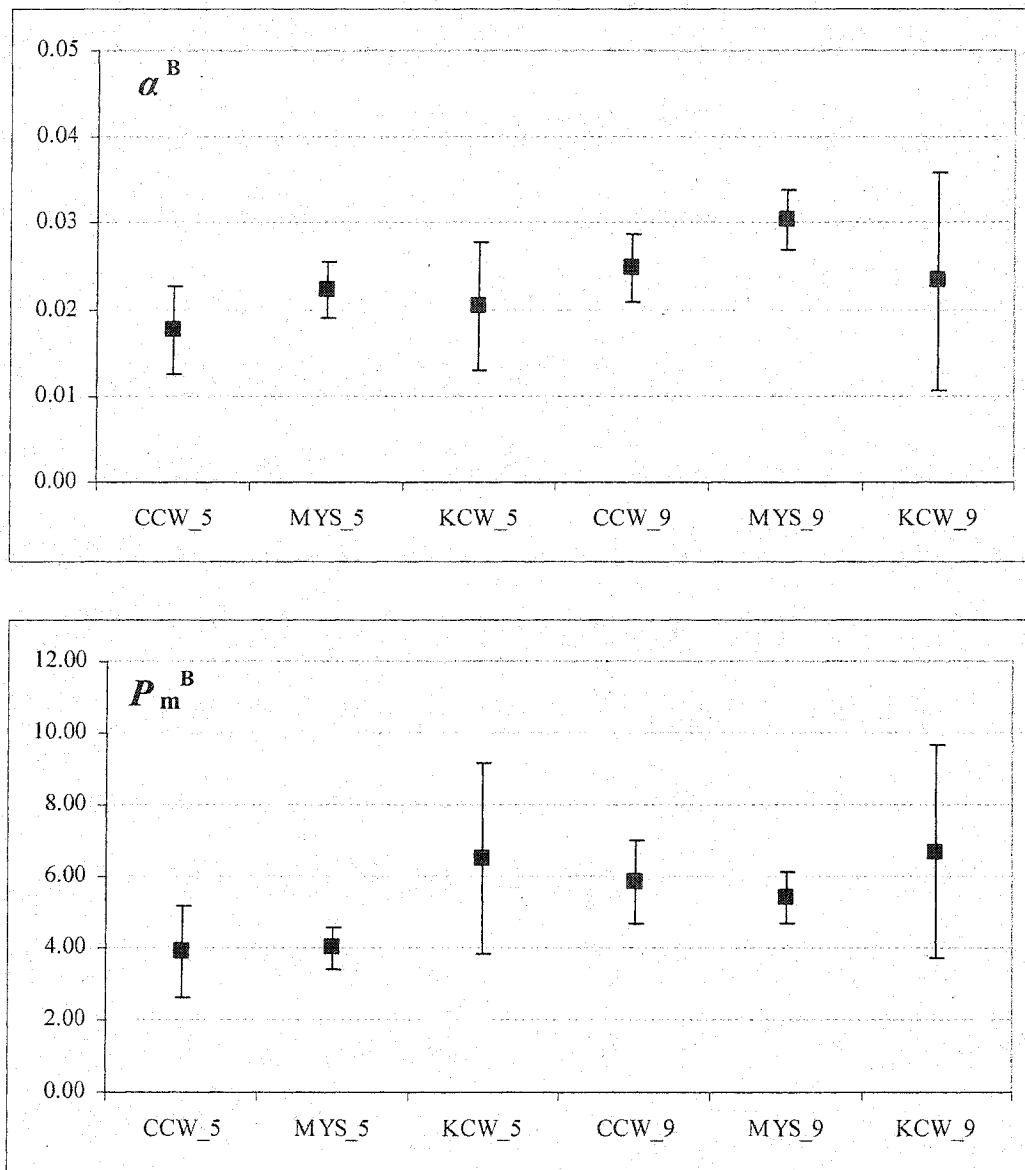


**Figure 4.6.** Mean values of  $\alpha^B$  and  $P_m^B$  in three different regions (CCW, MYS, and KCW) in May (left three) and December (right three) with 95% confidence intervals.

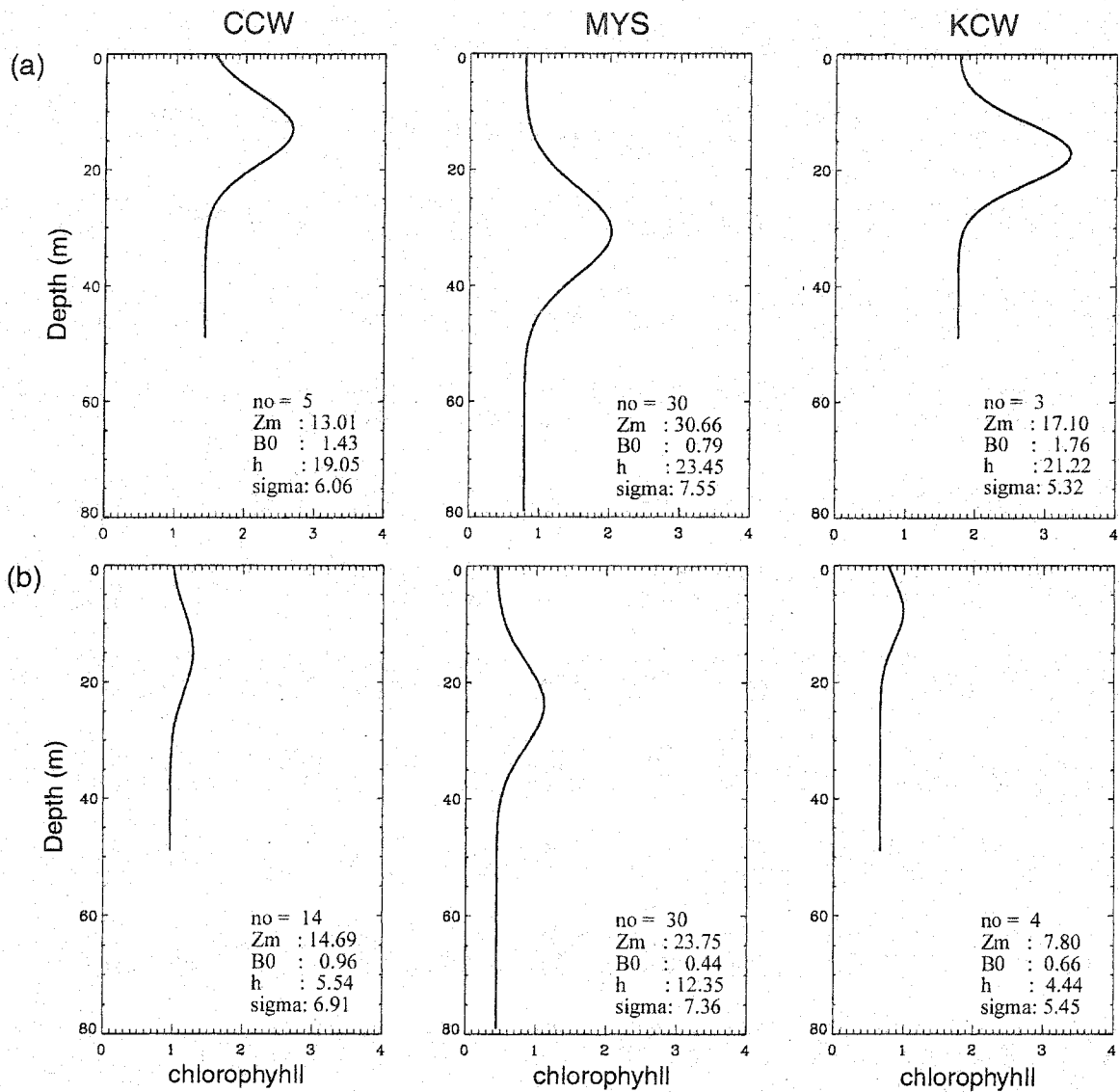


**Figure 4.7.** Mean fitted biomass (chlorophyll) profiles for the 3 sub-regions of the Yellow Sea in (a) May and (b) September. Number of data used (n) and four parameters of DCM model are shown on each graph.

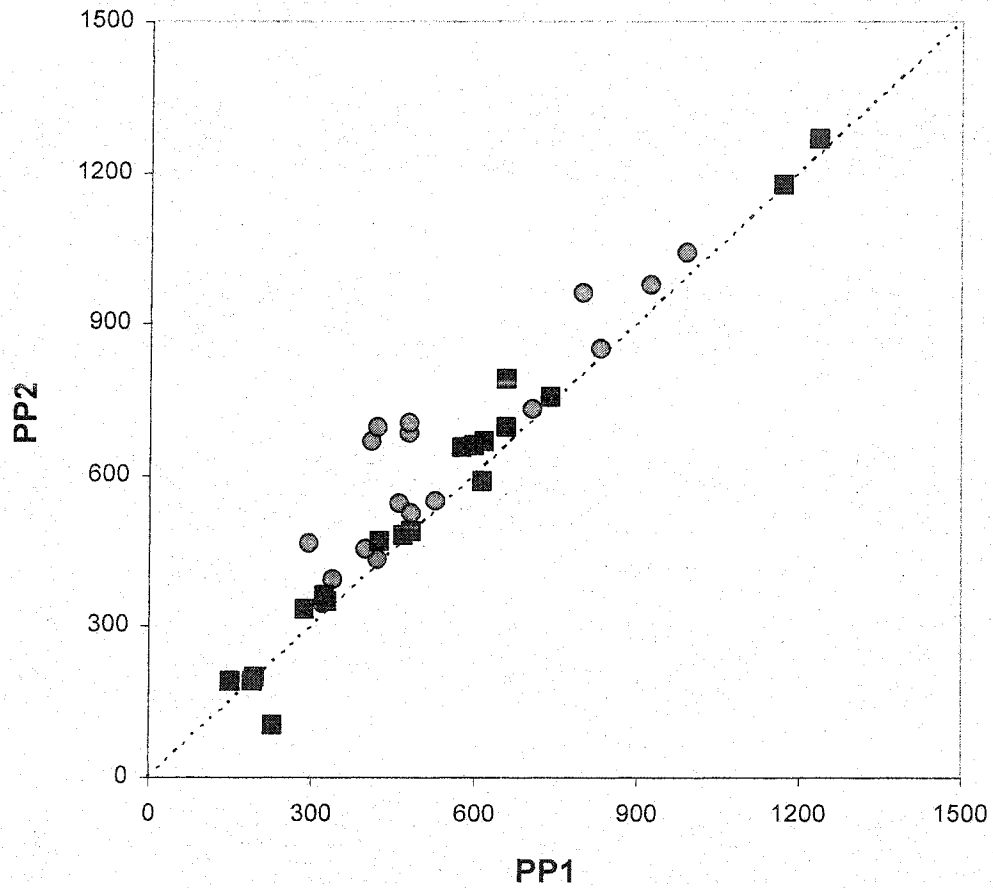


**Figure 4.8.** Scatter plots of primary production calculated using a uniform biomass profile (PP1) versus primary production using non-uniform biomass profile (PP2) at 37 stations of the Yellow Sea cruise in September, 1992 (Choi et al, 1995). Squares indicate primary production in deeper area (> 50m) and circles in the shallower areas (< 50m).

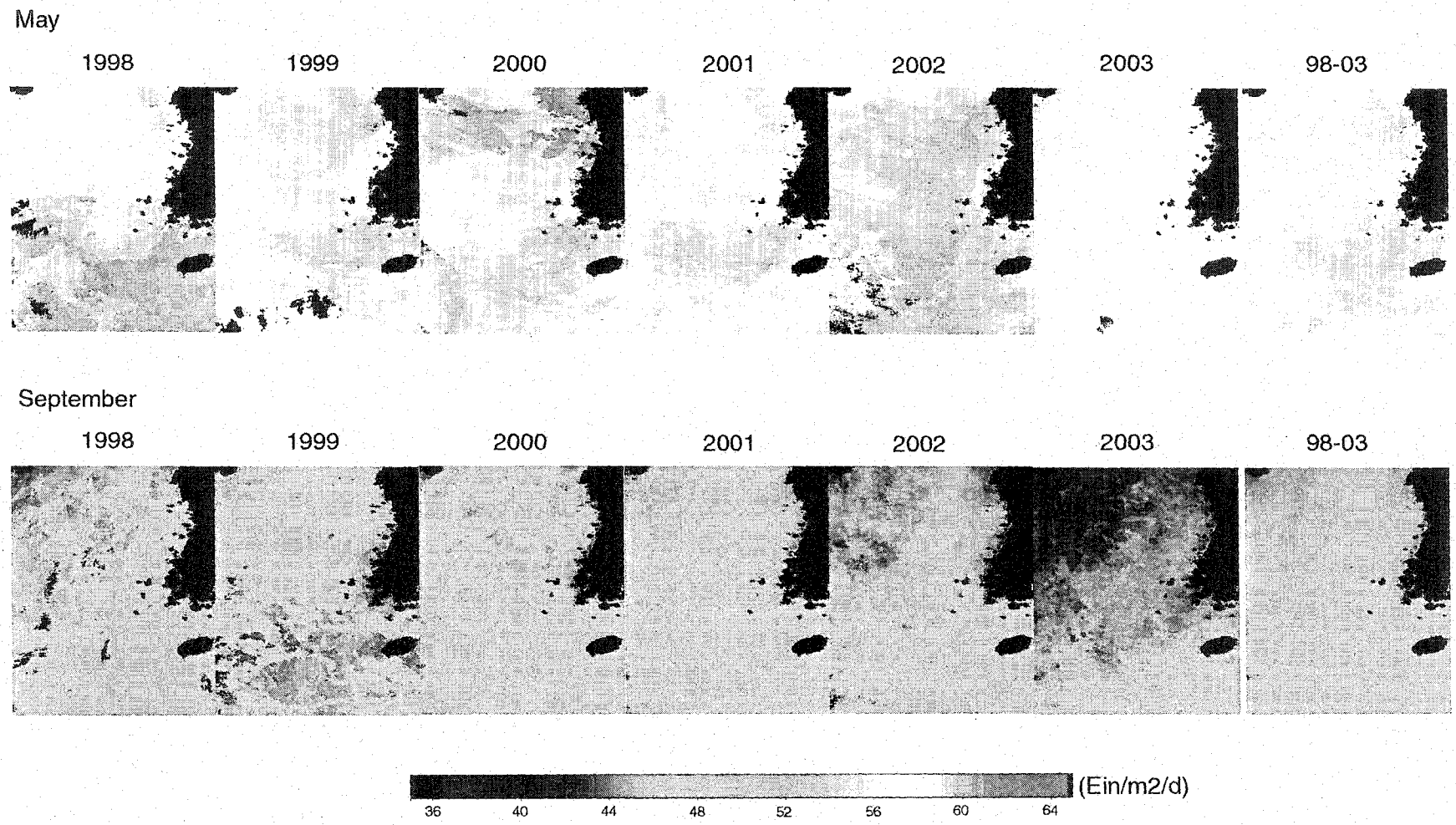


**Figure 4.9 (a).** Monthly composite SeaWiFS images from 1998 to 2003 in May (top) and September (bottom) as well as 6-year composite images on the right of each row (a) PAR, (b) diffuse attenuation ( $K_d$ ) derived from nLw555, (c) chlorophyll derived from Ahn's algorithm.



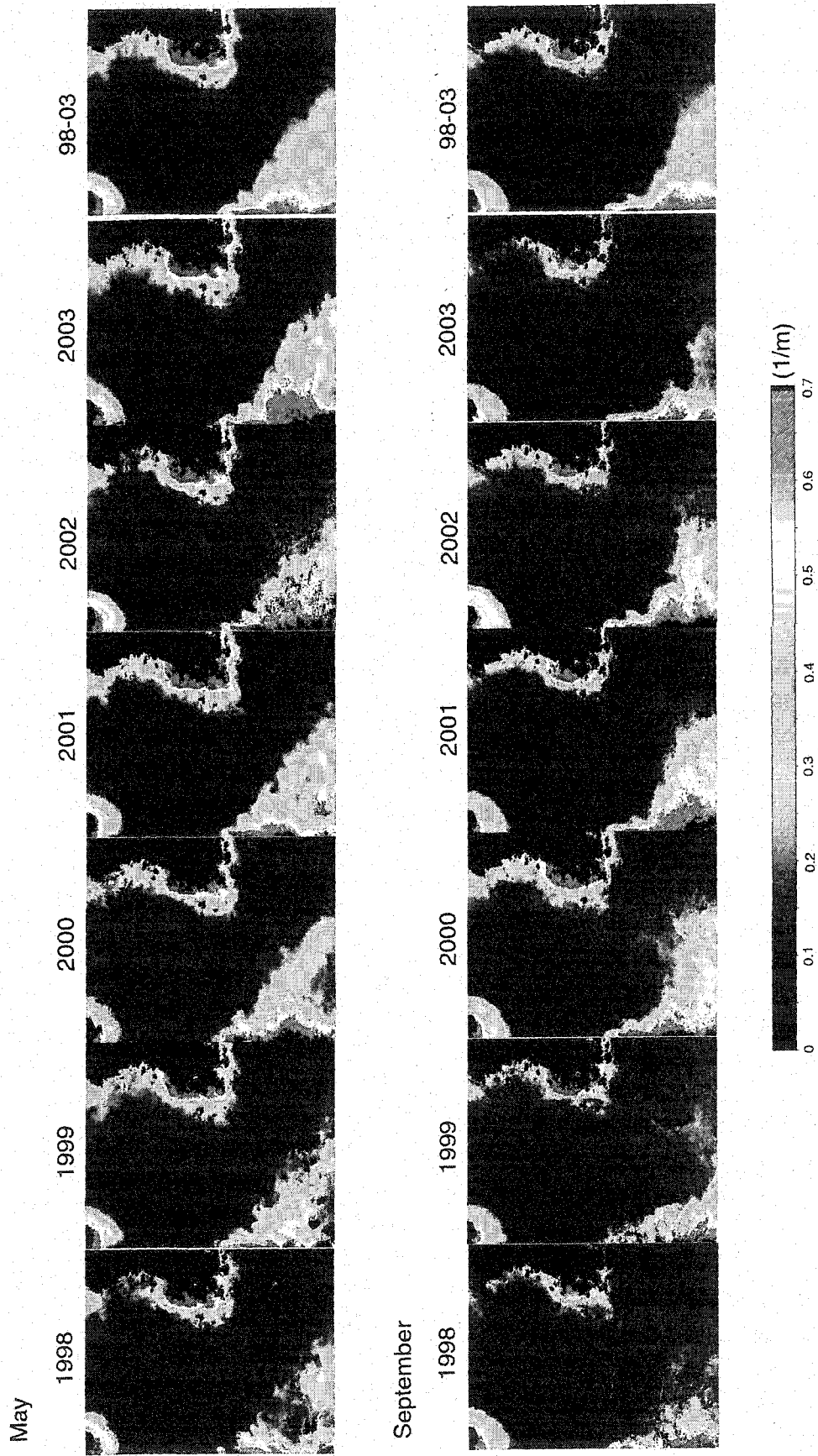


Figure 4.9 (b)

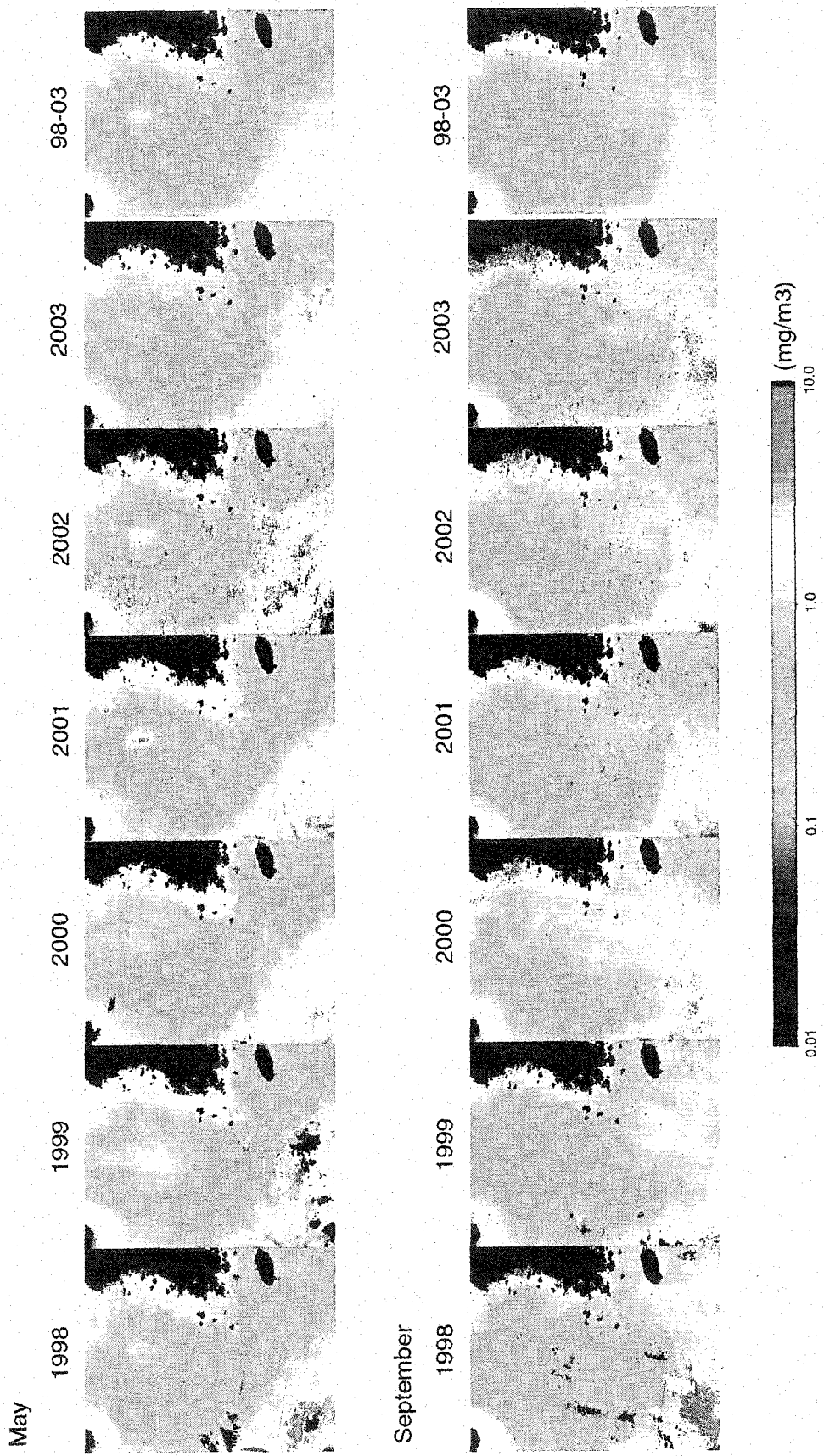
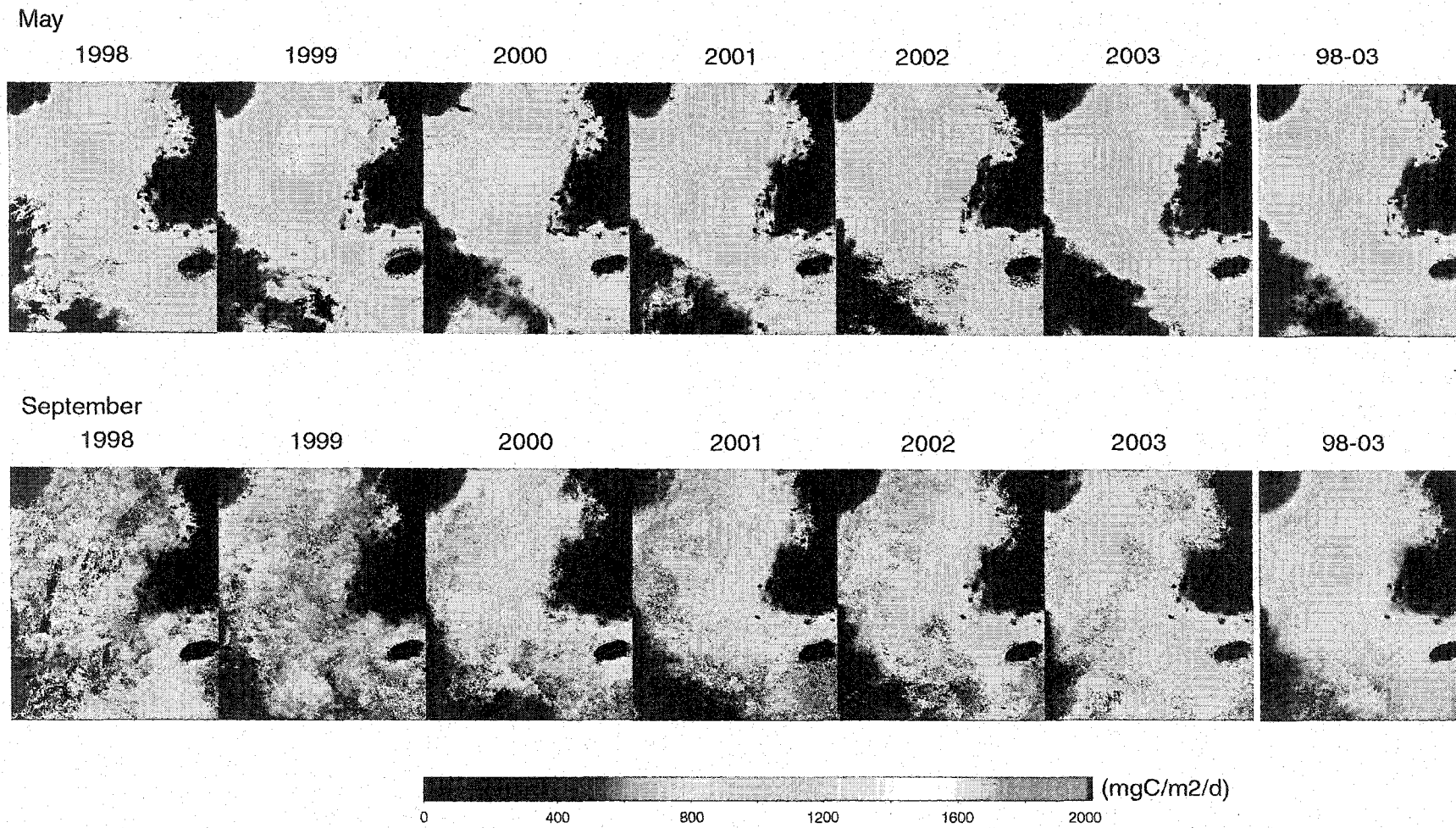
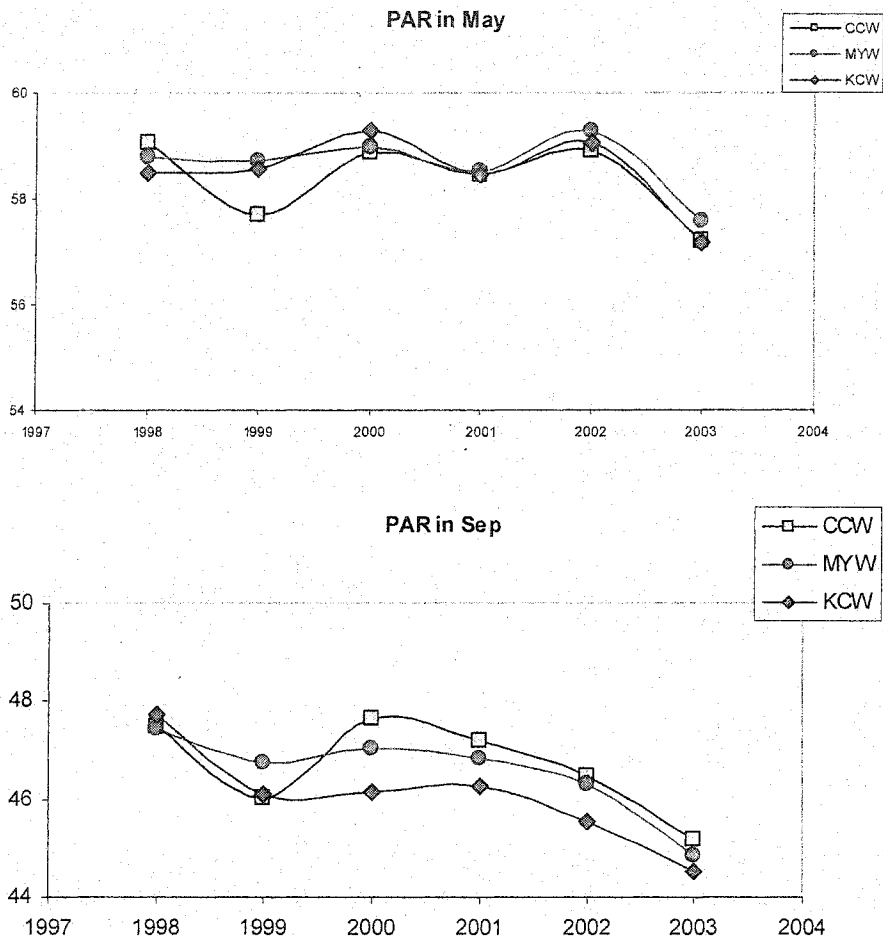


Figure 4.9(c)



**Figure 4.10.** Monthly-composite images of primary production based on SeaWiFS from 1998 to 2003 in May (top) and September (bottom) as well as 6-year composite images on the right of each row.



**Figure 4.11(a).** Year-to-year variations of the mean values of the SeaWiFS input values in the 3 sub-regions in May (top) and September (bottom). (a) PAR, (b) diffuse attenuation ( $K_d$ ) derived from nLw555, (c) chlorophyll derived from Ahn's algorithm, and (d) daily integrated primary production.

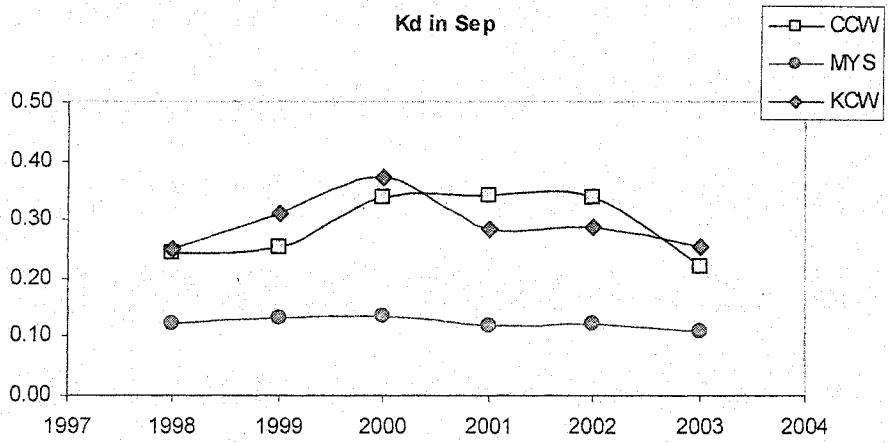
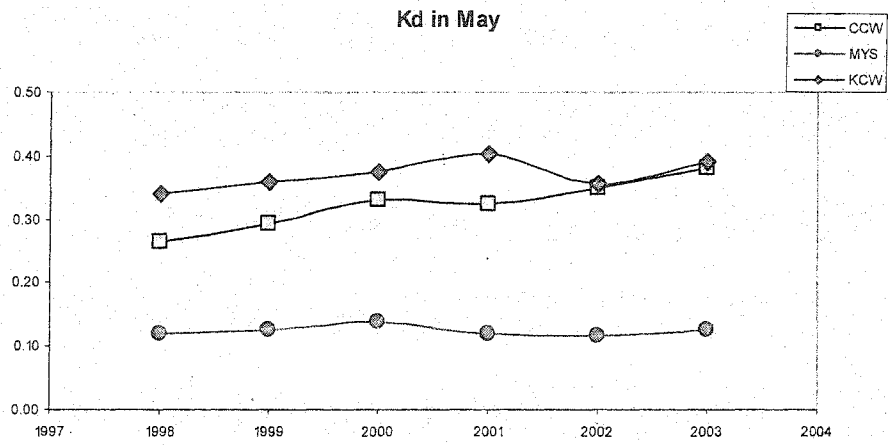


Figure 4.11(b)

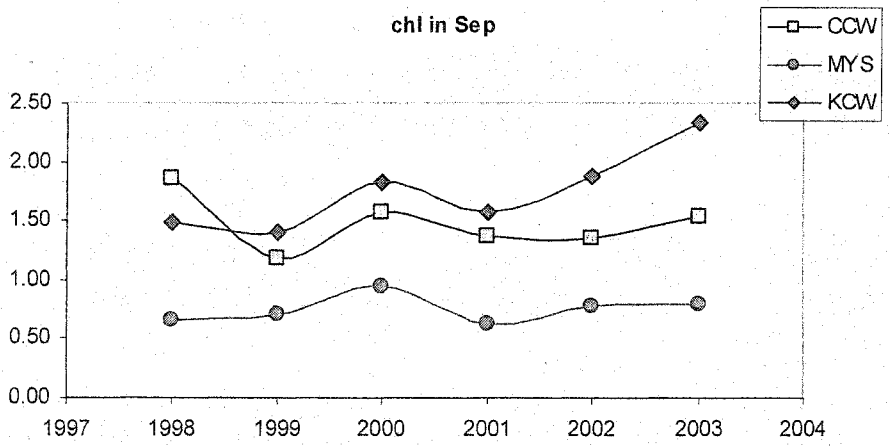
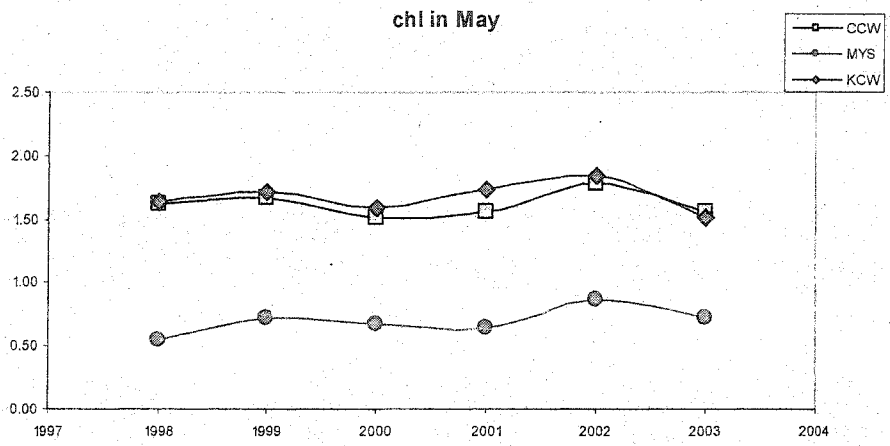
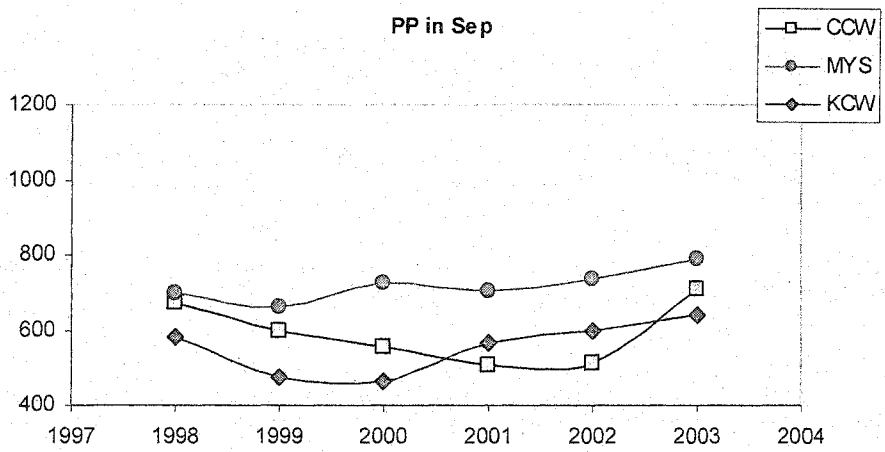
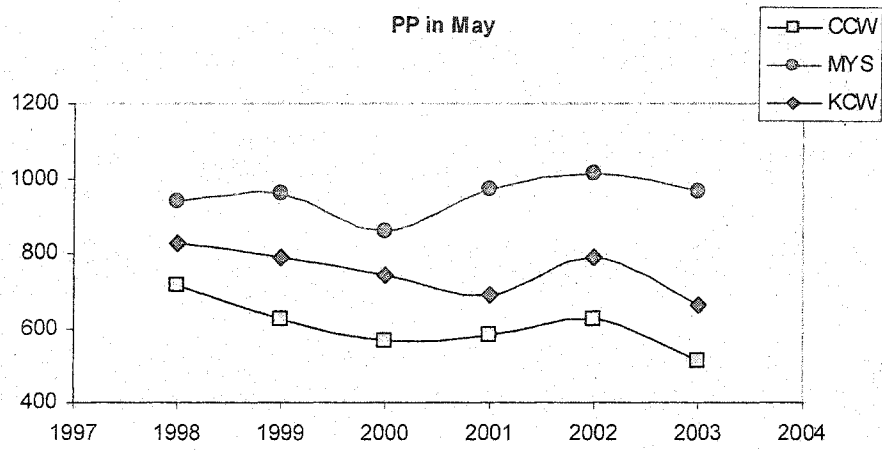
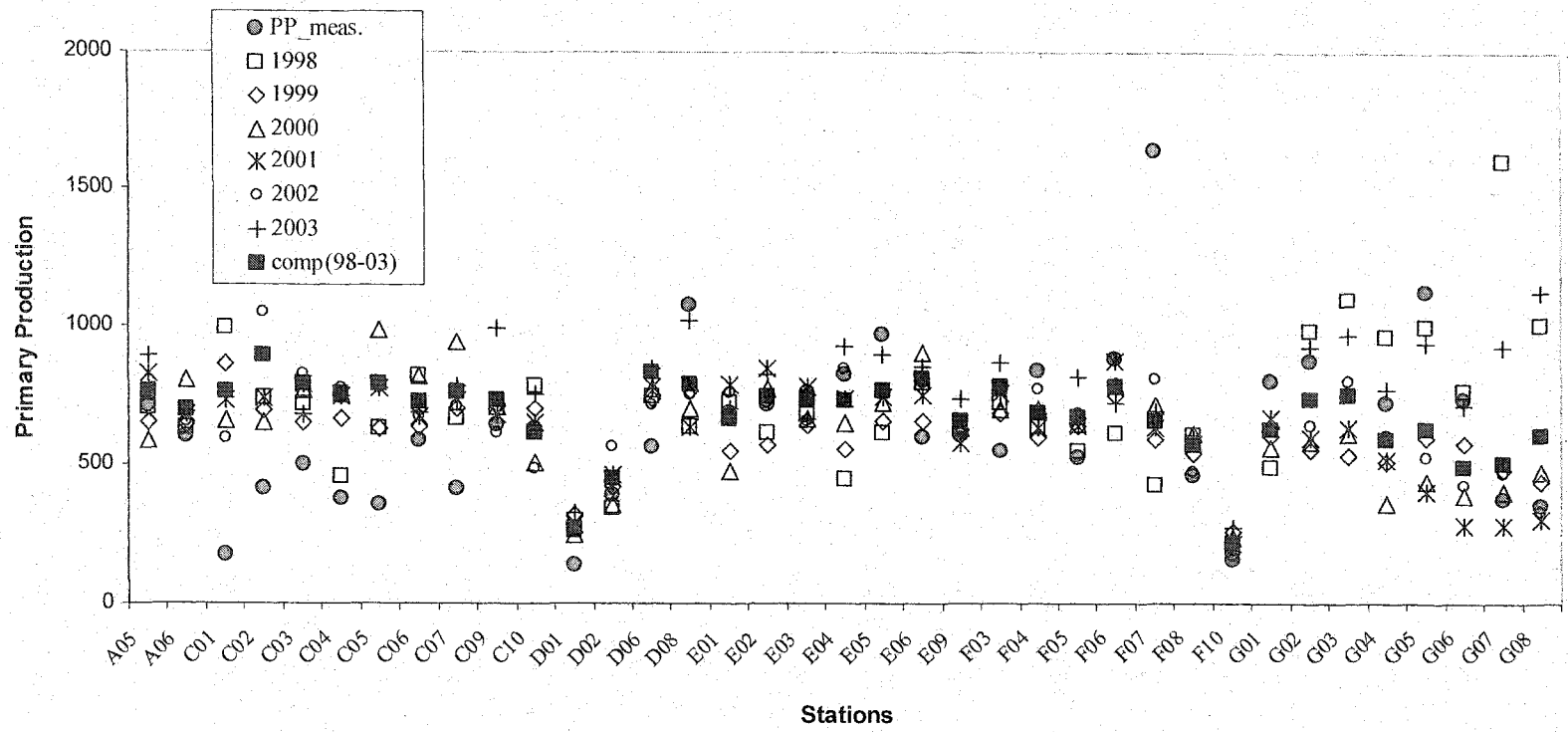


Figure 4.11(c)



**Figure 4.11(d)**



**Figure 4.12.** The values extracted from the monthly primary production images in 1998 to 2003 compared with the measured primary production at 37 stations of the Yellow Sea cruise in September, 1992 (Choi et al. 1995).



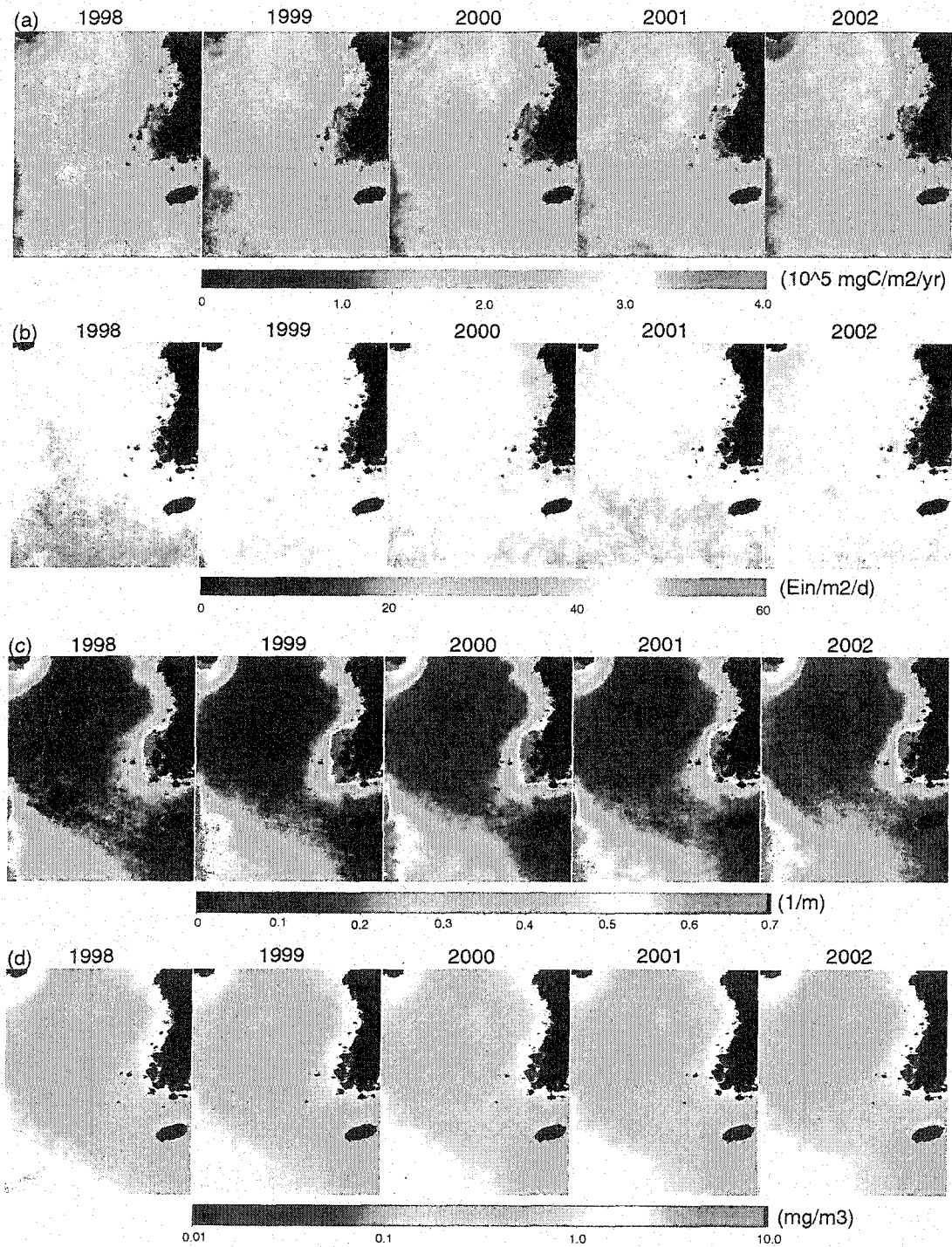


**Figure 4.13.** Annual results based on the SeaWiFS from 1998 to 2002: (a) total primary production (unit is  $10^5 \text{ mgC m}^{-2} \text{ yr}^{-1}$ ), and composite images of (b) PAR, (c)  $K_d$ , and (d) chlorophyll from Ahn's algorithm.

## CHAPTER 5

### SUMMARY, SIGNIFICANCE AND FUTURE RESEARCH

Coastal waters represent only about 10% of the ocean area, and yet coastal primary production contributes 15–30% of the global oceanic primary production. Coastal waters are vitally important for their role in fisheries. The coastal waters are influenced through human activities such as damming as well as by global-scale climate change. An important contribution of ocean color remote sensing data is to advance the understanding of long-term variations in primary production and phytoplankton biomass, and their relationship to environmental variables. This dissertation addresses primary production and decadal variation of ecological variables using remote sensing and *in situ* data in the Yellow Sea.

Two ocean color remote sensing data sets, Coastal Zone Color Scanner (CZCS) data from 1978–1984 and the Sea-viewing Wide Field-of-view Sensor (SeaWiFS) from 1998–2003, were compared in Chapter 2 to determine whether there have been decadal trends in the Yellow Sea. The water-leaving radiance measurements at 443 nm (Lw443) and 555 nm (Lw555) were compared, and chlorophyll derived from these values were also compared. CZCS pigment data were converted to chlorophyll concentration using an algorithm derived from *in situ* data to be comparable to the SeaWiFS OC4 chlorophyll. High Lw555 exhibited in the shallow coastal areas, including waters near the Changjiang River, during both periods indicate that these waters are sediment-dominated case-2 waters. Lw443 increased in these areas by 17%–61%, and Lw555 increased by 67–108% between the CZCS and the SeaWiFS eras. In the deeper waters

that are characterized as case-1 during summer, a decrease in  $L_w443$  by 25–31% during summer would indicate an increase in absorbing chlorophyll and colored dissolved organic matter (CDOM). The average chlorophyll concentration based on case-1 algorithms increased by 15–60% in these offshore deep waters between the two eras. Time series of *in situ* measurements from 1978 to 2002 of temperature, salinity, Secchi depth, and zooplankton biomass were obtained from the Korea Oceanography Data Center for comparison with the trends found in the satellite data. Between 1978 and 2002, there were increasing trends in temperature and zooplankton biomass, and decreasing trends in salinity and Secchi depth. The satellite data surrounding these stations showed an increase in  $L_w555$  (49 %), a decrease in the  $L_w443$  (-12 %), and an increase in chlorophyll (46 %). In this chapter, we discuss whether the decadal changes seen in the satellite data are real environmental changes, or whether they might be due to differences in the sensors and data processing methods. We cannot rule out the possibility that differences in the atmospheric correction might account for most of the differences.

In chapter three, we establish vertically well-mixed and stratified areas associated with monthly variations for the estimation of primary production and develop a method to differentiate those two areas using satellite observations in the Yellow Sea. To identify well-mixed areas, the criterion of temperature difference between surface and bottom layer,  $|\Delta T| < 0.8^\circ\text{C}$ , and the Simpson-Hunter criterion,  $\log(H/U^3) < 2$ , where both derived from a coupled ocean wave-circulation model (Moon, 2004). To develop a method to differentiate stratified and well-mixed waters using satellite data, remotely sensed sea surface temperature (SST) and water-leaving radiance at 667 nm ( $nL_w667$ )

from the Moderate Resolution Imaging Spectroradiometer (MODIS) were compared with the model results. During the winter season, most of the Yellow Sea is totally well-mixed. From spring through fall, the middle of the Yellow Sea is thermally stratified whereas the coastal areas are vertically well-mixed year-around due to tidal forces. However, the waters around the Changjiang River are stratified during the warmer months due to large amount of freshwater discharged from the river. A threshold based on nLw667 was found to work reasonably well along the southwest coast of Korea during the warmer months, where high nLw667 values indicate suspended sediments due to tidal mixing. Maps of the well-mixed area derived from the MODIS nLw667 using relationships between the nLw667 and the model  $\Delta T$  in the southeastern Yellow Sea were produced for the warmer months (April to September). The well-mixed waters were located in the areas where the nLw667 was higher than  $2-4 \text{ W}\cdot\text{m}^{-2}\cdot\text{nm}^{-1}\cdot\text{sr}^{-1}$  (the threshold varying with the month).

In chapter four, a local primary production algorithm was developed based on the algorithm of Platt and Sathyendranath (1988) parameterized with *in situ* data. The algorithm was applied to ocean color satellite data and primary production was estimated using for the Yellow Sea. To address the photosynthetic and the vertical biomass profile parameters, the Yellow Sea was divided into three sub-areas: Chinese coastal waters < 50 m deep, middle of the Yellow Sea, and Korean coastal waters < 50 m deep. More than 1300 individual scenes of the SeaWiFS were used for estimating primary production. The standard chlorophyll algorithms overestimate chlorophyll concentration since a large part of the Yellow Sea is considered as case 2 waters. Therefore, a local empirical chlorophyll algorithm was applied to derive more accurate chlorophyll concentration in

the Yellow Sea. A relationship was found between the SeaWiFS water-leaving radiance at 555nm and more than 300 measurements of Secchi depth obtained from the Korea Ocean Data Center. These Secchi measurements and satellite data measured within one day of each other were used to derive an algorithm for the diffuse attenuation coefficient.

Primary production derived using the local algorithm was higher in the middle of the Yellow Sea than in the coastal regions. Lower primary production in coastal areas was caused by light limitation due to high turbidity and shallow depth. The mean daily primary production was  $947 \text{ mgC m}^{-2} \text{ d}^{-1}$  in May and  $723 \text{ mgC m}^{-2} \text{ d}^{-1}$  in September in the middle of the Yellow Sea, and the values in Chinese coastal waters and Korean coastal waters were 590 and 589  $\text{mgC m}^{-2} \text{ d}^{-1}$ , respectively, in May, and 734 and 553  $\text{mgC m}^{-2} \text{ d}^{-1}$  in September. Our estimate of the daily primary production for the entire Yellow Sea was  $19.7 \times 10^4 \text{ tonC d}^{-1}$  in May and  $15.8 \times 10^4 \text{ tonC d}^{-1}$  in September, and the annual total primary production in the Yellow Sea was  $50.1 \times 10^6 \text{ ton C yr}^{-1}$ .

In this thesis, progress was made in characterizing and understanding contemporary and long-term variations in the marine ecosystem of the Yellow Sea. We compared different ocean color satellite data sets using a unified chlorophyll algorithm and constructed time series of environmental variables which reveal long-term variations of the ecosystem in the Yellow Sea. In particular, this will provide a framework to understand influences of the Changjiang River and the effect of its changing discharge before and after the Three Gorges dam which completed construction in 2003. We developed a method to differentiate well-mixed and stratified areas using satellite observations and established maps of the well-mixed and stratified areas in the southeastern Yellow Sea. These maps provide the basis for modeling vertical biomass

profiles for estimating primary production in these coastal waters. Finally, we developed a local primary production algorithm using ocean color satellite data for the Yellow Sea. The calculation using the local algorithm provides the first synoptic maps allowing a quantitative assessment of primary production in this coastal environment.

No attempt was made to unify the atmospheric correction algorithms for the CZCS and SeaWiFS data. We evaluated the consequences of the differences for a limited period (November 2003) and concluded that differences in the atmospheric correction between the ocean color sensors might account for the differences we found in the water-leaving radiances. Probably both atmospheric corrections need improvement in this area influenced by Asian dust. To resolve this we would need a unified algorithm that can correct for absorbing aerosols. Furthermore, for these Case 2 waters where mixtures of organic and inorganic materials affect the color of the water, more sophisticated bio-optical algorithms must be developed to account for their unique optical characteristics and variation of environmental parameters.

Our proposed method to classify well-mixed and stratified areas using satellite water-leaving radiance at 667nm can be applied only to limited regions and seasons. There is still a difficulty in applying satellite data for the classification in the shallow coastal regions which are affected by a large river discharge. The *in situ* measurements such as photosynthetic and DCM parameters for the primary production were spatially and temporally limited. We do not have ship-measured primary production data in the study area coincident with the operating period of the ocean color sensors for validation of our algorithm results. In addition, there was no available bio-optical measurement to model the light fields associated with primary production in the Yellow Sea. Therefore,

obtaining more data is really required for more accurate estimation of primary production as well as for validation. The development of a more sophisticated chlorophyll algorithm for these case 2 waters which could be applied to unify different ocean color satellite data would provide better understating of long-term changes in primary production associated with climate change and human impacts in the Yellow and East China Seas.

## BIBLIOGRAPHY

- Ahn, Y.H., 2004. Study on prediction of oceanographic variability of the Yellow Sea (The second phase), The Korea Ocean Research & Development Institute Report, BSPN 50900-1627-1 (in Korean).
- Antoine, D. and A. Morel, 1996. Ocean primary production 2. Estimation at global scale from satellite (Coastal Zone Color Scanner) chlorophyll. *Global Biogeochemical Cycles*, 10: 57–69.
- Antoine, D., A. Morel, and J. Andre, 1995. Algal pigment distribution and primary production in the eastern Mediterranean as derived from coastal zone color scanner observations. *J. Geophys. Res.* 100(8): 16193–16209.
- Baines, P. and C. Fandry, 1983. Annual cycle of density field in Bass Strait, *Australian J. Marine and Freshwater Res.*, 34: 143–153.
- Balch, W., R. Evans, J. Brown, G. Feldman, C. McClain, and W. Esaias, 1992. The remote sensing of ocean primary productivity: Use of a new data compilation to test satellite algorithms. *J. Geophys. Res.*, V97(2): 2279–2293.
- Beamish, R.J. and D.R. Bouillon, 1993. Pacific salmon production trends in relation to climate. *Canadian J. Fisheries and Aquatic Sciences*: 50, 1002–1016.
- Beardsley, R.C., R. Limeburner, K. Le, D. Hu, G.A. Cannon, and D.J. Pashinski, 1983. Structure of the Changjiang plume in the East China Sea during June 1980. In: *Proceedings of the International Symposium on Sedimentation on the Continental Shelf, with Special Reference to the East China Sea, April 12-16, Hangzhou, P. R. China, 1*, China Ocean Press, Beijing, pp.265–284.
- Beardsley, R.C., R. Limeburner, H. Yu, and G.A. Cannon, 1985. Discharge of the Changjiang (Yangtze River) into the East China Sea. *Continental Shelf Research*, 4: 57–76.
- Behrenfeld, M. and P. Falkowski, 1997. Photosynthetic rates derived from satellite-based chlorophyll concentration, *Limnol. Oceanogr.* 42(1): 1–20.
- Bowman, M. and W. Esaias, 1981. Fronts, stratification, and mixing in Long Island and Block Island Sounds, *J. Geophys. Res.*, 86(5): 4260–4264.
- Cadee, G.C. and J. Hegeman, 1974. Primary production of phytoplankton in the dutch wadden sea. *Netherl. J. Sea Res.*, 8(2): 240–259.



- Chen, C., R. Beardsley, Limburner, R. and Kim, K. 1994. Comparison of winter and summer hydrographic observations in the Yellow and East China Seas and adjacent Kuroshio during 1986. *Cont. Shelf. Res.*, 14(7-8): 909–929.
- Choi, J. K., 1991. The influence of the tidal front on primary productivity and distribution of phytoplankton in the mid-eastern coast of Yellow Sea. *The jour. Oceano. Soc. Korea*, 26(3): 223–241 (*in Korean*).
- Choi, J.K., J.H. Noh, and S.H. Cho, 2004. Temporal and spatial variation of primary production in the Yellow Sea (*in preparation*).
- Choi, J. K., J. H. Noh, K. S. Shin, and K. H. Hong, 1995. The early autumn distribution of chlorophyll-a and primary productivity in the Yellow Sea, 1992. *The Yellow Sea*, 1: 68–80.
- Choi, J.K., Y.C. Park, Y.C. Kim, Y.C. Lee, S.K. Son, H.J. Hwang, B.S. Han and C.S. Jung, 1988. The study of biological productivity of the fishing ground in the western coastal area of Korea, Yellow Sea. *Bull. Nat. Fish. Ref. Dev. Agency*, 42: 143–168 (*in Korean*).
- Choi, J. K. and J. H. Shim, 1986. The ecological study of phytoplankton in Kyeonggi Bay, Yellow Sea: II. Light intensity, transparency, suspended substances. *The Journ. Oceano. Soc. Korea*, 21(2): 101–109.
- Chung, K.H. and Y.C. Park, 1988. Primary production and nitrogen regeneration by macrozooplankton in the Kyunggi Bay, Yellow Sea. *J. Oceanol. Soc. Korea*, 23(4): 194–206.
- Conkright, M.E. and W.W. Gregg, 2003. Comparison of global chlorophyll climatologies: In situ, CZCS, Blended in situ-CZCS and SeaWiFS. *Int. J. Remote Sensing*, 24: 969–991.
- Evans, R.H. and H.R. Gordon, 1994. Coastal zone color scanner ‘system calibration’: a retrospective examination. *J. Geophys. Res.*, 99: 7293–7307.
- Feldman, G.C., N. Kuring, C. Ng, W. Esaias, C. McClain, J. Elrod, N. Maynard, D. Endres, R. Evans, J. Brown, S. Walsh, M. Carle, and G. Podesta, 1989. Ocean color, availability of the global data set. *Eos Trans.*, AGU. 70(23): 635–640.
- Garrett, C., J. Keeley, and D. Greenberg, 1978. Tidal mixing versus thermal stratification in the Bay of Fundy and Gulf of Maine, *Atmosphere-Ocean*, 16: 403–423.
- Gong, G.-C. and G.-J. Liu, 2003. An empirical primary production model for the East China Sea. *Cont. Shelf Res.* 23: 213–224.

- Gordon, H.R., D.K. Clark, J.W. Brown, O.B. Brown, R.H. Evans, and W.W. Broenkow, 1983. Phytoplankton pigment concentrations in the Middle Atlantic Bight: comparison of ship determinations and CZCS estimates. *Appl. Optics*, 22(1): 20–36.
- Gregg, W.W. and M.E. Conkright, 2001. Global seasonal climatologies of ocean chlorophyll: Blending in situ and satellite data for the Coastal Zone Color Scanner era. *J. Geophys. Res.*, 106(2): 2499–2515.
- Hoepffner, N., B. Sturm, Z. Finenko., and D. Larkin, 1999. Depth-integrated primary production in the eastern tropical and subtropical North Atlantic basin from ocean colour imagery. *Int. J. Remote Sensing*, 20(7): 1435–1456.
- Kang, Y. S., 1992. Primary productivity and assimilation number in the Kyonggi bay and the mid-eastern coast of Yellow Sea. *The Jour. Oceanogr. Soc. Korea*, 27(3): 237–246 (*in Korean*).
- Kang, Y. S., 1998. Climate shifts and zooplanktons in Korean Water. *Proceedings of the 1<sup>st</sup> Workshop on Climate Changes & Fisheries Resources*. P39–54 (*in Korean*).
- Kang, S., S. Kim, and S. Bae. 2000. Changes in ecosystem components induced by climate variability off the eastern coast of the Korean Peninsula during 1960-1990. *Progress in Oceanogr.*, 47: 205–222.
- Kang, Y. S., J.K. Choi, K.H. Chung, and Y.C. Park, 1992. Primary productivity and assimilation number in the Kyonggi bay and the mid-eastern coast of Yellow Sea. *The jour. Oceano. Soc. Korea*, 27(3): 237–246 (*in Korean*).
- Kara, A.B., P.A. Rochford, and H.E. Hurlburt, 2000. An optimal definition for ocean mixed layer depth. *J. Geophys. Res.*, 105(7): 16803–16821.
- Kywalyanga, M., T. Platt, and S. Sathyendranath, 1992. Ocean primary production calculated by spectral and broad-band models. *Marine Ecology Progress Series*. 85: 171–185.
- Kim, S. and S., Kang. 2000. Ecological variations and El Nino effects off the southern coast of the Korean Peninsula during the last three decades. *Fish. Oceanogr.*, 9(3): 239–247.
- Kim, S., S. Kang, and D. Kang, 1998. Effects of climate change in Korean Waters, *Proceedings of the 1<sup>st</sup> workshop on Climate changes & fisheries resources*. 68–81 (*in Korean*).
- Kim, S. and S. Yoo, 1996. Did climate regime shift in 1976 in the North Pacific occur in Korean waters?, *Ocean Res.*, 11(1): 133–149 (*in Korean*).

- Kirk, J.T.O., 1994. Light and photosynthesis in aquatic ecosystems, 2<sup>nd</sup>. Cambridge University Press, pp119–120.
- KORDI (Korea Ocean Res. Dev. Instit.), 1998. The Large Marine Ecosystem in the Yellow Sea, BSPN 97359-00-1159-3.
- Lewis, M., J. Cullen, and T. Platt. 1983. Phytoplankton and thermal structure in the upper ocean: consequences of nonuniformity in chlorophyll profile, *J. Geophys. Res.*, 88(4): 2565–2570.
- Longhurst, A., S. Sathyendranath, T. Platt, and C. Caverhill, 1995. An estimate of global primary production in the ocean from satellite radiometer data, *J. Plankton Res.*, 17(6): 1245–1271.
- Lie, H., 1989. Tidal fronts in the southeastern Hwanghae (Yellow Sea), *Cont. Shelf Res.*, 9(6): 527–546.
- Mask, A.C., J.J. O'Brien, and R. Preller, 1998. Wind-driven effects on the Yellow Sea Warm Current. *J. Geophys. Res.* 103(13): 30713–30729.
- McFarlane, G. and R.M. Beamish, 1992. Climate influence linking copepod production with strong year-classes in sablefish, *Anoplopoma fimbria*. *Canadian J. Fisheries and Aquatic Sciences*, 49: 743–753.
- Milliman, J.D., 1997. Blessed dams or damned dams. *Nature*, 386, 325-326.
- Monterey, G. and S. Levitus, 1997. Seasonal variability of mixed layer depth for the world ocean, NOAA Atlas NESDIS 14, 100 pp., U.S. Govt. Print. Off., Washington, D.C.
- Moon, I., 2004. Impact of a coupled ocean wave-tide-circulation system on coastal modeling. *Ocean Modelling*, (*in press*).
- Moon, J.E., Y.H. Ahn, and J.K. Choi, 2002. Compatible study on the SeaWiFS chlorophyll standard algorithm in Korean waters. Proceedings of the fall meeting, 2002 of the Korean Soc. of Oceanogr., Seoul, Korea, pp103–107 (*in Korean*).
- Morel, A. and J.-F. Berthon, 1989. Surface pigments, algal biomass profiles, and potential production of the euphotic layer: Relationships reinvestigated in view of remote-sensing applications, *Limnol. Oceanogr.*, 34(8): 1545–1562.
- Morel, A. and S. Maritorena, 2001. Bio-optical properties of oceanic waters: a reappraisal. *J. Geophys. Res.*, 106: 7163–7180.
- Morel, A. and L. Prieur, 1977. Analysis of variations in ocean color, *Limnol. Oceanogr.*, 22(4): 709–722.

- Naimie, C.E., C.A. Blain, and D.R. Lynch, 2001. Seasonal mean circulation in the Yellow Sea – a model-generated climatology. *Continental Shelf Res.*, 21: 667–695.
- Ning, X., Z. Liu, Y. Cai, M. Fang, and F. Chai, 1998. Physicobiological oceanographic remote sensing of the East China Sea: Satellite and in situ observations, *J. Geophys. Res.*, 103(10): 21623–21635.
- Obata, A., J. Ishizaka, and M. Endoh, 1996. Global verification of critical depth theory for phytoplankton bloom with climatological in situ temperature and satellite ocean color data. *J. Geophys. Res.*, 101: 20657–20667.
- O'Reilly, J.J., S. Maritorena, B.G. Mitchell, D.A. Siegel, K.L. Carder, M. Kahru, S.A. Garver, C.R. McClain, 1998. Ocean color algorithms for SeaWiFS, *J. of Geophys. Res.*, **103**: 24937–24953.
- O'Reilly, J.J. (and 21 co-authors), 2000. Ocean Color Chlorophyll *a* Algorithms for SeaWiFS, OC2 and OC4: Version 4. SeaWiFS Post-launch Technical Memorandum Series, **11**, NASA.
- O'Reilly, J.E., and 24 co-authors, 2000. SeaWiFS Postlaunch calibration and validation analyses, Part 3. NASA Tech. Memo. 2000-206892, Vol. 11, S.B. Hooker and E.R. Firestone, Eds., NASA Goddard Space Flight Center, 49pp.
- Park, J., 2000. Vertical distribution and primary productivity of phytoplankton in the Yellow Sea in spring time. M.S. thesis, Inha University, 83p (*in Korean*).
- Park, J.H., Y.M. Choi, and S.H. Kang, 1998. El Nino and fluctuations in fishing conditions in Korean Waters. Proceedings of the 1<sup>st</sup> Workshop on Climate Changes & Fisheries Resources. 83-91 (*in Korean*).
- Pernetta, J. C. and J. D. Milliman, 1995. Land-Ocean Interactions in the coastal zone implementation plan. IGBP Report No. 33, Stockholm, 215p.
- Pingree, R. and D. Griffiths, 1978. Tidal fronts on the shelf seas around the British Isles, *J. Geophys. Res.*, 83(9): 4615–4622.
- Platt, T., C. Caverhill, and S. Sathyendranath, 1991. Basin-scale estimates of oceanic primary production by remote sensing: The North Atlantic. *J. Geophys. Res.* **96(8)**: 15147–15159.
- Platt, T., C. Gallegos, and W.G. Harrison, 1980. Photoinhibition of photosynthesis in natural assemblages of marine phytoplankton. *J. Mar. Res.* 38: 687–701.
- Platt, T. and S. Sathyendranath, 1988a. Oceanic primary production: Estimation by remote sensing at local and regional scales. *Science*. 241: 1613–1620.

- Platt, T., S. Sathyendranath, C. Caverhill, and M. Lewis, 1988b. Ocean primary production and available light: further algorithms for remote sensing. *Deep-Sea Res.* 35(6): 855–879.
- Platt, T., S. Sathyendranath, and A. Longhurst, 1995. Remote sensing of primary production in the ocean: promise and fulfillment. *Phil. Trans. R. Soc. London Ser.*, pp447–465.
- Polovina, J.J., Mitchum, G.T., and Evans, G.T. (1995). Decadal and basin-scale variation in mixed layer depth and the impact on biological production in the Central and North Pacific, 1969–88. *Deep Sea Res.*, 42: 1701–1716.
- Polovina, J.J., G.T. Mitchum, N.E. Graham, M.P. Craig, E.E. Dartini, and E.N. Flint, 1994. Physical and biological consequences of a climate event in the central North Pacific. *Fisheries Oceanography*, 3: 15–21.
- Riedlinger, S. and R. Preller, 1995. Validation test report for the Yellow Sea shallow water analysis and forecast system. Draft NRL Report, Stennis Space Center, MI.
- Robinson, I., 1985. *Satellite oceanography: An introduction for oceanographers and remote-sensing scientists*, John Wiley & Sons, 454pp.
- Salisbury, J.E., 2003. *Satellite indices of fluvial influence in coastal waters*, University of New Hampshire, Ph.D. dissertation, 117pp.
- Sathyendranath, S., A. Longhurst, C. Caverhill, and T. Platt, 1995. Regionally and seasonally differentiated primary production in the North Atlantic. *Deep-Sea Res.* 42(10): 1773–1802.
- Sathyendranath, S. and T. Platt, 1988. The spectral irradiance field at the surface and in the interior of the ocean: A model for applications in oceanography and remote sensing. *J. Geophys. Res.*, 93(8): 9270–9280.
- Sathyendranath, S. and T. Platt, 1989. Remote sensing of ocean chlorophyll: consequence of nonuniform pigment profile. *Applied Optics*, 28(3): 490–495.
- Sathyendranath, S., and Platt, T., 1993. Underwater light field and primary production: Application to remote sensing. In: *Ocean Colour: Theory and Applications in a Decade of CZCS Experience*, V. Barale and P. M. Schlittenhardt (eds.), Kluwer Academic Publishers, Brussels, pp.79–93.
- Schubel, J.R., H.T. Shen, and M.J. Park, 1984. A comparison of some characteristic sedimentation processes of estuaries entering the Yellow Sea. In: *Marine geology and physical processes of the Yellow Sea*, proceedings of Korea-U.S. Seminar and Workshop, June 19-23, 1984, Seoul, Korea. pp.286–308.

- Seung, Y.H., J.H. Chung, and Y.C. Park, 1990. Oceanographic Studies Related to the Tidal Front in the Mid-Yellow Sea off Korea: Physical Aspects, *J. Oceanological Soc. Of Korea*, 25(2): 84–95.
- Siegel, D.A., M. Wang, S. Maritorea, and W. Robinson, 2000. Atmospheric correction of satellite ocean color imagery: the black pixel assumption. *Applied Optics*, 39(21): 3583–3591.
- Simpson, J. and J. Hunter, 1974. Fronts in the Irish Sea, *Nature*, 250: 404–406.
- Siswanto, E., J. Ishizaka, and Y. Katsumi, 2004. Estimating chlorophyll vertical profiles and the importance of subsurface chlorophyll maximum on primary production in Kuroshio front of the East China Sea (*in preparation*).
- Smith, R.C., R.W. Eppley, and K.S. Baker, 1982, Correlation of primary production as measured aboard ship in Southern California coastal waters and as estimated from satellite chlorophyll images. *Marine Biology*, 66: 281–288.
- Son, S., M. Dowell, J. Campbell, and S. Yoo, 2001. Primary production modeling in Case II waters: Significances of the vertical distribution of diffuse attenuation. Aquatic Sciences Meeting by American Society of Limnology and Oceanography, Feb. 12–16, 2001, Albuquerque, New Mexico, USA.
- Son, S., S. Yoo, M. Dowell, T. Moore, and J. Campbell, 2000. Decadal Trends in the Yellow Sea as Revealed by Satellite Ocean Color Data (1979-1998), Proceedings PORSEC 2000 in Goa, INDIA. pp.59–62.
- Steeman Nielsen, E., 1952. The use of radioactive carbon (C14) for measuring organic production in the sea. *J. Cons. Int. Explor. Mer*, 18: 117–140.
- Su, J., 1998. Circulation dynamics of the China Seas North of 18N. In: Robinson, A.R., Brink, K.H.(Eds.), *The Sea*, Vol. 11. Wiley, New York, pp.483–505.
- Sugimoto, T. and K. Tadokoro, 1997. Interannual-interdecadal variations of in zooplankton biomass, chlorophyll concentration and physical environment in the subarctic Pacific and Bering Sea. *Fisheries Oceanography*, 6(2), 74–93.
- Sugimoto, T. and K. Tadokoro, 1998. Interdecadal variations of plankton biomass and physical environment in the North Pacific. *Fisheries Oceanography*, 7 (3/4): 289–299.
- Trenberth, K.E. and J.W. Hurrell, 1994. Decadal coupled atmospheric-ocean variations in the Pacific. *Climate Dynamics*. 9: 303–319.
- Wallace, J. M. and S. Vogel, 1994. El Nino and climate prediction. Reports to the nation (Spring, 1994). NOAA. USA. 25pp.

- Wang, F., W. Li, and Q. Zheng, 1998. Seasonal and interannual varying scales of phytoplankton pigment concentrations in the East China Sea, Proceedings PORSEC 1998 in Qingdao, China. pp.130–133.
- Wu, Y., Y. Guo, and Y. Zhang, 1995. Distributional characteristics of chlorophyll-a and primary productivity in the Yellow Sea. *The Yellow Sea*, 1: 81–92.
- Yang, S., Q. Zhao, and I.M. Belkin, 2002. Temporal variation in the sediment load of the Yangtze river and the influences of human activities. *J. Hydrology*, 263: 56–71.
- Yentsch, C. and N. Garfield, 1981. Principal areas of vertical mixing in the waters of the Gulf of Maine, with reference to the total productivity of the area, oceanography from space, edited by J.F.R. Gower, Plenum Publishing Corp., pp.303–312.
- Yoo, S. and J. Park, 1998. Bio-optical properties in the Yellow Sea. *J. Korean Soc. Remote Sens.*, 14(3): 285–294.
- Yoo, S. and K. Shin, 1995. Primary productivity properties in the nearshore region of Taean Peninsula. *Ocean Res.*, 17(2): 91–99 (*in Korean*).
- Zhang, C., J. Lee, S. Kim, and J. Oh. 2000. Climatic regime shifts and their impacts on marine ecosystem and fisheries resources in Korean Waters. *Prog. Oceanogr.*, 47: 171–190.